Particle identification

Peter Križan

Introduction: Why Particle ID?

Efficiency and purity in particle identification

Time-of-flight

Basics: dE/dx, Čerenkov, Trans. Rad.

dE/dx measurement

Čerenkov counters

Transition radiation counters

Calorimeters

Muon and K_L detection

Introduction: Why Particle ID?

Particle identification is an important aspect of particle, nuclear and astroparticle physics experiments.

Some physical quantities in particle physics are only accessible with sophisticated particle identification (B-physics, CP violation, rare decays, search for exotic hadronic states).

Nuclear physics: final state identification in quark-gluon plasma searches, separation between isotopes

Astrophysics/astroparticle physics: identification of cosmic rays – separation between nuclei (isotopes), charged particles vs high energy photons

Introduction: Why Particle ID?

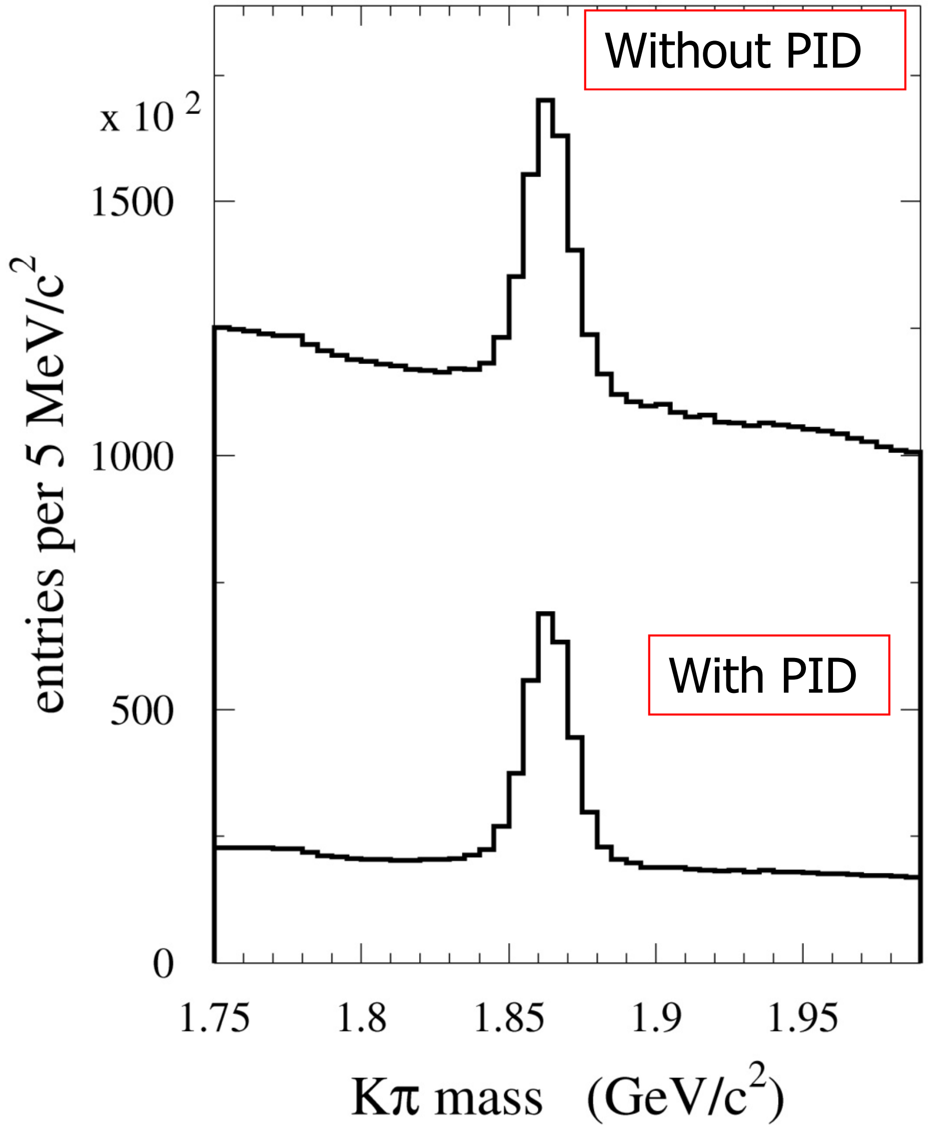

Example 1: BaBar

Particle identification reduces combinatorial background by ~5x

Introduction: Why Particle ID?

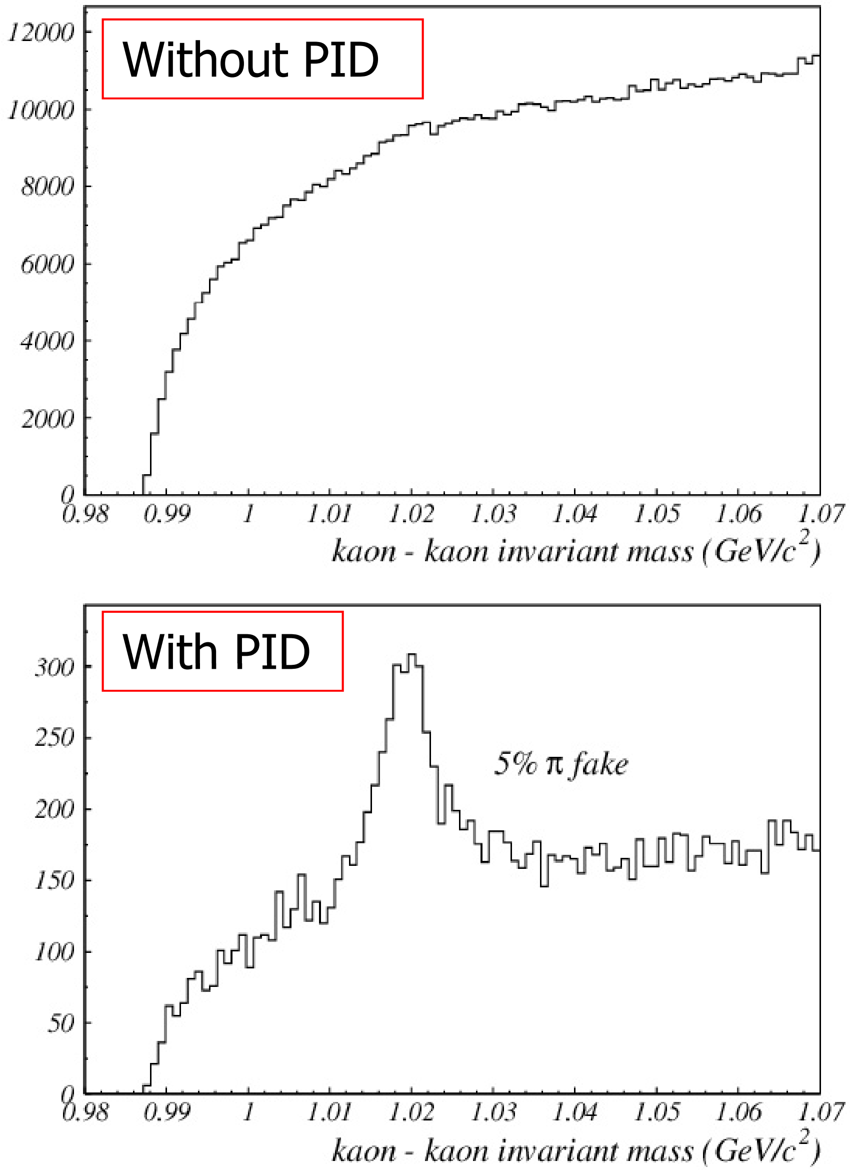

Example 2: HERA-B

K^+K^- invariant mass.

The $\phi \rightarrow K^+K^-$ decay only becomes visible after particle identification is taken into account.

Particle identification systems in Belle

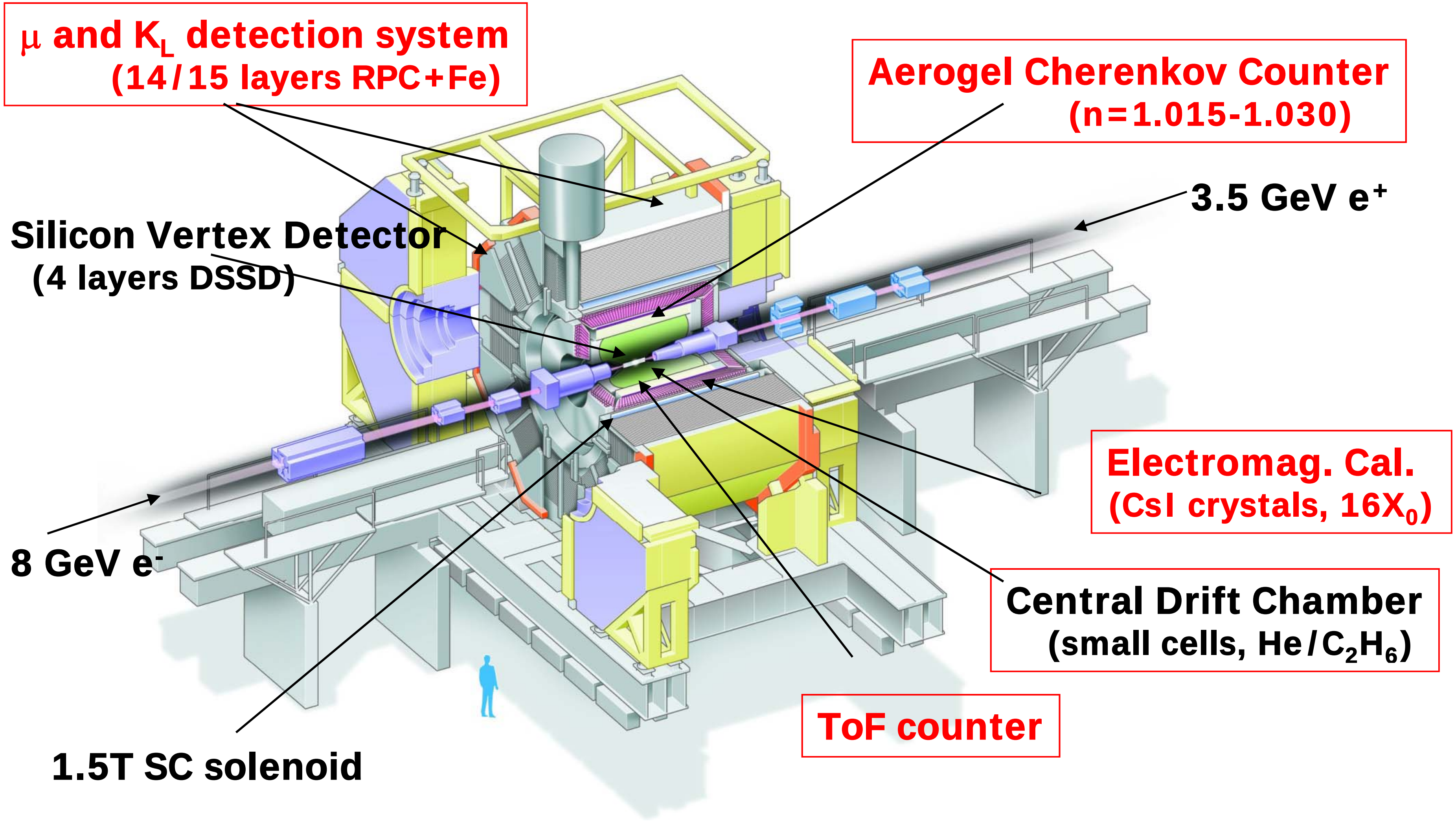

Efficiency and purity in particle identification

Efficiency and purity are tightly coupled!

Two examples:

particle type 1 type 2

eff. vs fake probability

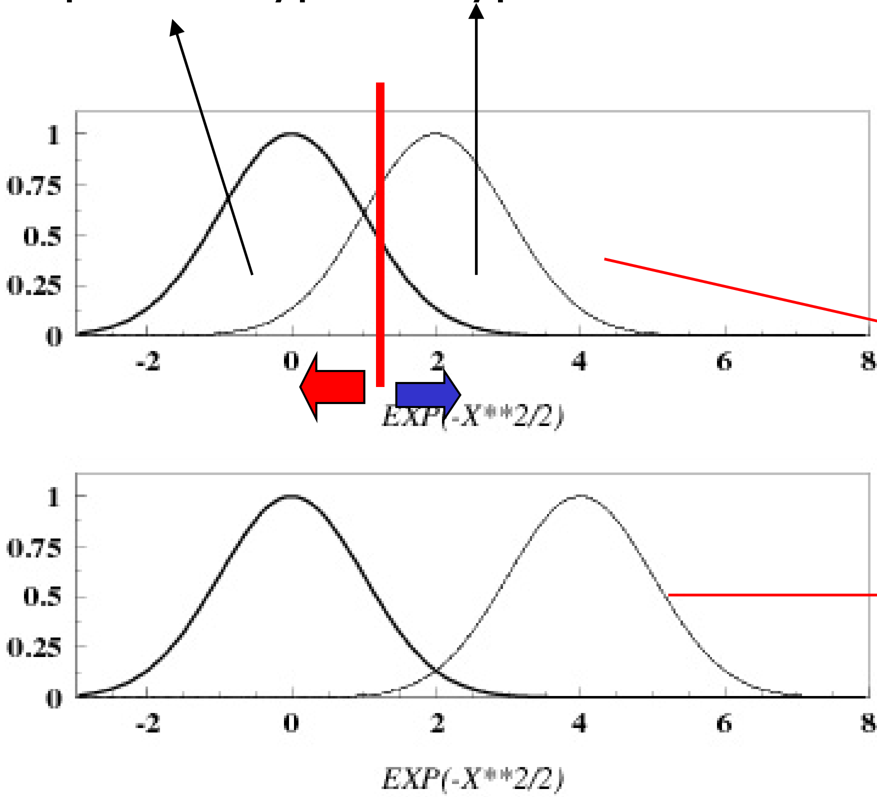

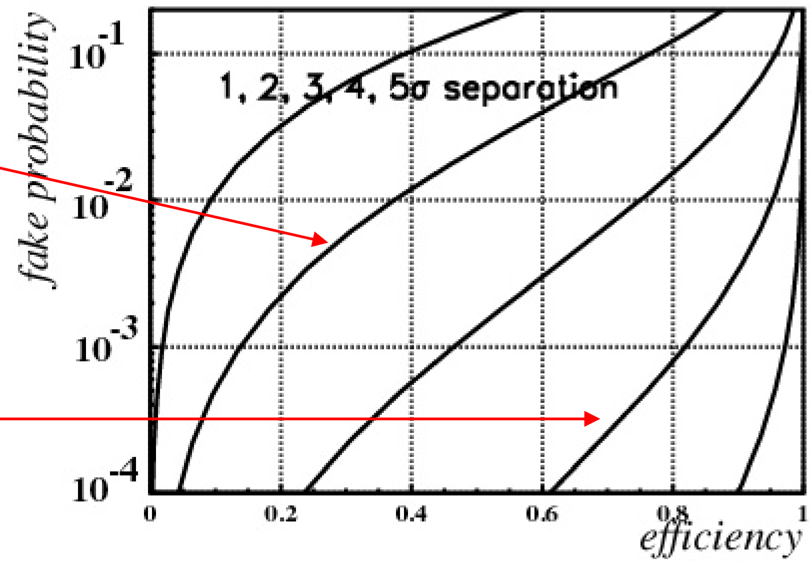

some discriminating variable

Identification of charged particles

Particles are identified by their mass or by the way they interact.

Determination of mass: from the relation between momentum and velocity, $p=\gamma mv$.

Momentum known (radius of curvature in magnetic field)

→Measure velocity:

- time of flight
- ionisation losses dE/dx
- Cherenkov angle
- transition radiation

Mainly used for the identification of hadrons.

Identification through interaction: electrons and muons

Time-of-flight measurement (TOF)

Measure time difference over a known distance, determine velocity

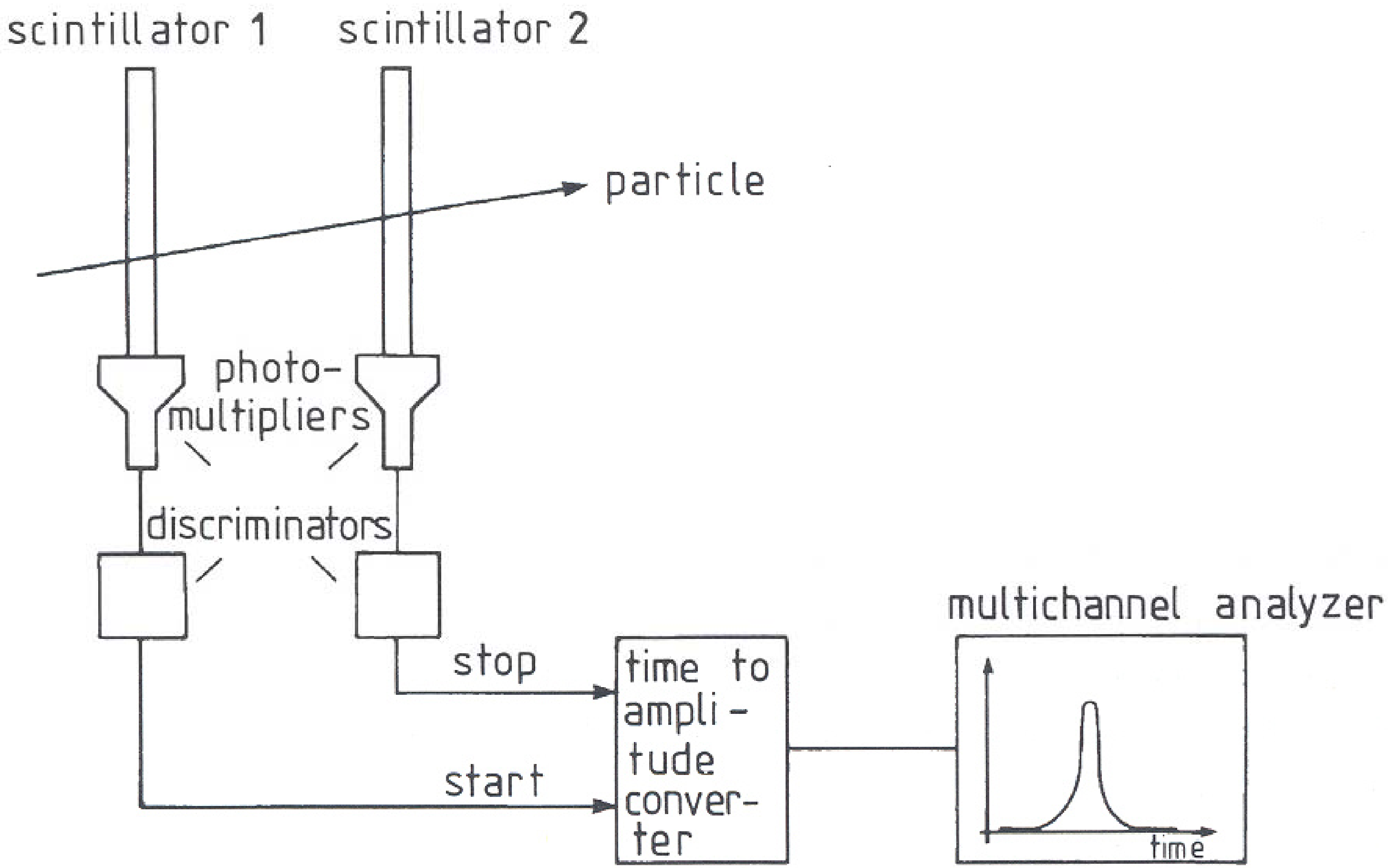

Fig. 6.5. Working principle of time-of-flight measurement.

Photomultiplier tube

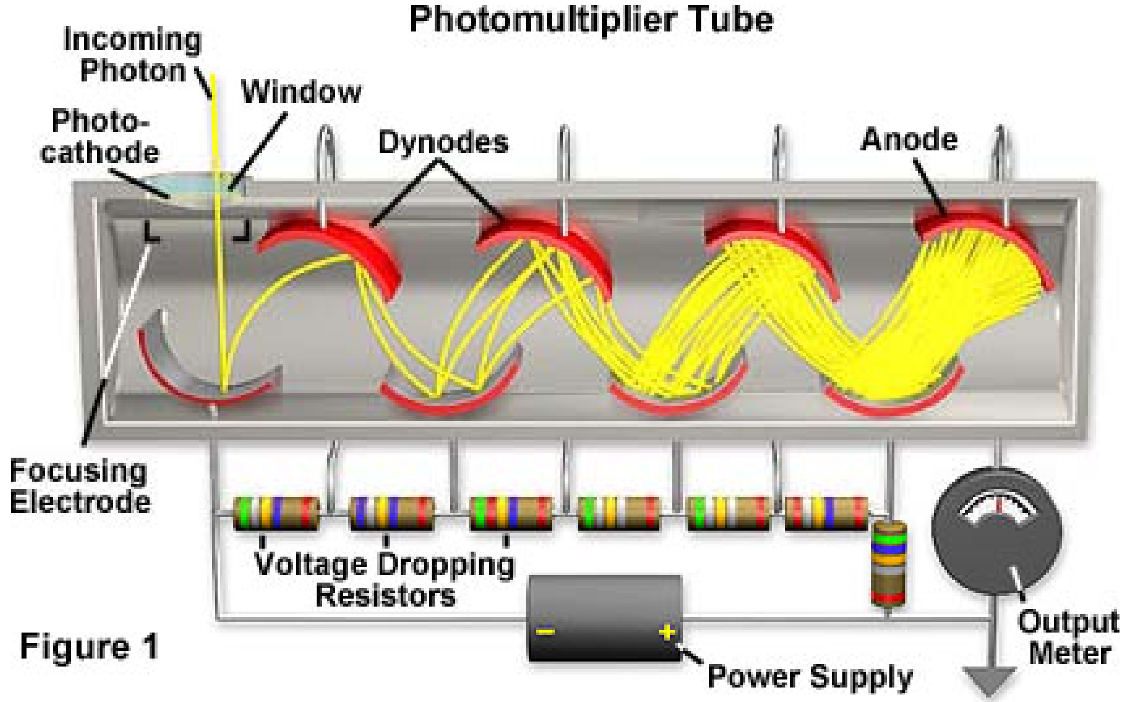

Time-of-flight measurement 2

Required resolution, example:

π/K difference at 1GeV/c: 300ps

For a 3σ separation need σ(TOF)=100ps

Resolution contributions:

- PMT: transient time spread (TTS)
- Path length variation
- Momentum uncertainty

Time difference between two particle species for path length=1m

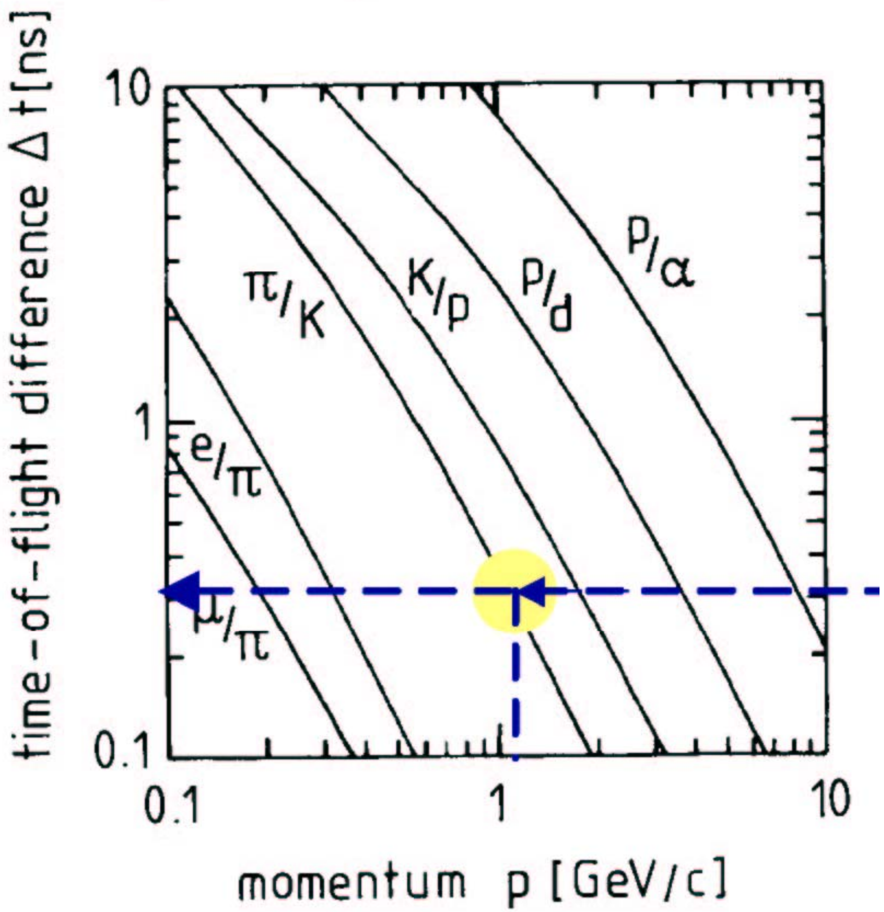

Time-of-flight measurement 3

Resolution of a PMT: transient time spread (TTS), time variation for single photons

Tubes for TOF have to be optimized for small TTS.

Main contribution after the optimisation: photoelectron time spread before it hits the first dynode.

Estimate: take two cases, one with T=1eV and the other with T=0 after the photoelectron leaves the photocathode; take U=200V and d=10mm

T=1eV: $v_0 = \sqrt{(2T/m)} = 0.002\ c$, $a=F/m=200eV/(10mm\ 0.5\ 10^6 eV/c^2)$

$d = v_0 t + at^2/2 \rightarrow t = \sqrt{(2d/a+(v_0/a)^2)} - v_0/a$

T=0eV : $v_0 = 0 \rightarrow t=\sqrt{(2d/a)}=2.3ns$

Time difference: 170ps is a typical value.

Good tubes: σ(TTS)=100ps

For N photons: $\sigma \sim \sigma$(TTS) / $\sqrt{(N)}$

Very fast: MCP-PMT

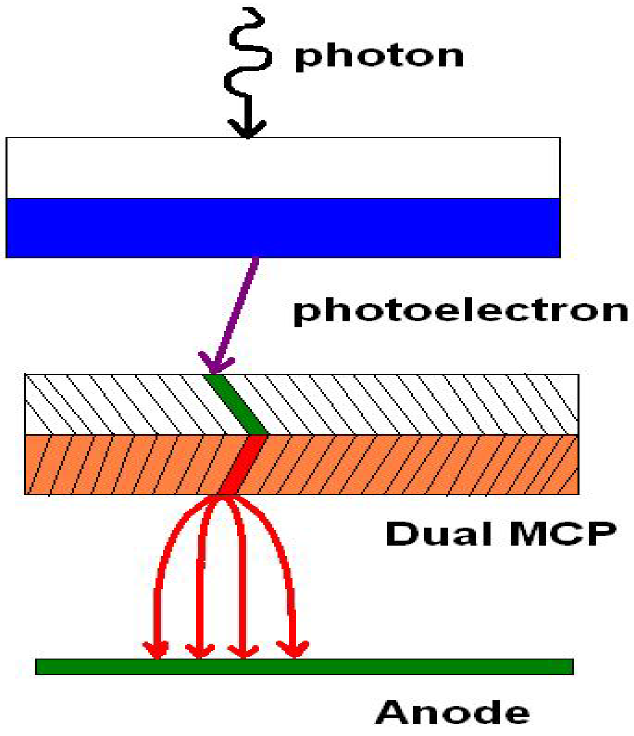

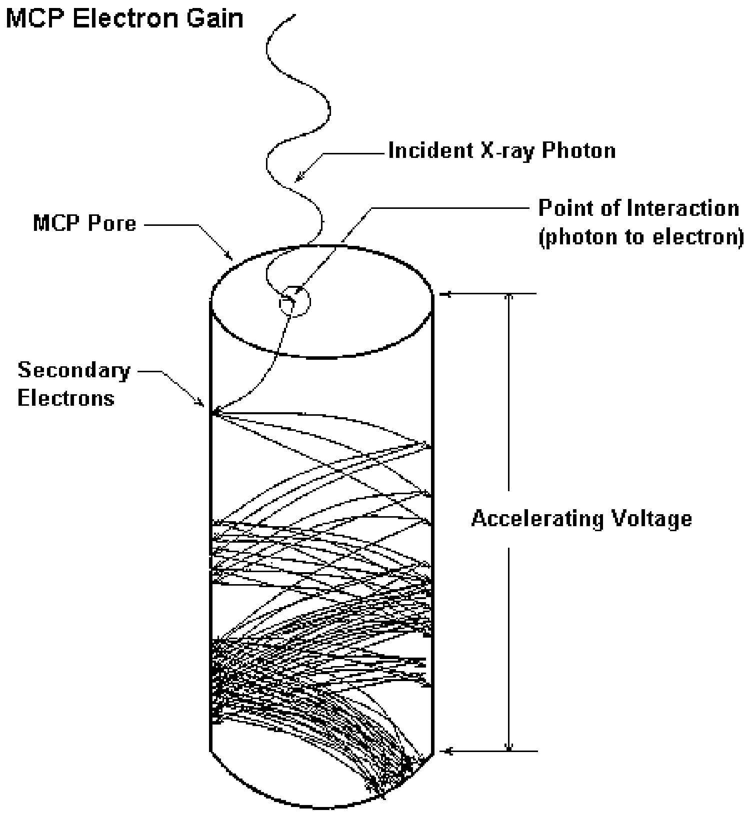

Very fast: MCP-PMT

BURLE 85011 microchannel plate (MCP) PMT: multi-anode PMT with two MCP stages

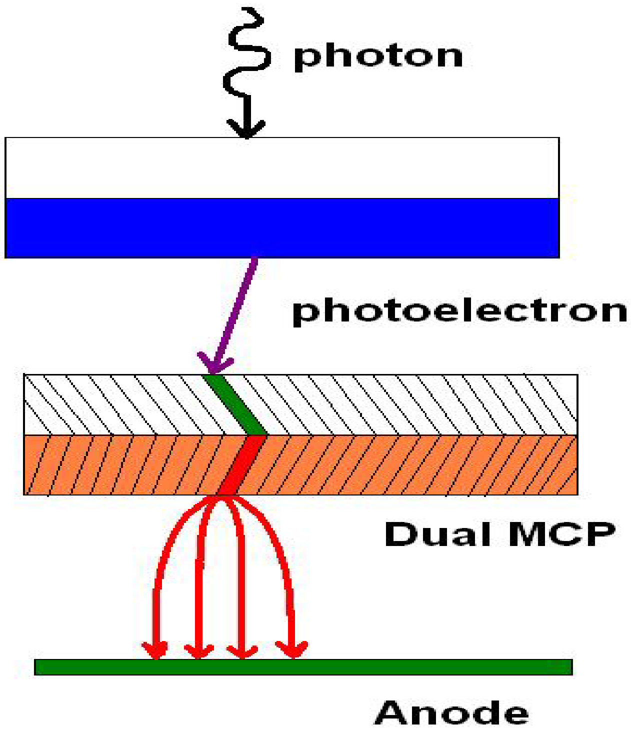

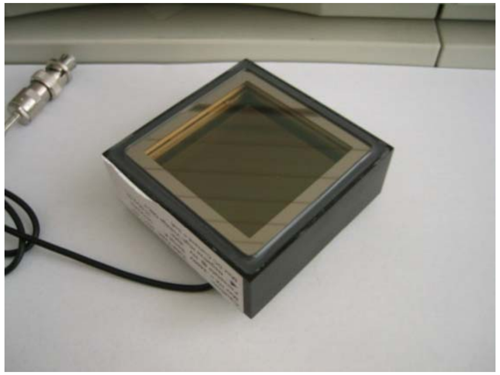

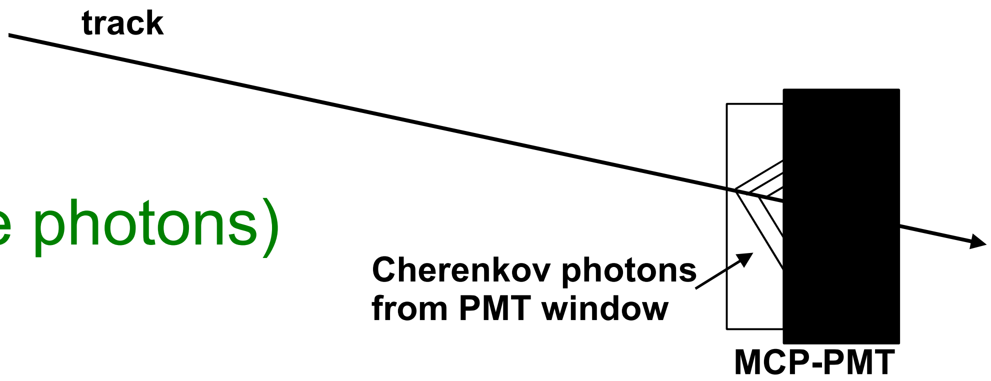

→ very fast (σ=40ps for single photons)

TOF capability: window photons

Expected number of detected Cherenkov photons emitted in the PMT window (2mm) is ~15

→ Expected resolution ~35 ps

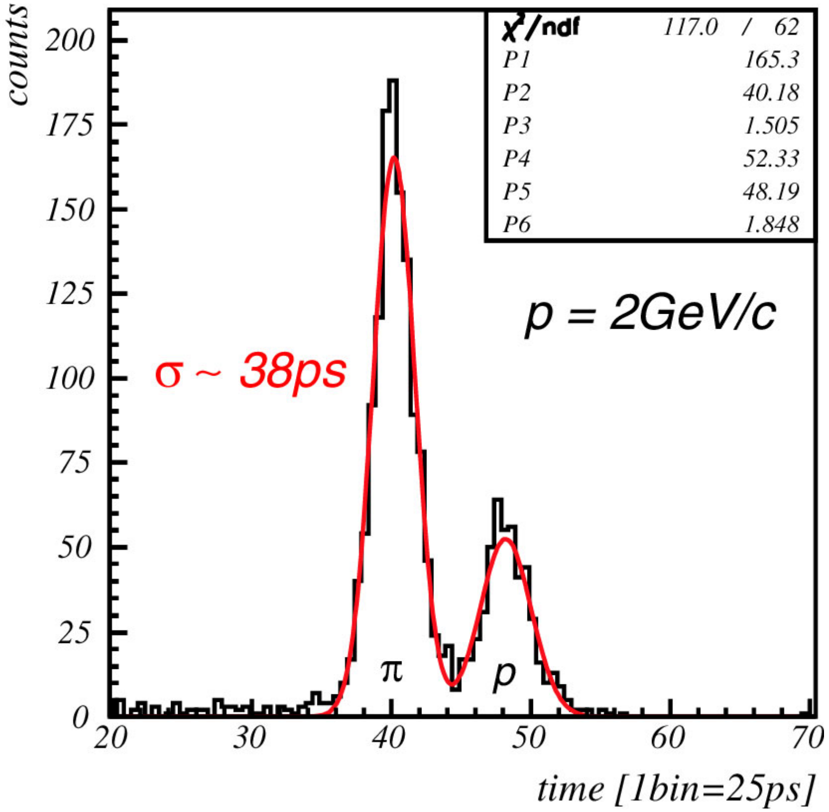

TOF test with pions and protons at 2 GeV/c.

Distance between start counter and MCP-PMT is 65cm

→ In the real detector ~2m

→ 3x better separation

Read out: time walk with a leading edge discriminator

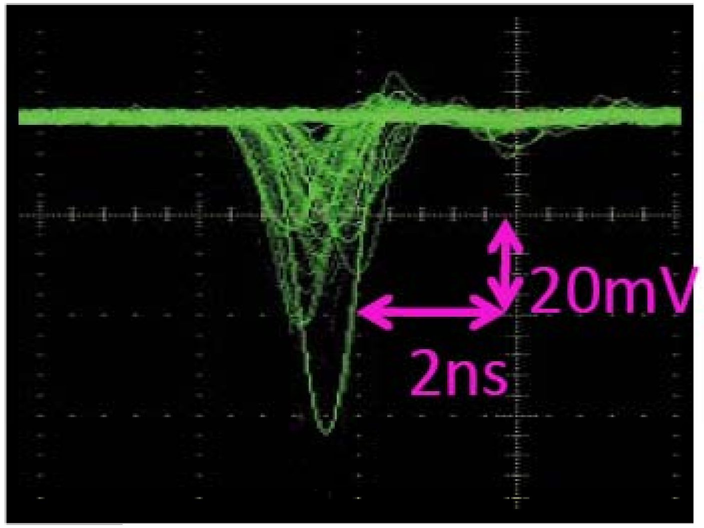

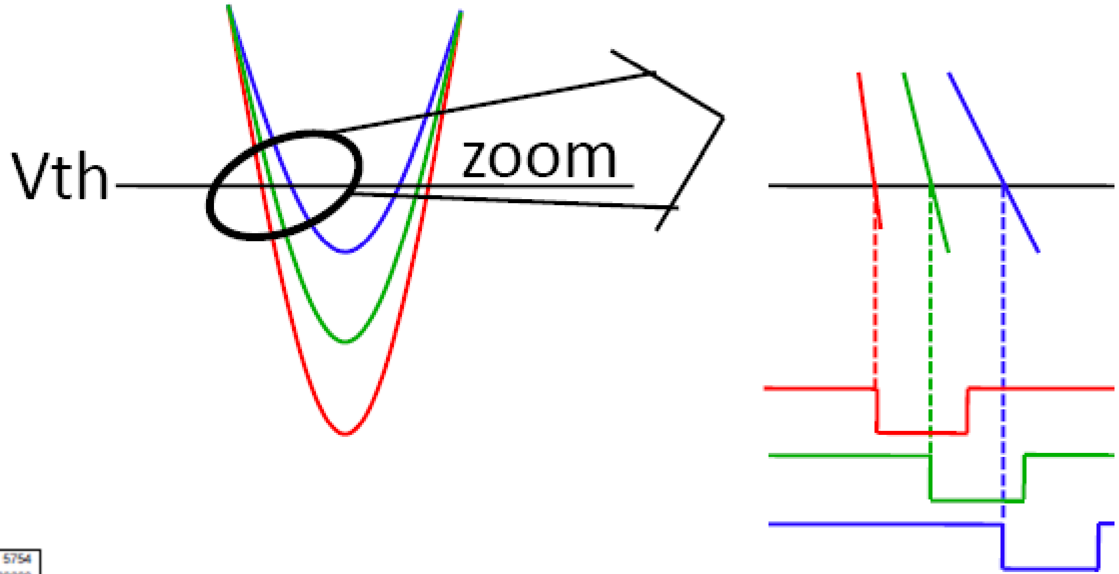

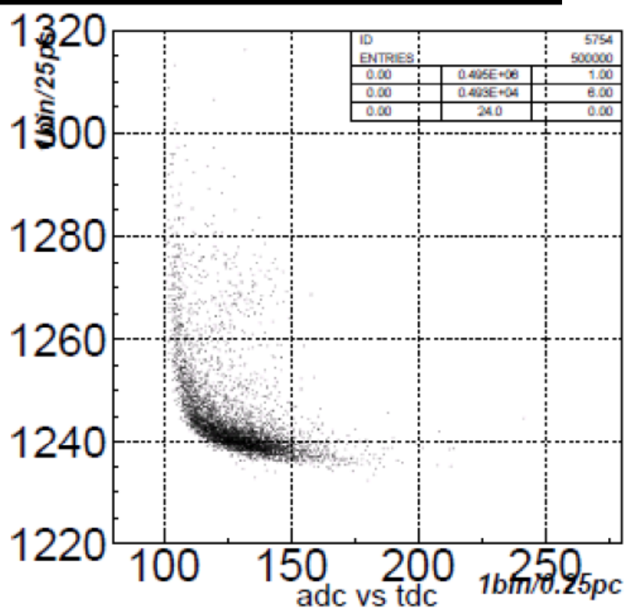

Variation of time determined with a leading edge discriminator: smaller pulses give a delayed signal

→ Has to be corrected!

Time walk correction 1

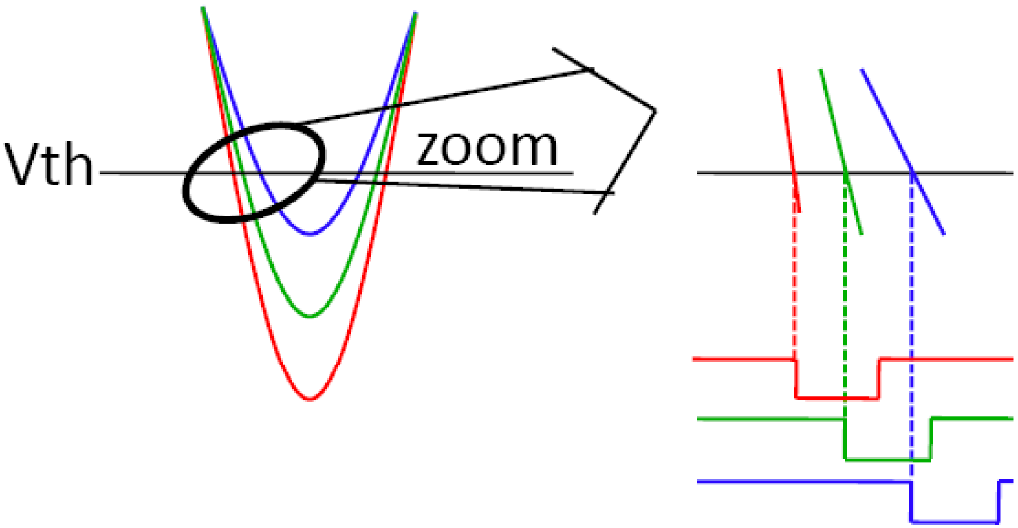

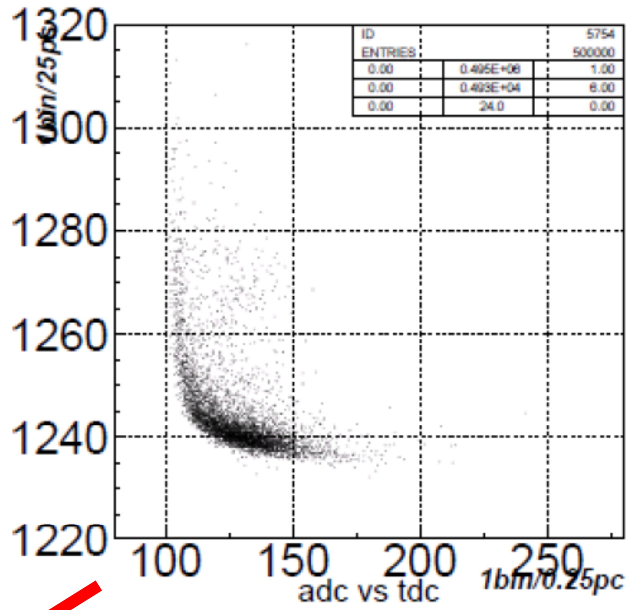

One possibility: measure both time (TDC) and amplitude (ADC)

→ Correct time of arrival by using a ΔT(ADC) correction

Time walk correction

TDC vs. ADC correlation is fitted with

$$TDC = P1 + \sqrt{\frac{P2}{ADC - P3}}$$

and used for TDC correction

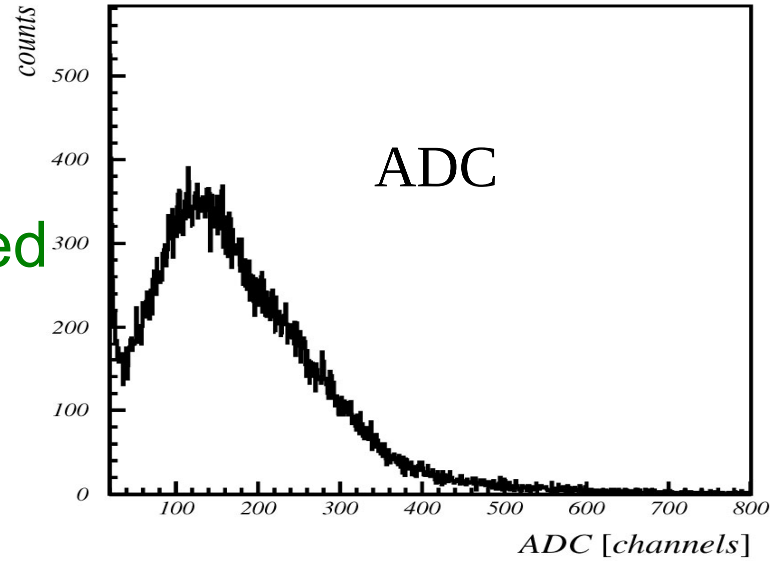

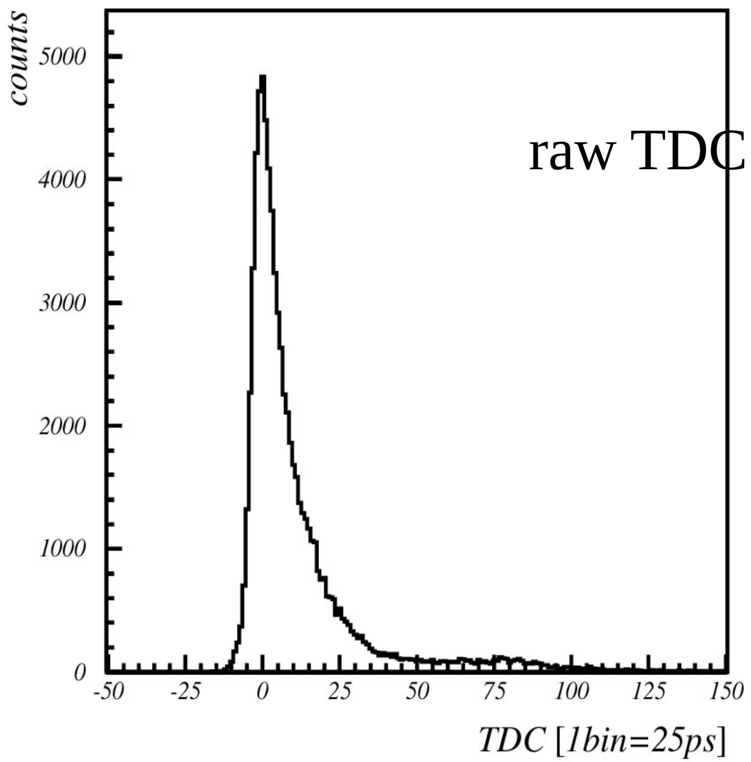

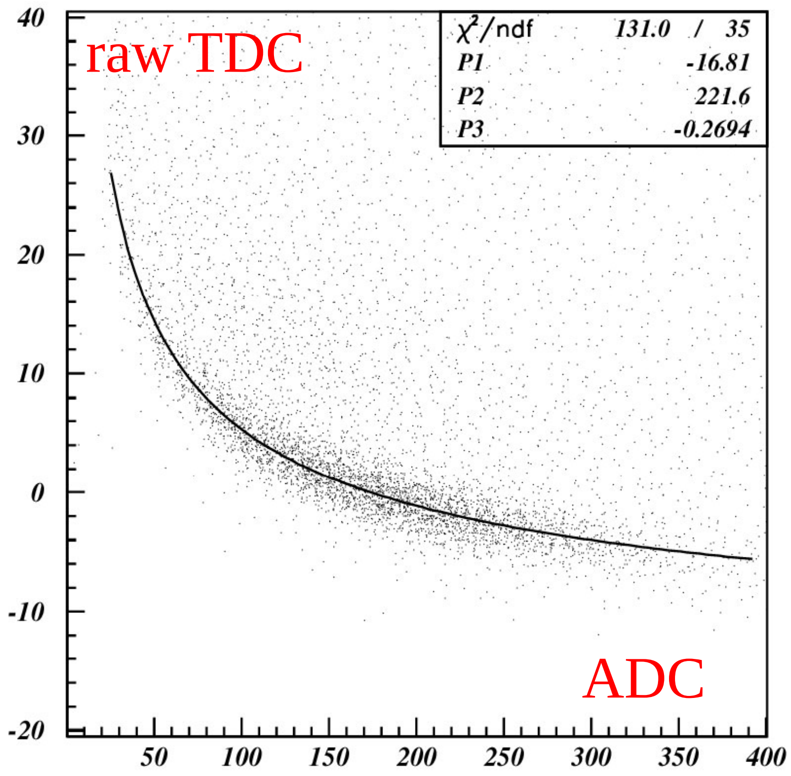

Corrected TDC

Corrected TDC distributions for all pads

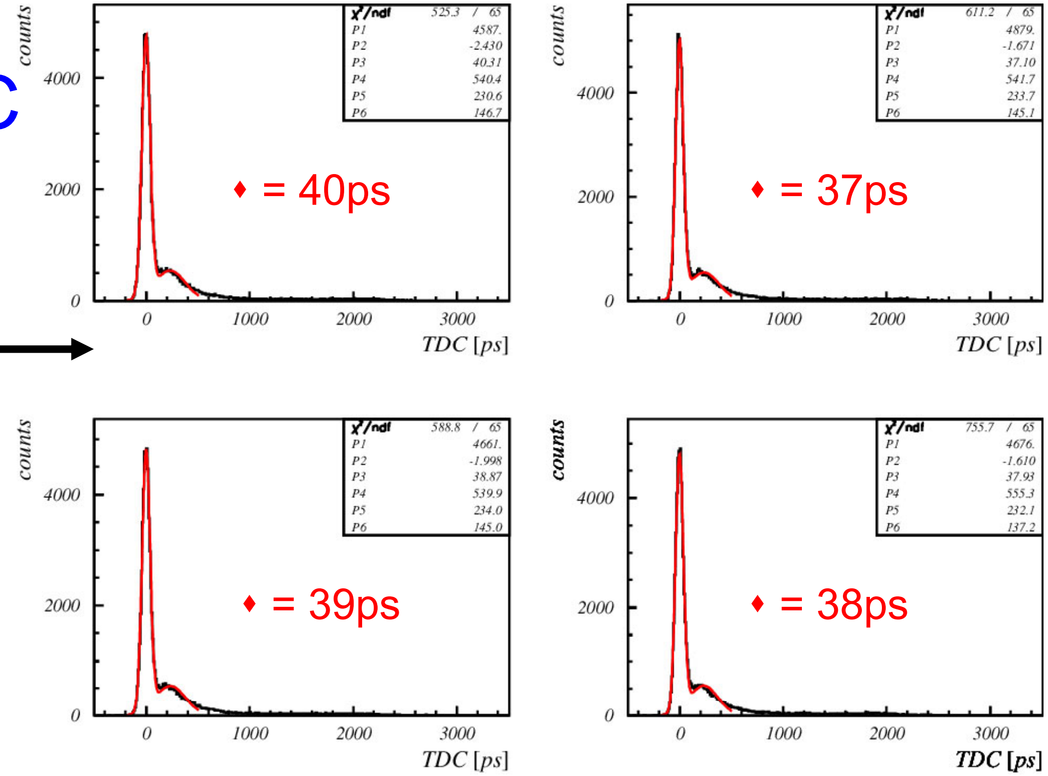

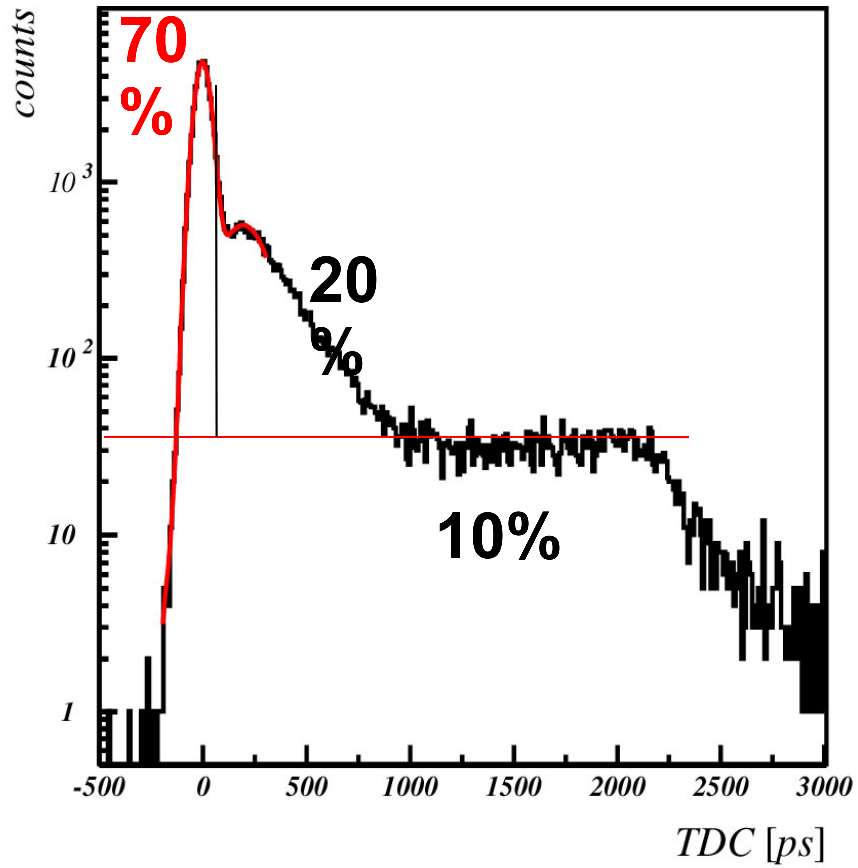

Response:

- prompt signal ~ 70%
- short delay ~ 20%
- ~ 10% uniform distribution

Photon electron detection: modeling

Parameters used:

- $U = 200$ V
- $l = 6$ mm
- $E_0 = 1$ eV
- $m_e = 511$ keV/c^2
- $e_0 = 1.6\ 10^{-19}$ As

Photo-electron:

- $d_{0,max} \sim 0.8$ mm
- $t_0 \sim 1.4$ ns
- $\Delta t_0 \sim 100$ ps

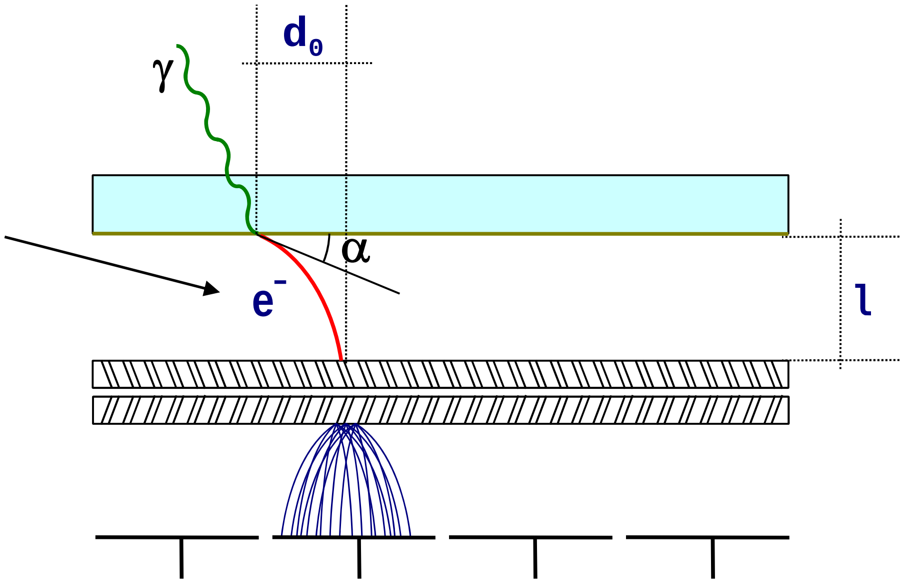

Backscattering:

- $d_{1,max} \sim 12$ mm
- $t_{1,max} \sim 2.8$ ns

Charge sharing

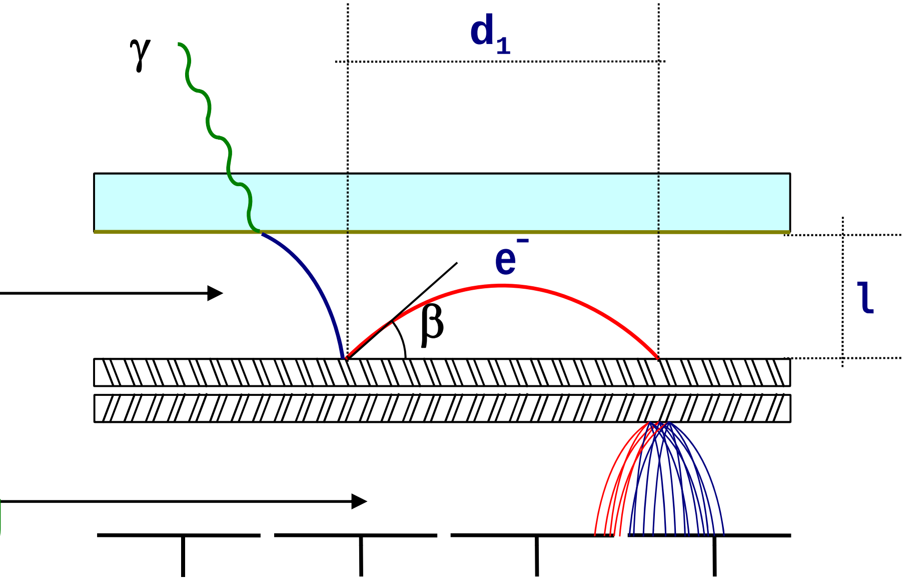

Photo-electron: simple estimates

$$t_0 \approx l\sqrt{\frac{2m_e}{Ue_0}}$$

$$d_0 \approx 2l\sqrt{\frac{E_0}{Ue_0}}\cos\alpha$$

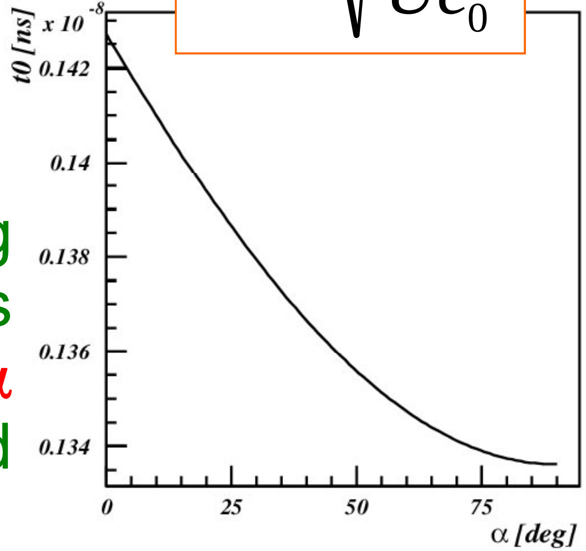

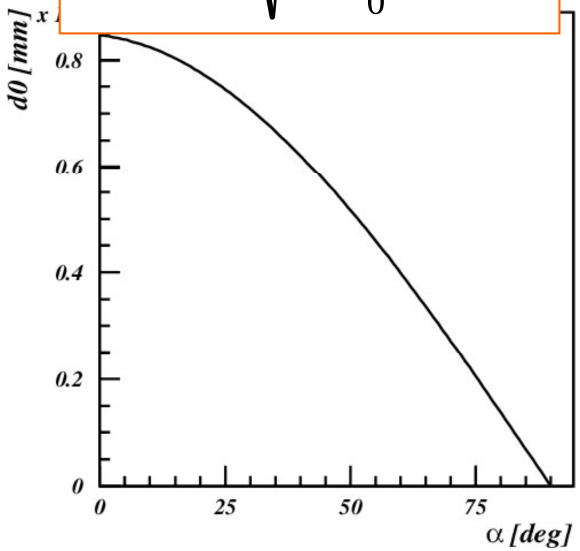

Distributions assuming that photo-electron is emitted at angle α uniformly over the solid angle

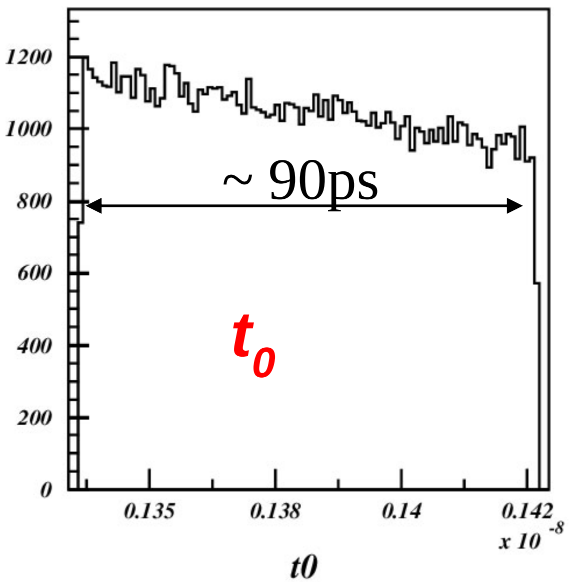

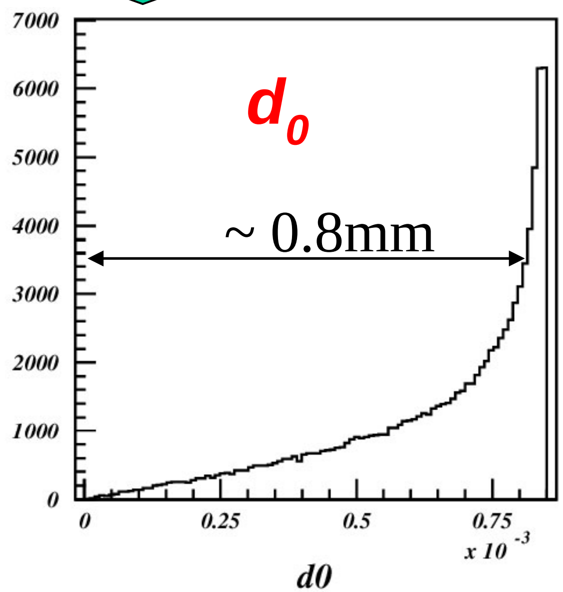

Maximum variation of photo-electron travel time.

$$\Delta t_0 \approx t_0\sqrt{\frac{E_0}{Ue_0}} \approx \frac{l}{Ue_0}\sqrt{2m_eE_0}$$

Elastic back-scattering

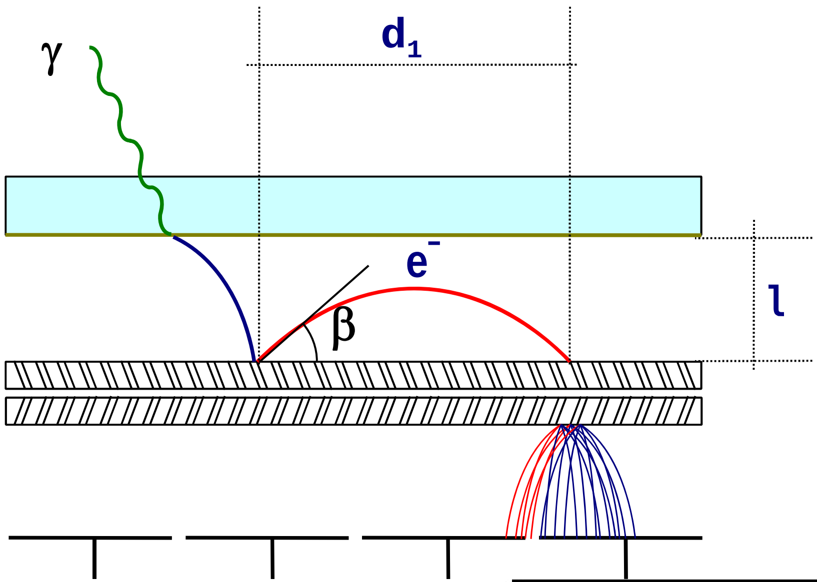

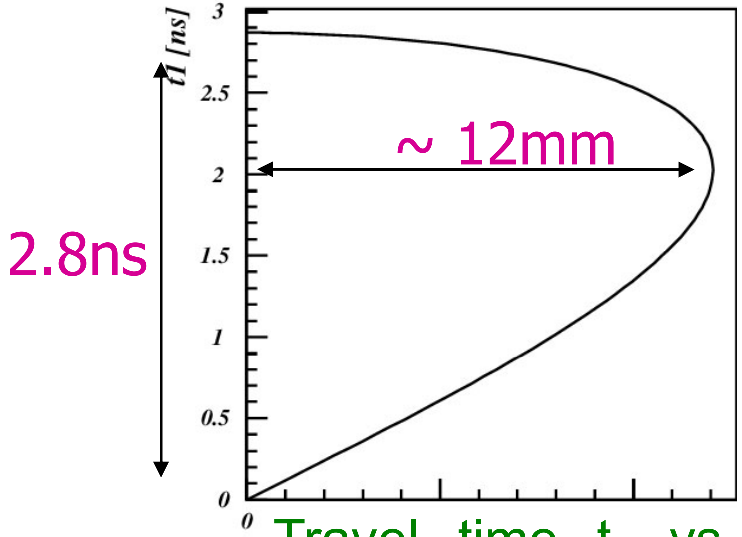

Travel time t_1 vs. travel distance d_1

Distributions assuming that back-scattering by angle β is uniform over the solid angle

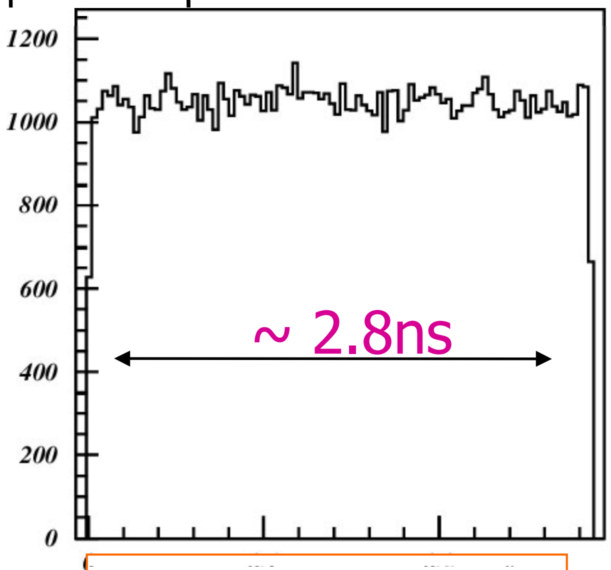

$$t_1 \approx 2t_0 \sin \beta$$

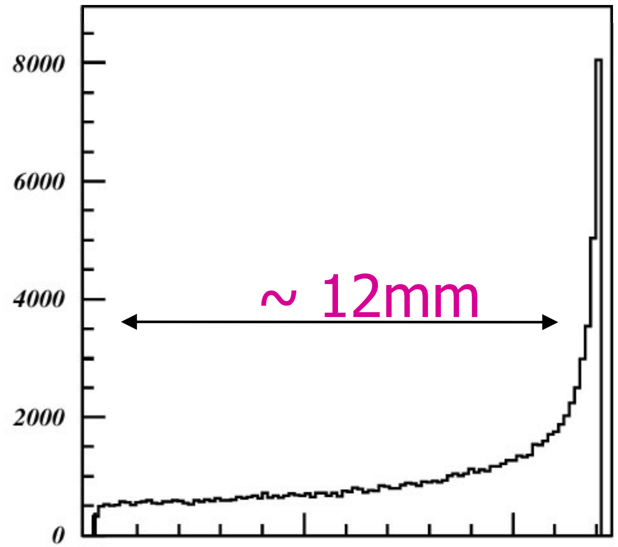

$$d_1 \approx 2l \sin 2\beta$$

Understanding time-of-arrival distribution

Normal photo-electrons

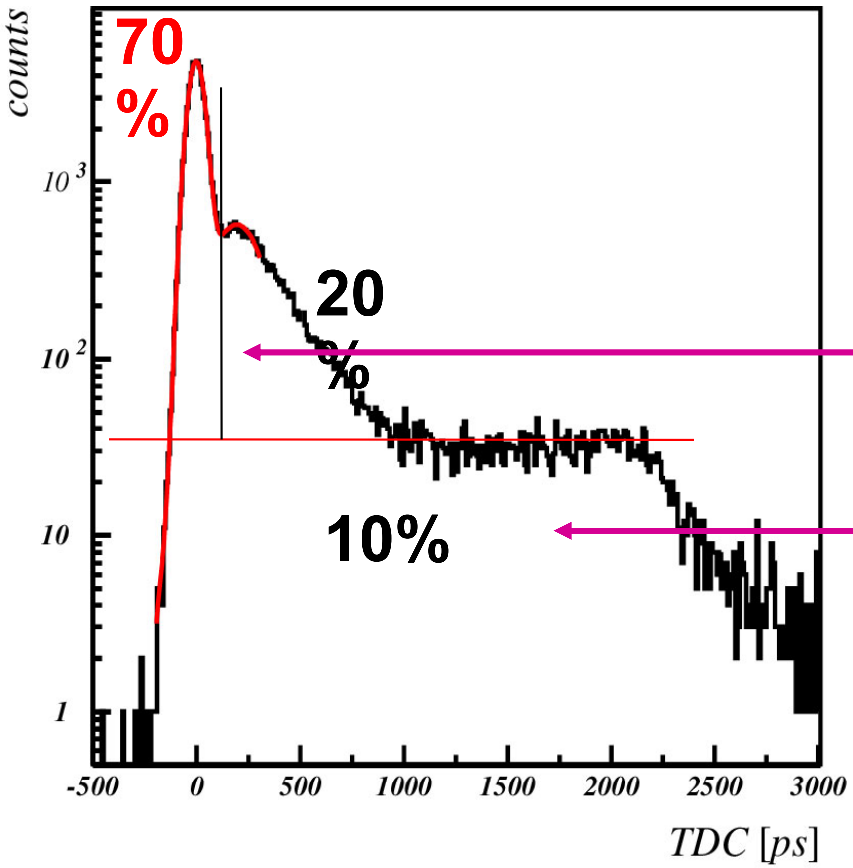

Inelastically scattered photo-electrons?

Elastically scattered photo-electrons

Time walk correction 2: constant fraction discriminator

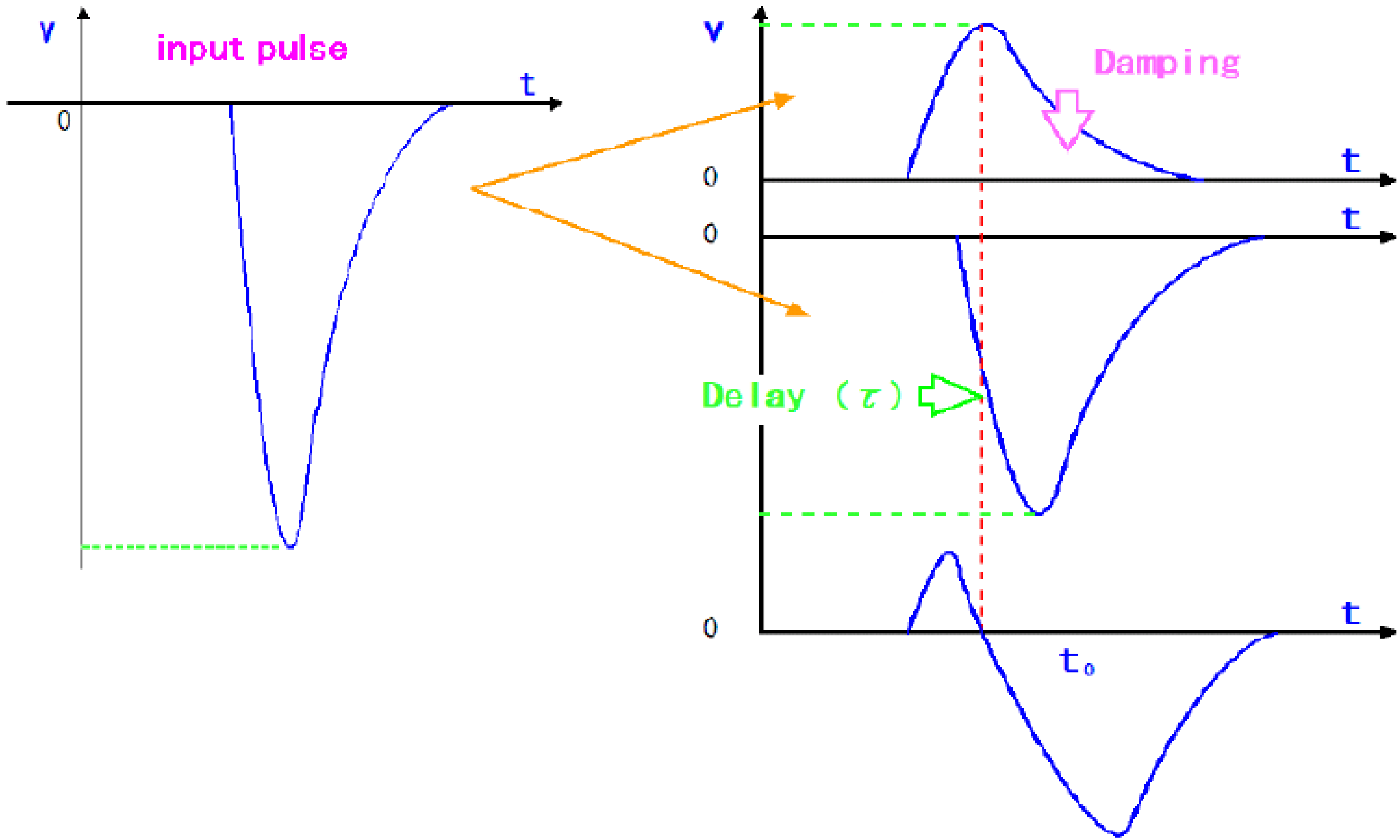

Basics:
dE/dx,
Čerenkov,
Trans. Rad.

Charged particle of mass m and velocity $\vec{\beta}c$ interacts electromagnetically with detector medium via a photon of energy $\hbar\omega$ and momentum $\hbar\vec{k}$

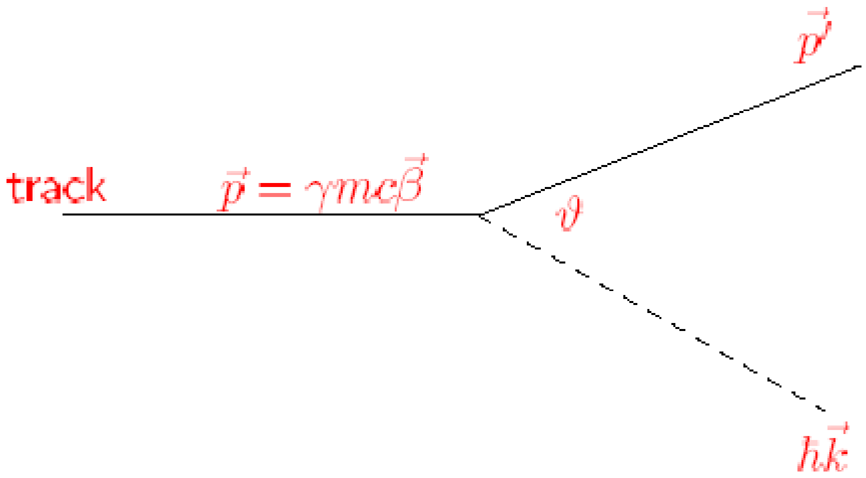

Conservation of energy and momentum gives

$\hbar\omega(1 - \frac{\hbar\omega}{2\gamma mc^2}) = \hbar\vec{k}\cdot\vec{\beta}c - \frac{\hbar^2 k^2}{2\gamma m}$

typically $\hbar\omega << \gamma mc^2$ and $\hbar k << \gamma mc \rightarrow$

$$\omega = \vec{k}\cdot\vec{\beta}c = \beta ck\cos\vartheta. \quad (1)$$

Basics: dE/dx, Čerenkov, Trans. Rad - 2

The photon also has to satisfy the dispersion relation for a given medium with a dielectric constant ϵ

$$\omega^2 - \frac{k^2c^2}{\epsilon} = 0 \tag{2}$$

From (1) and (2) we get

$$\sqrt{\epsilon}\beta\cos\vartheta = 1$$

which has a solution with a real value of ϑ if

$$\sqrt{\epsilon}\beta = n\beta > 1. \tag{3}$$

In this case **real** (Čerenkov) photons are emitted, and the emission angle is called Čerenkov angle ϑ_c.

N.B. In discontinuous media diffraction causes real photon emission even if (3) is not fulfilled (transition radiation).

Cross-section for emission (see Appendix for details)

$$\begin{aligned}
\frac{d\sigma}{d(\hbar\omega)} &= \frac{\alpha}{\beta^2\pi}\frac{\sigma_\gamma(\hbar\omega)}{\hbar\omega Z}\log\left[(1-\beta^2\epsilon_1)^2+\beta^4\epsilon_2^2\right]^{-\frac{1}{2}} \\
&+ \frac{\alpha}{\beta^2\pi}\frac{\sigma_\gamma(\hbar\omega)}{\hbar\omega Z}\log\left[\frac{2mc^2\beta^2}{\hbar\omega}\right] && \text{(ionis., excit.} \rightarrow \text{dE/dx)} \\
&+ \frac{\alpha}{\beta^2\pi}\frac{1}{n_e\hbar c}\left[\beta^2-\frac{\epsilon_1}{|\epsilon|^2}\right]\Theta && \text{(Čerenkov, TRD)} \\
&+ \frac{\alpha}{\beta^2\pi}\frac{1}{(\hbar\omega)^2}\int_0^{\hbar\omega}\frac{\sigma_\gamma(\hbar\omega')}{Z}d(\hbar\omega') && (\delta\text{ electrons})
\end{aligned}$$

Basics: dE/dx, Čerenkov, Trans. Rad – 3

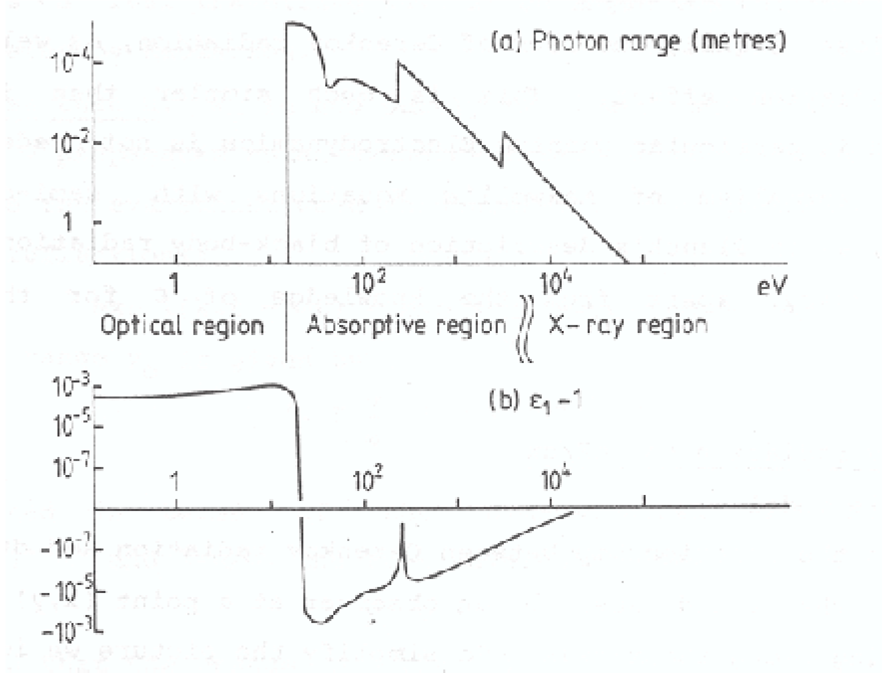

Three frequency ranges: ε_1, ε_2 vs frequency

1) Optical region: ε real and >1. The medium is transparent. and Čerenkov radiation is emitted by particles with velocity above the threshold.
2) Absorptive region: ε complex. Imaginary part makes the range of photons short.
3) X-ray region: ε nearly real and <1. Čerenkov threshold is greater than c, but sub-threshold Čerenkov radiation can be emitted at discontinuities in the medium --> X-ray Transition Radiation.

Identification with dE/dx measurement 1

dE/dx is a function of velocity. For particles with different mass the Bethe-Bloch curve gets displaced → separation is possible if the resolution is good enough

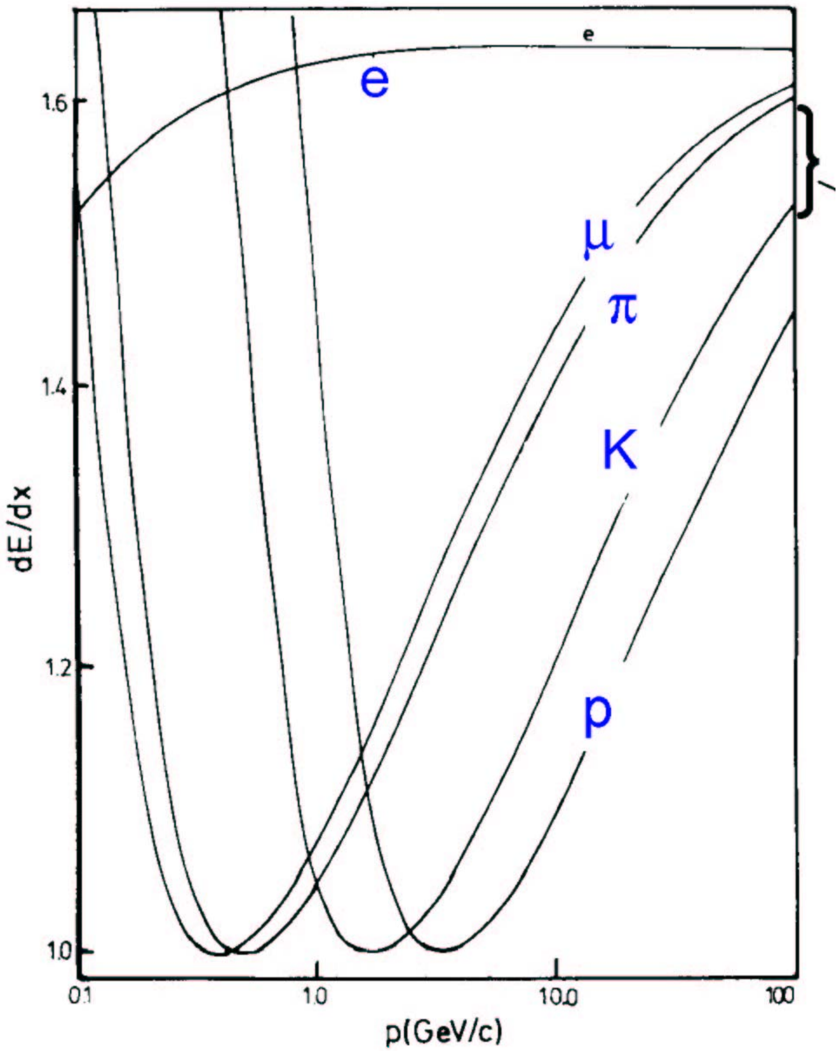

Identification with dE/dx measurement 2

Problem: long tails (Landau distribution, not Gaussian)

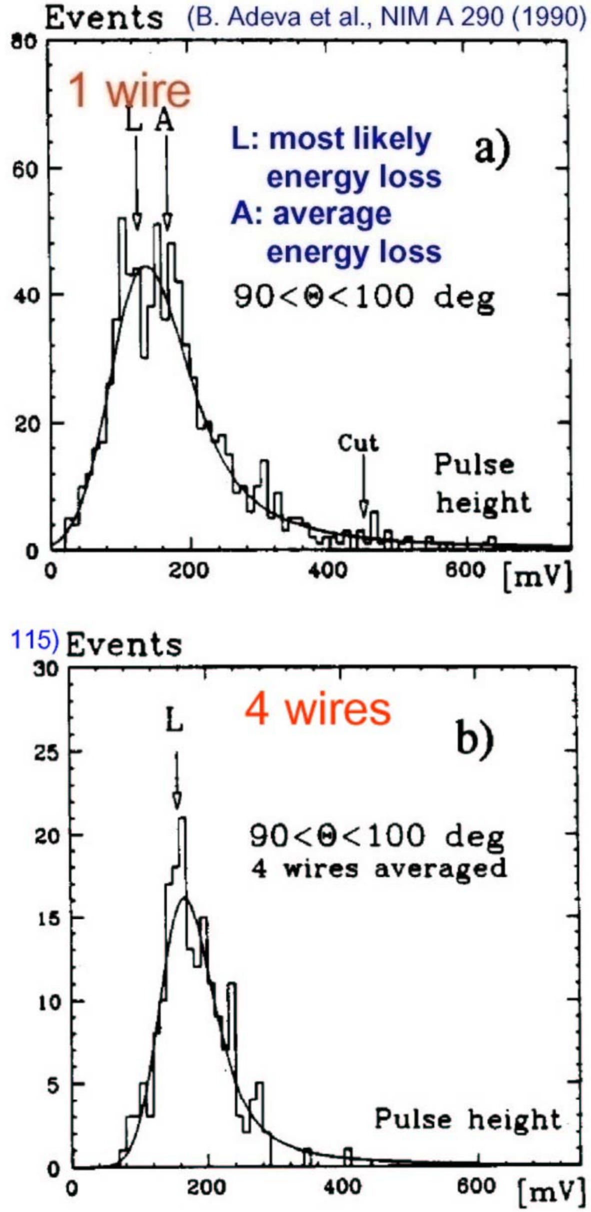

Identification with dE/dx measurement 3

Optimisation of the counter: length L, number of samples N, resolution (FWHM)

If the distribution of individual measurements were Gaussian, only the sample thickness would be relevant.

Tails: eliminate the largest 30% values → the optimumm depends also on the number of samples.

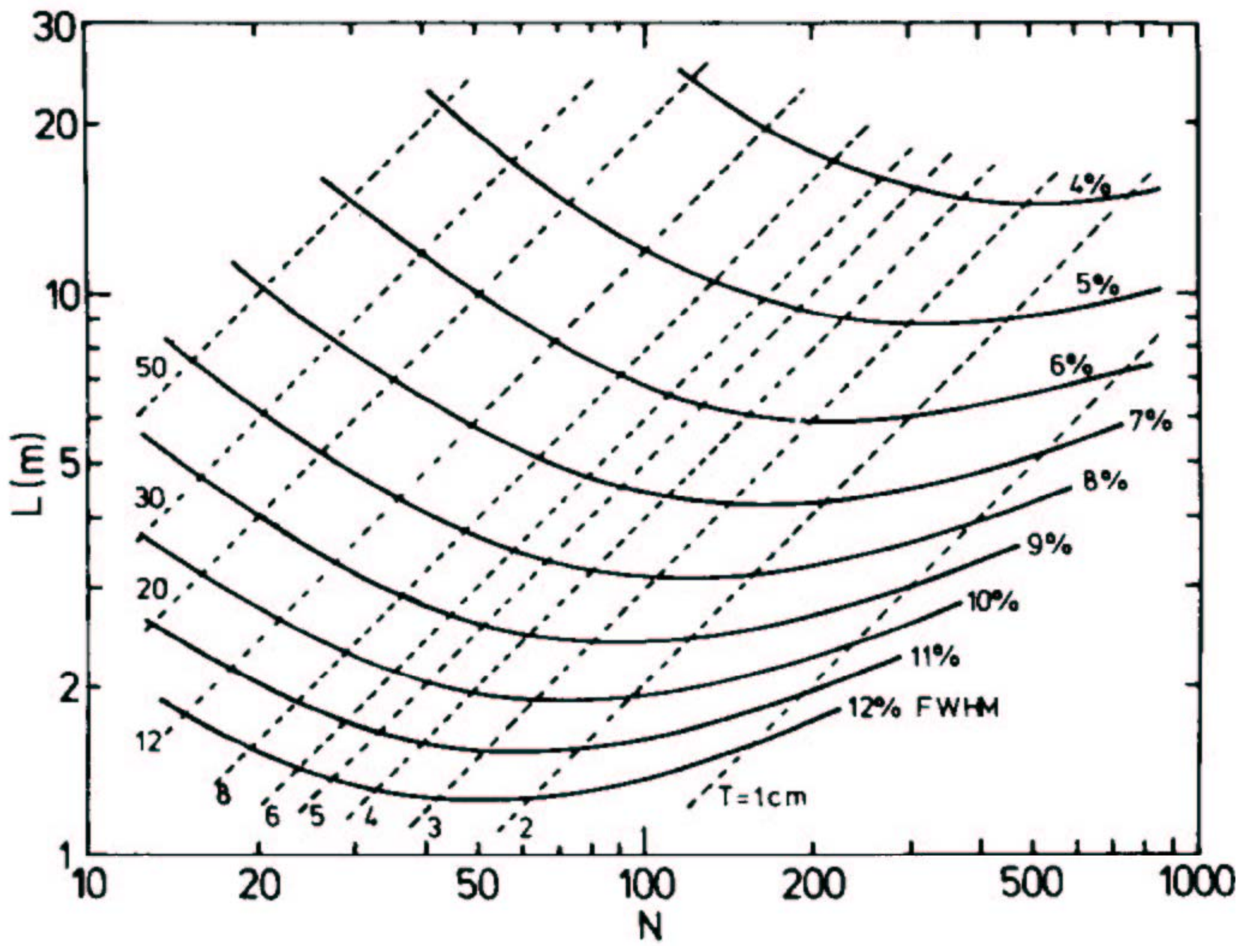

Identification with dE/dx measurement 4

Example of a dE/dx performance
in a large drift chamber.

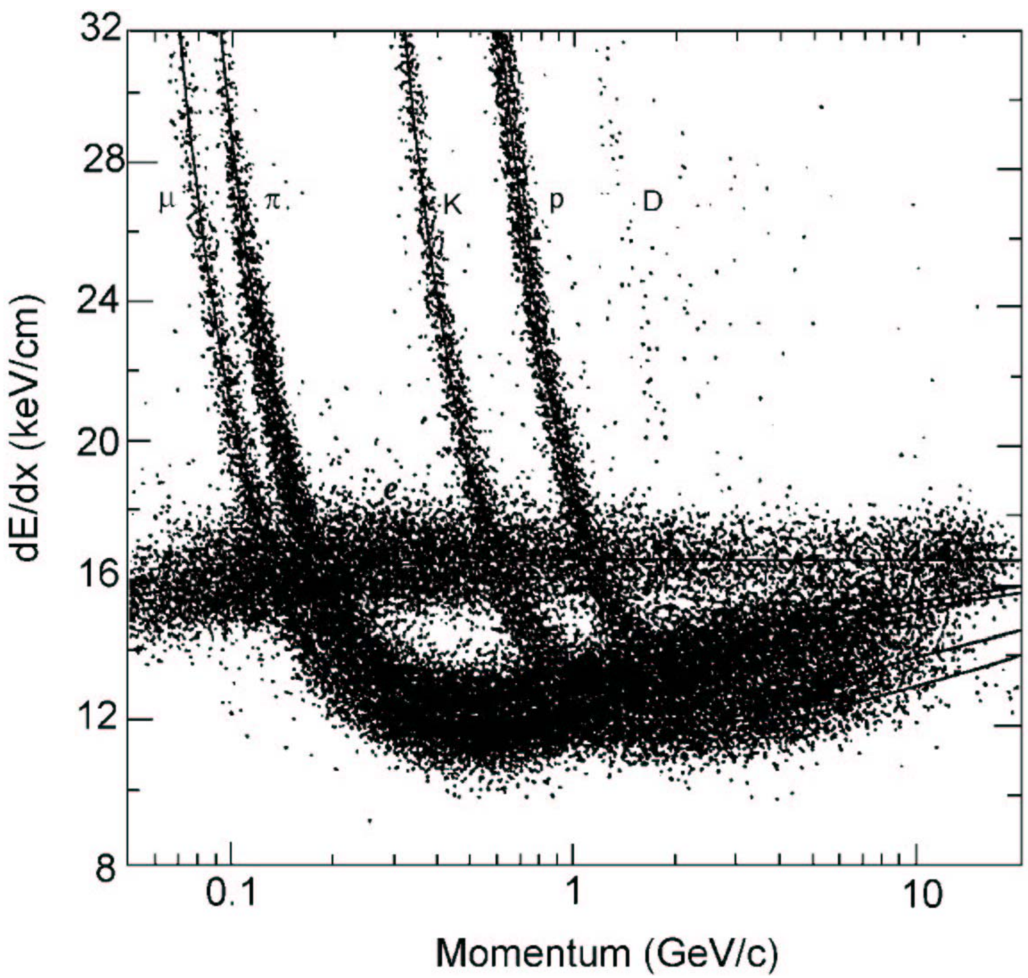

Identification with dE/dx measurement 5

dE/dx performance in the huge STAR TPC

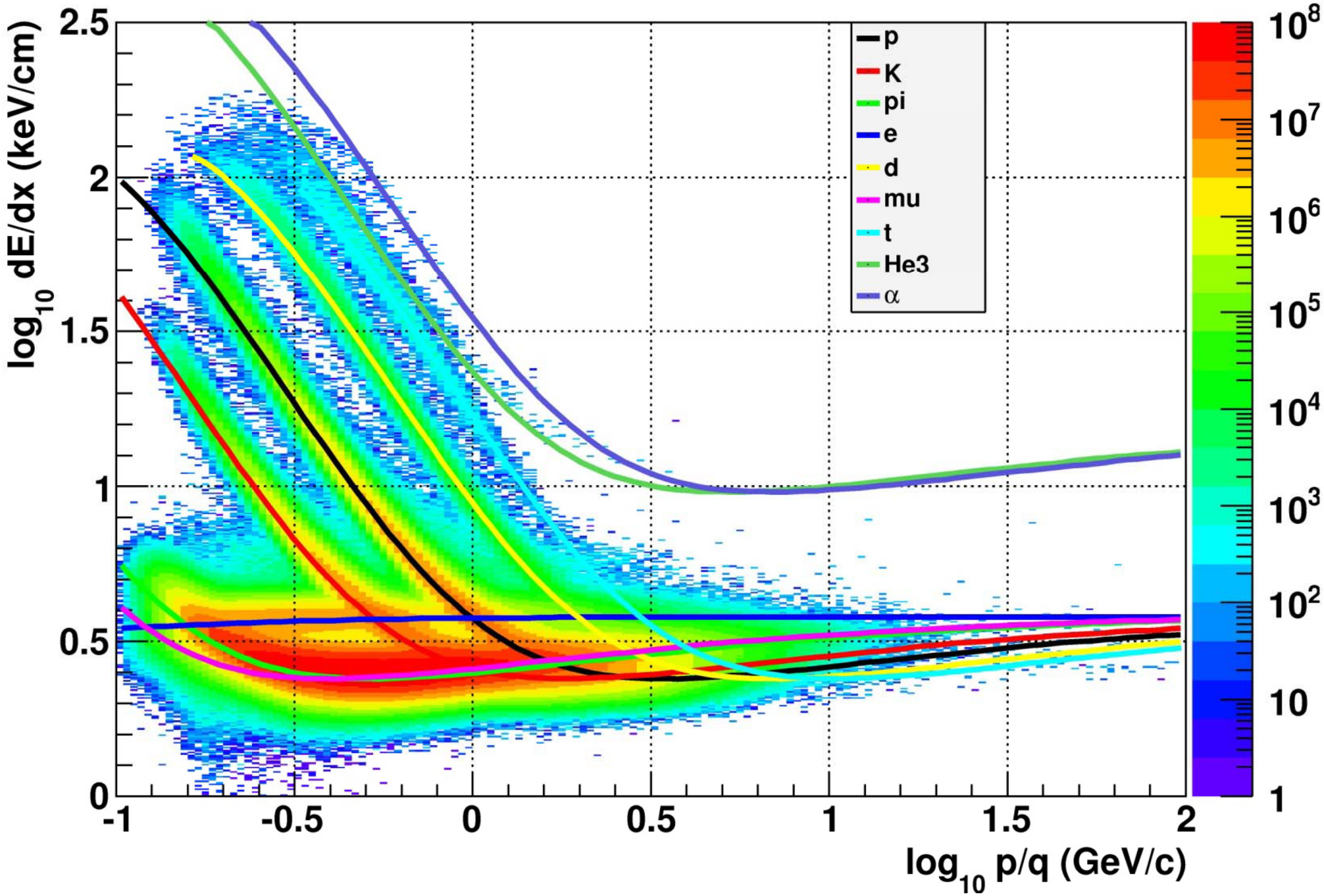

Čerenkov radiation

A charged track with velocity v=βc above the speed of light c/n in a medium with index of refraction n= √ε emits polarized light at a characteristic (Čerenkov) angle,

cosθ = c / nv = 1/βn

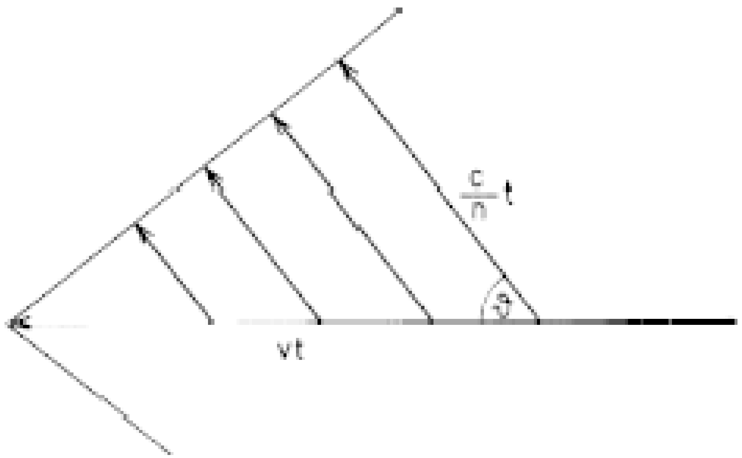

Two cases:

1) β < β_t = 1/n: below threshold no Čerenkov light is emitted.

2) β > β_t : the number of Čerenkov photons emitted over unit photon energy E=hν in a radiator of length L amounts to

$$\boxed{\frac{dN}{dE} = \frac{\alpha}{\hbar c} L \sin^2\theta = 370(cm)^{-1}(eV)^{-1} L \sin^2\theta}$$

Number of detected photons

Example: in 1m of air (n=1.00027) a track with β=1 emits N=41 photons in the spectral range of visible light (ΔE ~ 2 eV).

If Čerenkov photons were detected with an average detection efficiency of ε=0.1 over this interval, N=4 photons would be measured.

In general: number of detected photons can be parametrized as

$N = N_0 L \sin^2\theta$

where N_0 is the figure of merit, $$N_0 = \frac{\alpha}{\hbar c}\int Q(E)T(E)R(E)dE$$

and Q T R is the product of photon detection efficiency, transmission of the radiator and windows and reflectivity of mirrors employed.

Typically: N_0 = 50 - 100/cm

Rewrite the basic relations:

- the threshold Lorenz factor $\gamma_t = (1 - 1/n^2)^{-1/2}$
- the asymptotic value of Čerenkov angle (for $\beta = 1$)
  $\sin^2\theta_{max} = \frac{1}{\gamma_t}$
- the asymptotic number of Čerenkov photons:
  $N_{max} = \frac{N_0 L}{\gamma_t^2}$
- number of photons, non-asymptotic case:
  $\frac{N}{N_{max}} = 1 - \frac{(\beta_t\gamma_t)^2}{(\beta\gamma)^2}$
- Čerenkov angle, non-asymptotic case:
  $\frac{\sin\theta^2}{\sin\theta_{max}{}^2} = \sqrt{1 - \frac{(\beta_t\gamma_t)^2}{(\beta\gamma)^2}}$

The basic relations are functions of the ratio $\frac{\beta\gamma}{\beta_t\gamma_t} = \frac{p}{p_t}$

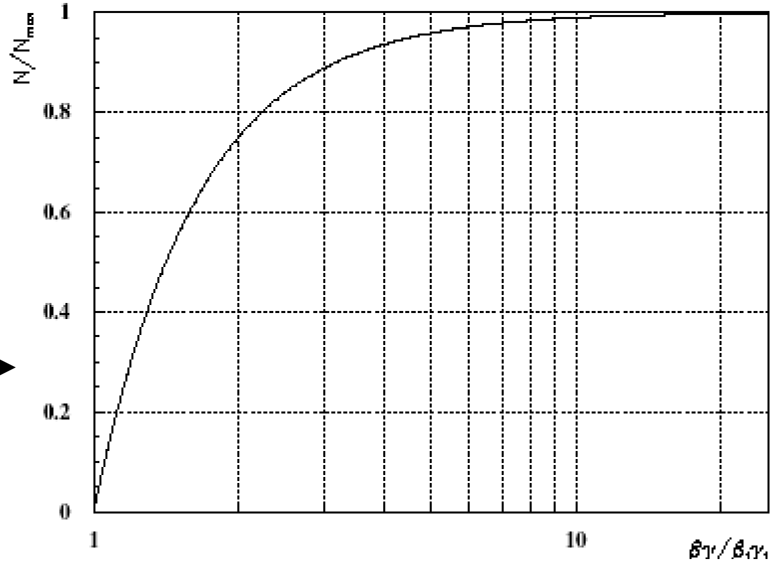

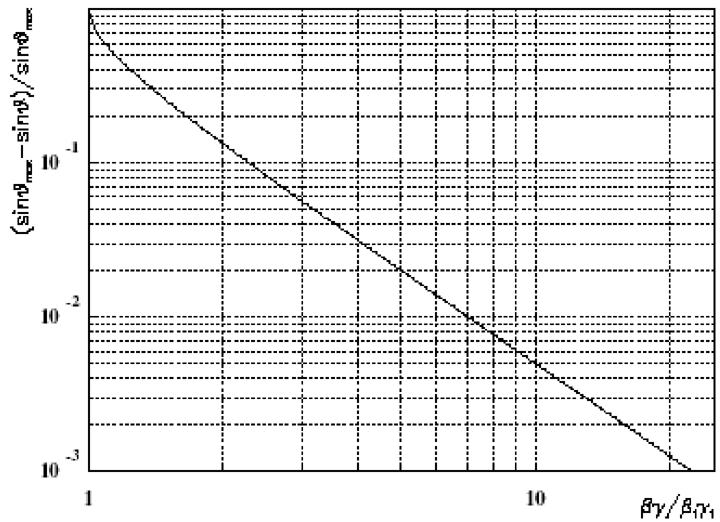

Types of Čerenkov counters

Threshold counters --> count photons to separate particles below and above threshold

Ring Imaging (RICH) --> measure Čerenkov angle and count photons

Short historical excursion

- 1934 Čerenkov characterizes the radiation
- 1938 Frank, Tamm give the theoretical explanation
- 50-ties - 70-ties Čerenkov counters are developed and are being used in nuclear and particle physics experiments, as differential and threshold counters
- 1958: Nobel prize for Čerenkov
- 1977 Ypsilantis, Seguinot introduce the idea of a RICH counter with a large area wire chamber based photon detector
- 1981-83 first use of a RICH counter in a particle physics experiment (E605)
- 1992--> first results from the DELPHI RICH, SLD CRID, OMEGA RICH

Threshold Čerenkov counters

- Beam veto counters
- Detection of sub-threshold particles in a RICH
- Aerogel Čerenkov counter in Belle: K (below) vs. π (above thr.) by properly choosing n for a given kinematic region

Threshold Čerenkov counter: Belle ACC (aerogel Cherenkov counter)

Aerogel Čerenkov counter Belle: K (below) vs. π (above thr.) by properly choosing n for a given kinematic region (more energetic particles fly in the 'forward region')

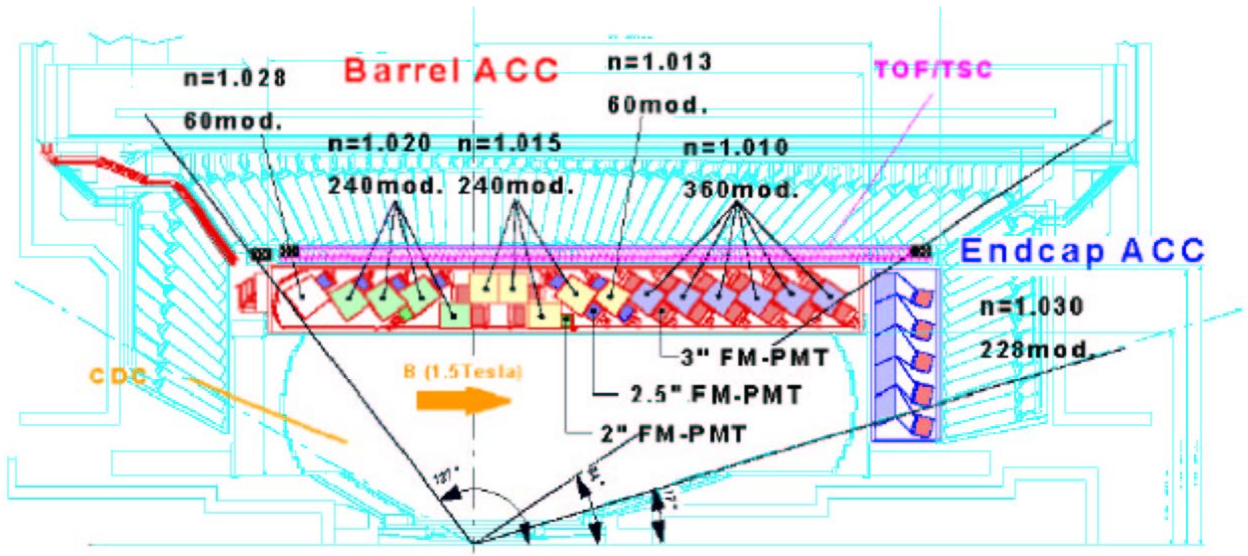

Detector unit: a block of aerogel and two

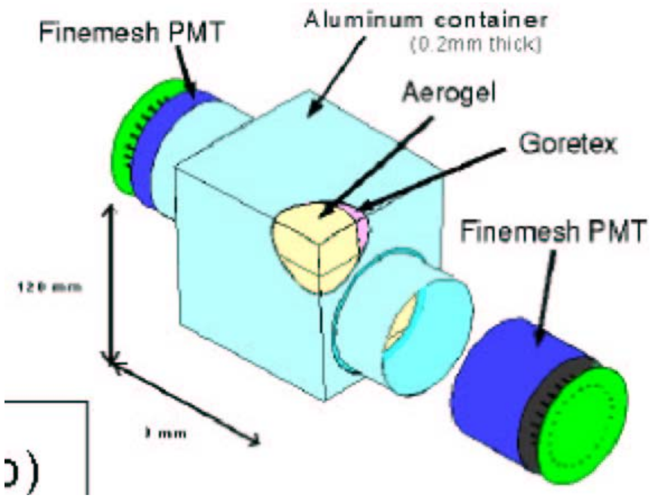

Fine-mesh PMT: works at high B fields

Threshold Čerenkov counter: Belle ACC (aerogel Cherenkov counter)

expected yield vs p

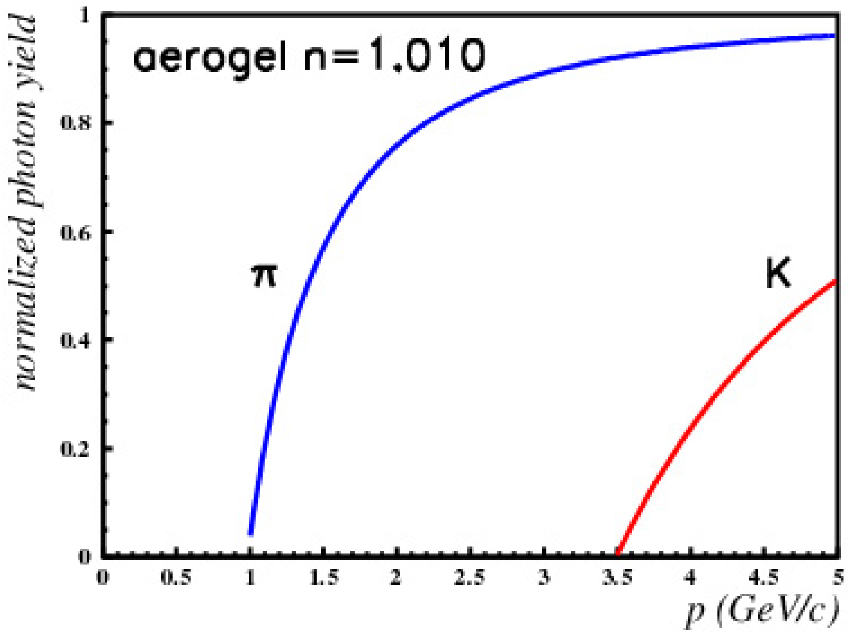

measured for 2 GeV < p < 3.5 GeV
expected and measured number of hits

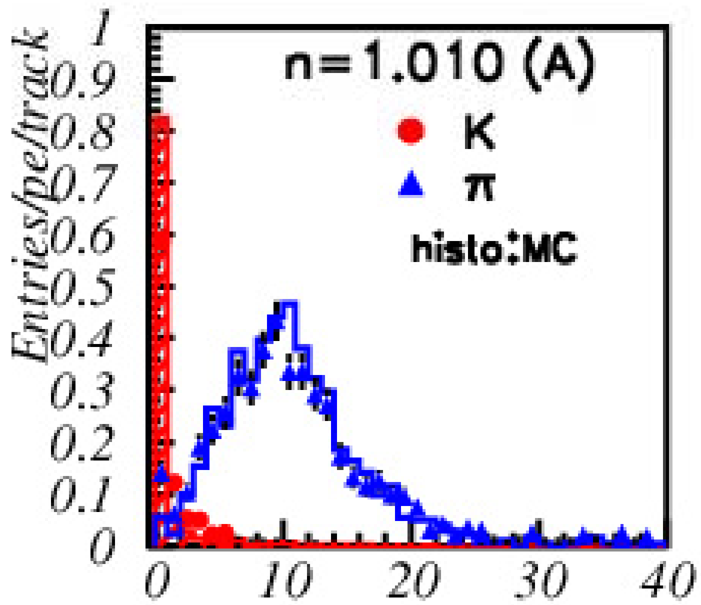

RICH counter

Aim: measure the direction of Čerenkov photons emitted by a charged track.

Idea: transform the direction into a coordinate.

Take a spherical mirror: parallel rays intersect on the focal surface. Since photons are emitted uniformly over the azimuthal angle around the track, a ring is formed on the focal plane. With a position sensitive photon detector in the focal plane we get a Ring Imaging Čerenkov counter (RICH).

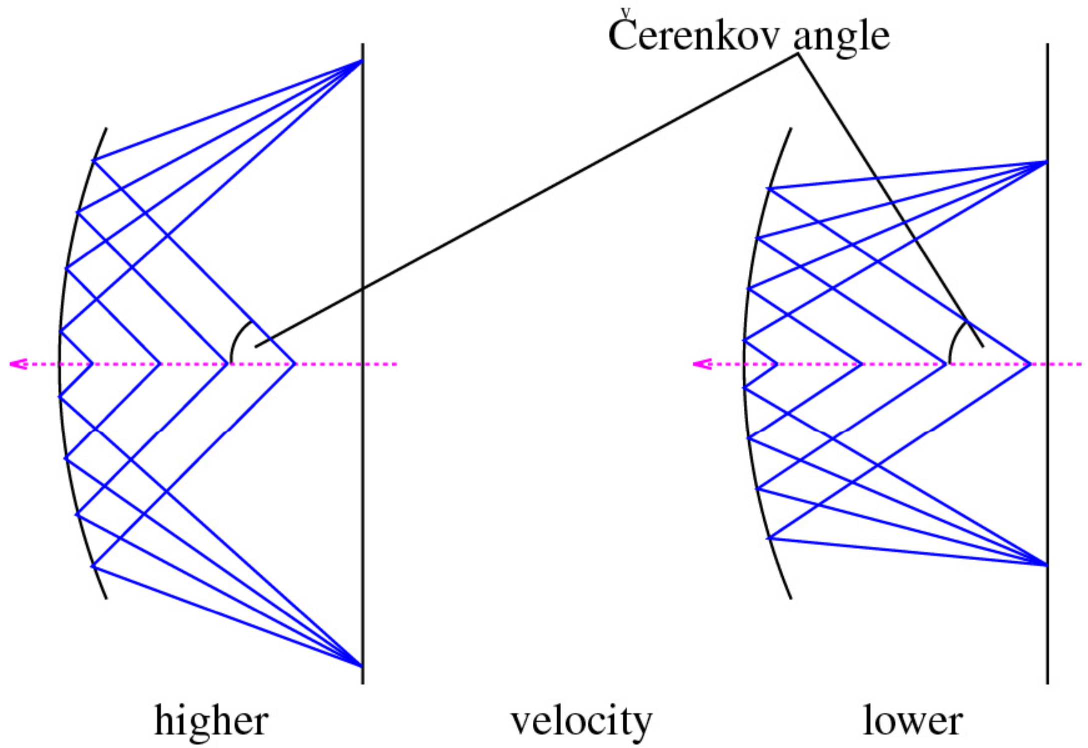

RICH counter 2

From the image on the photon detector, the Čerenkov angle of the track can be reconstructed, i.e. from the known track direction (ring center) and hit coordinate the angle is calculated and plotted

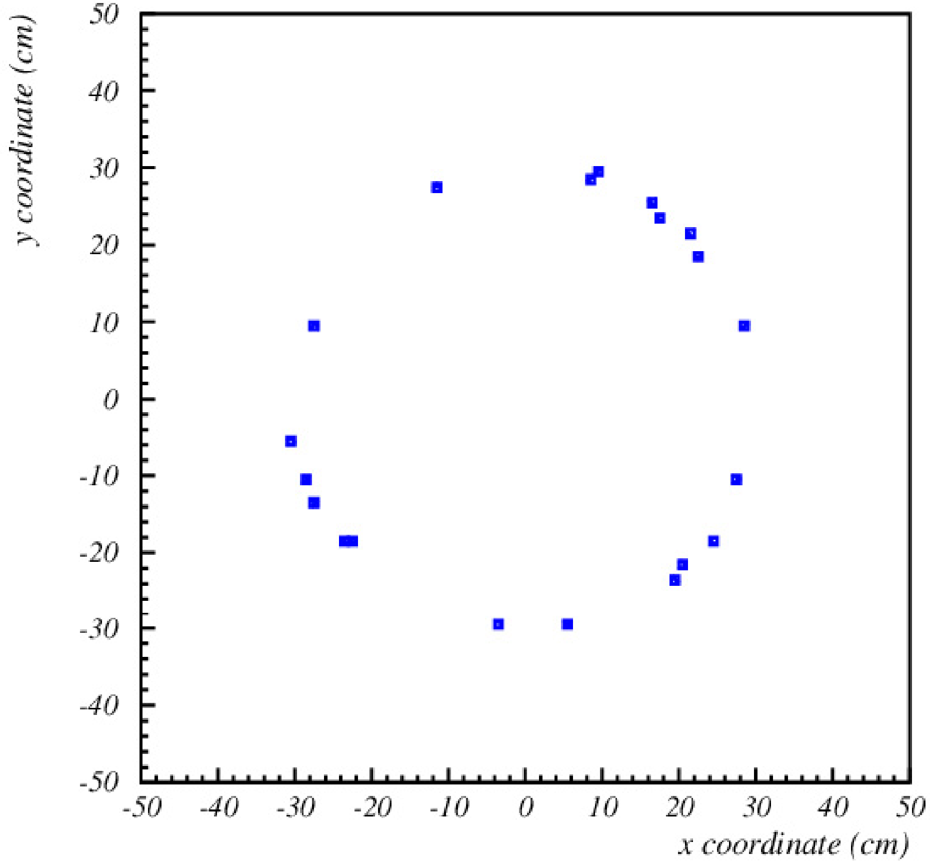

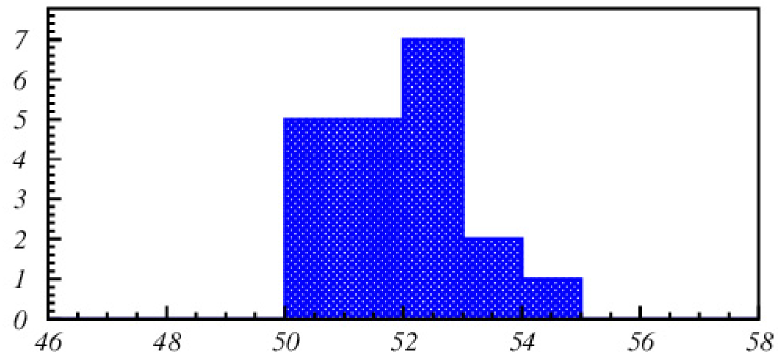

Cherekov angle distribution (mradian)

Analysis of RICH data

Rings are accompanied by noise hits and other rings

How to choose between the hypotheses e, μ, π, K, p?

1) Count photons within 2.5 σ of each hypothesis
2) Determine likelihood for each track and each hypothesis independently (extended maximum likelihood)
3) Global max. likelihood: maximize likelihood for all tracks in the event at teh same time
4) Iterative pattern analysis: associate each photon predominately with a single track
5) If only poor tracking information is available: look for rings in a stand-alone mode, use some form of Hough transform Essential:

->number of photons

->single photon resolution

Summary: need about 10 for isolated rings, more than 20 for high density cases.

Resolution of a RICH counter

- Photon impact point resolution (photon detector resolution
- Emission point uncertainty
- Dispersion: $n=n(\lambda)$ in $\cos\theta = 1/\beta n$
- Track parameters
- Errors of the optical system

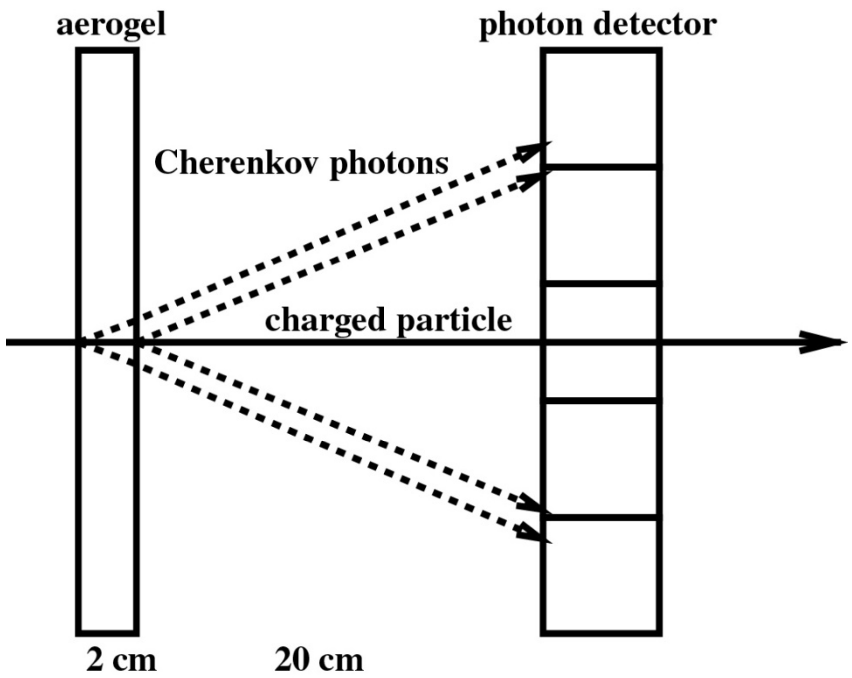

Resolution of a RICH counter

Sources of error in the Č. angle measurement

- finite coordinate resolution of the photon detector

$$\sigma_\theta = \frac{a}{f\sqrt{12}}$$

  for detector pad size a and mirror focal length f, e.g. $\sigma_\theta = 0.45$ mrad for $a = 9$ mm, $f = 5.75$ m.

- dispersion, variation of the refractive index $(\mathrm{d}n/\mathrm{d}E)$ over the energy range with RMS width σ_E of detected Čerenkov photons,

$$\sigma_\theta = \frac{1}{\beta n^2 \sin\theta} \frac{\mathrm{d}n}{\mathrm{d}E} \sigma_E$$

  solid radiators: $5-7$ mrad, liquids: $3-4$ mrad, gases: $0.1-0.5$ mrad (depends on the radiator and detector!).

- optical error due to the imperfections on the mirror surface and mirror misalignment, typically $\approx 0.1-0.2$ mrad

- finite precision in track slope parameters as determined by the tracking system

Resolution of a RICH counter

- spread in track slope parameters as caused by multiple scattering within the radiator
  $\sigma_\theta = \frac{1}{\sqrt{6}} 15\mathrm{MeV/c} \frac{\sqrt{L/X_0}}{\beta p}$
- spread in track slope parameters due to stray magnetic fields in the radiator
  $\sigma_\theta = \frac{1}{\sqrt{12}} \frac{B_\perp L}{p} \frac{0.3\mathrm{GeV/c}}{\mathrm{Tm}}$
- the optical error due to the finite angle of incidence of photons upon the spherical mirror (spherical aberration)

In a typical case the first two dominate since they are hardest to overcome.

The combined single photon error σ_1 is a quadratic sum of the contributions.

Assuming N detected photons, the overall resolution is

$$\sigma_N = \frac{\sigma_1}{\sqrt{N}}$$

for isolated tracks.

RICH Designs: mirror focused 1

Original mirror
focused set-up

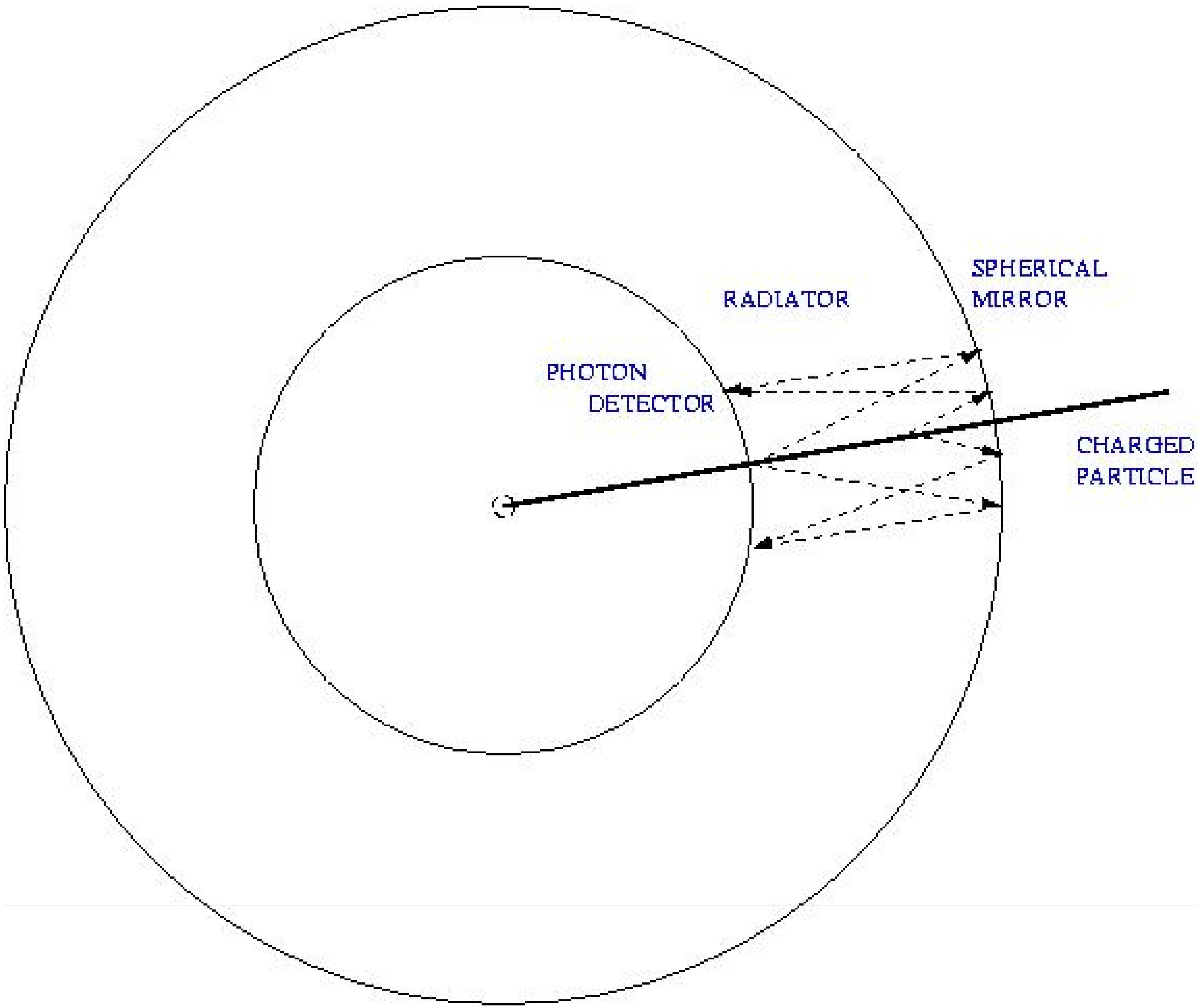

RICH Designs: mirror focused 2

OMEGA

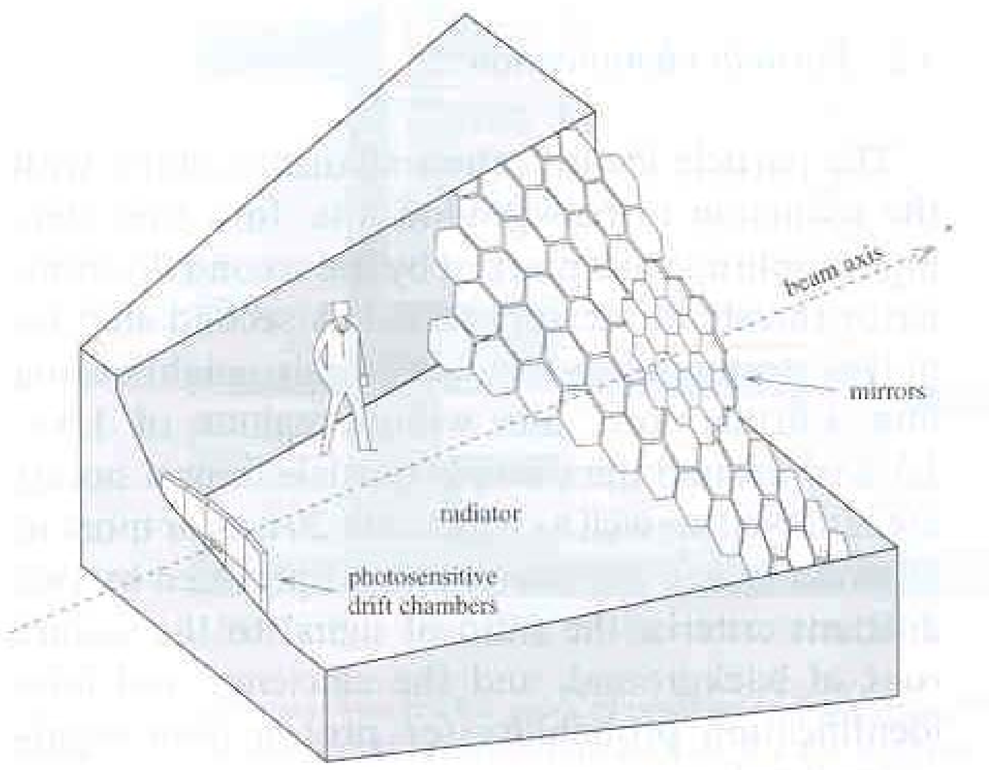

HADES

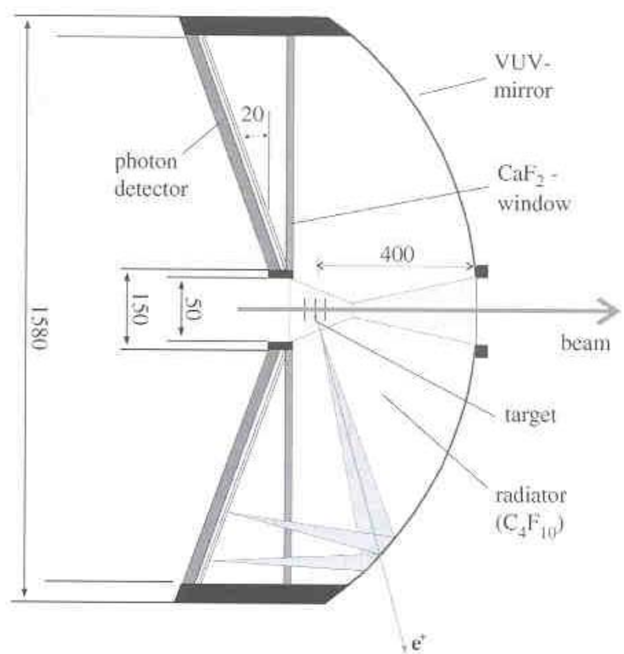

RICH Designs: HERA-B

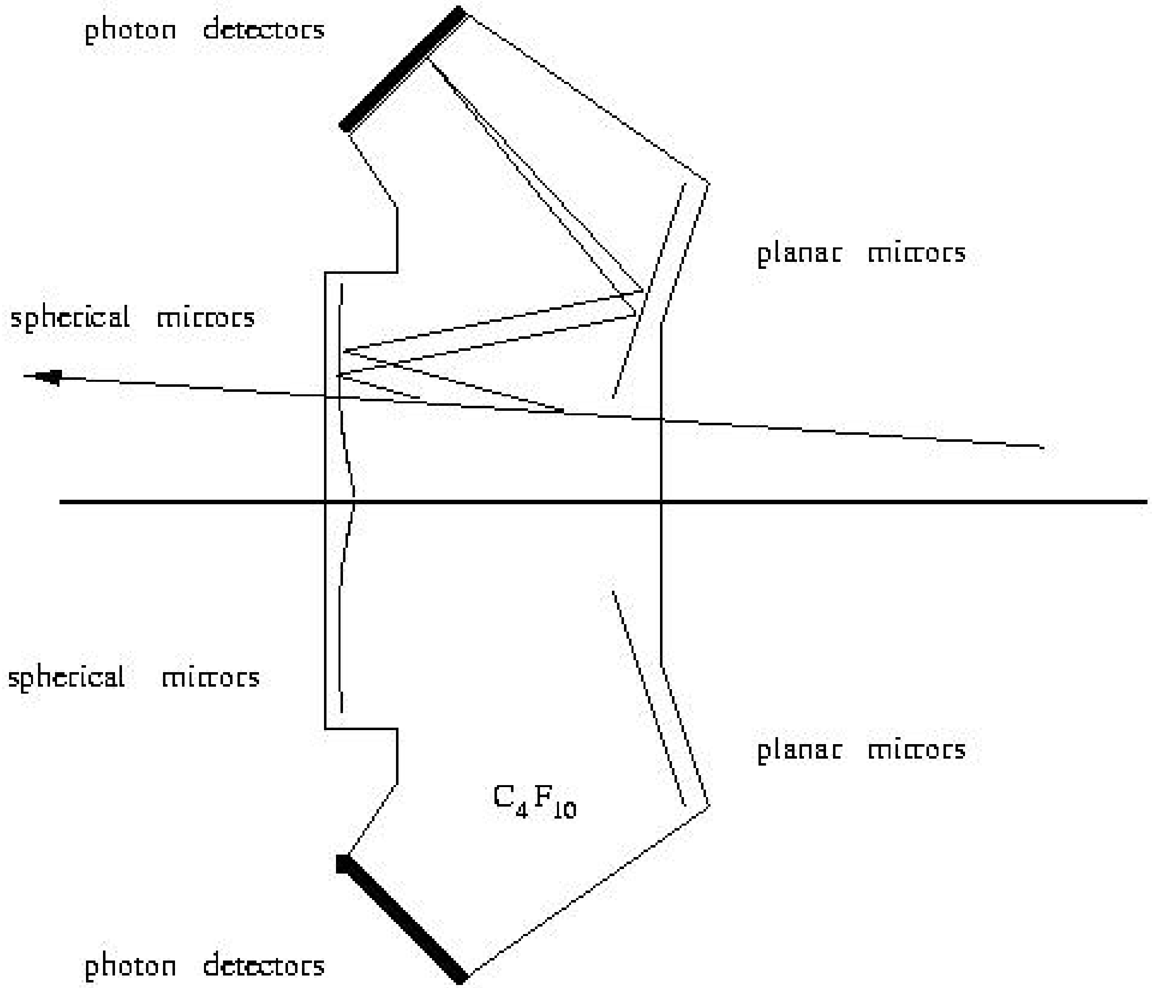

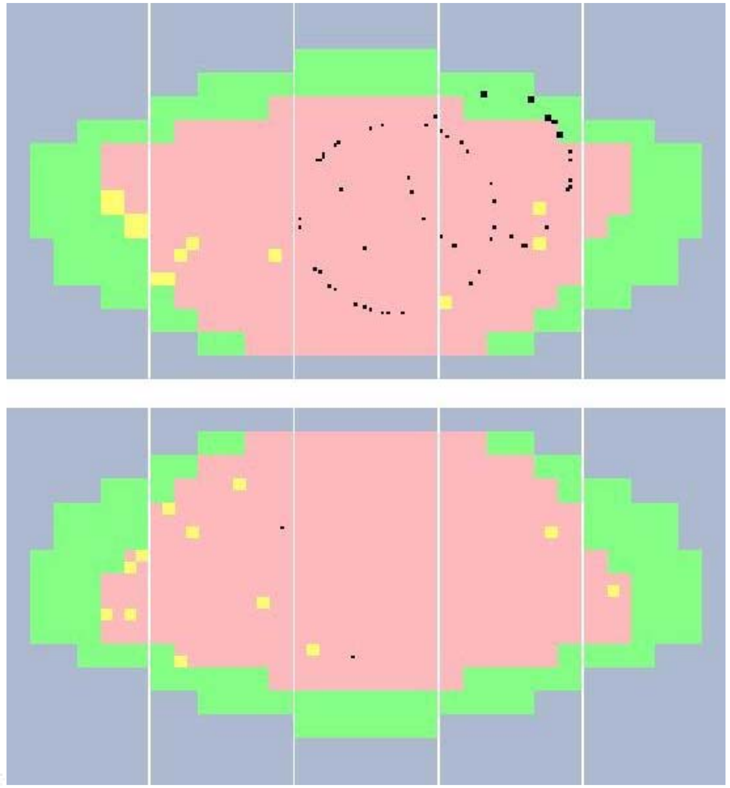

The light source is of particular nature: one has to be careful about the position, orientation, form of the photon detector plane: impact on resolution!

→ T. Ypsilantis, J. Seguinot, NIM A343 (1994) 30

→P. Križan, M. Starič, NIM A379 (1996) 124

Proximity focusing RICH

Geometry variation: in case of a solid or liquid radiator, the radiator can be rather thin (only about 1 cm) - one does not need a spherical mirror.

Photons are led to propagate over a distance of 10-20~cm, until they reach the photon detector.

Errors in the proximity focusing case depend on the photon angle:

- detector granularity
- emission point error
- dispersion

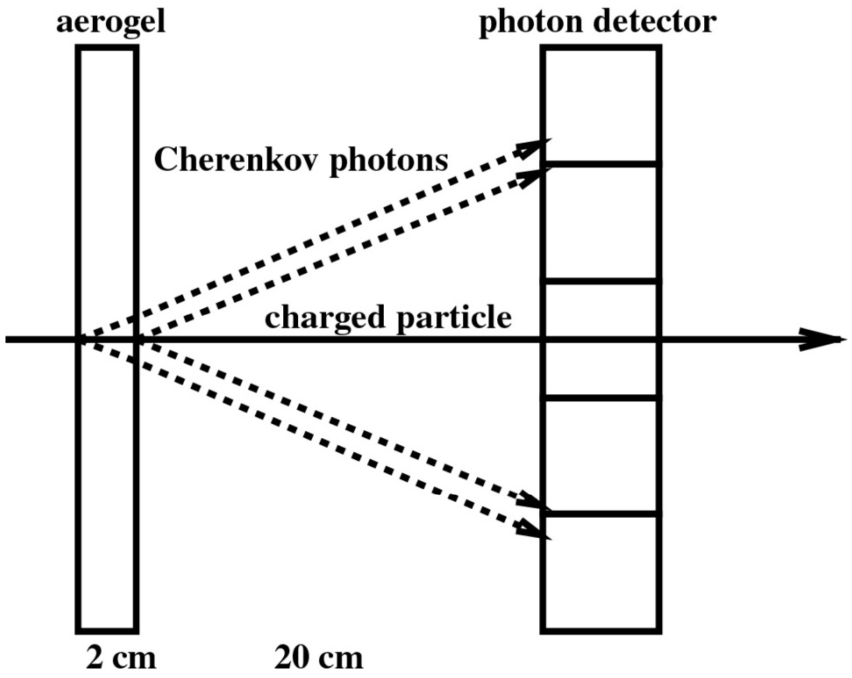

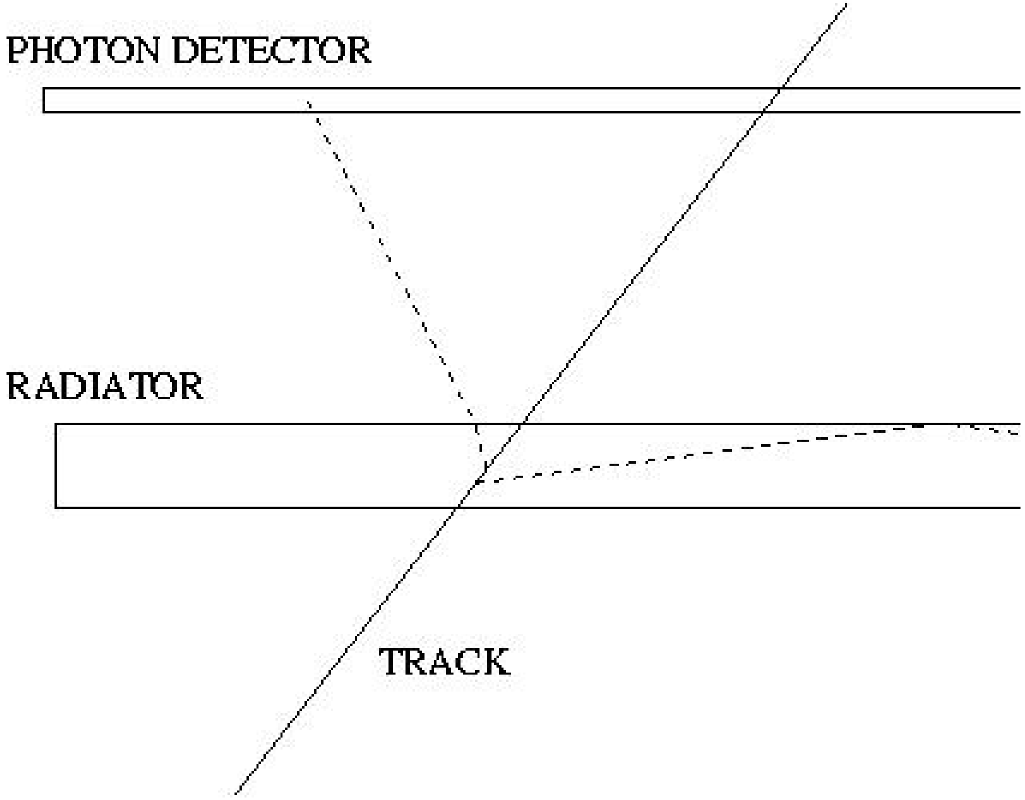

Radiator with multiple refractive indices

How to increase the number of photons without degrading the resolution?

→ stack two tiles with different refractive indices: "focusing" configuration

normal

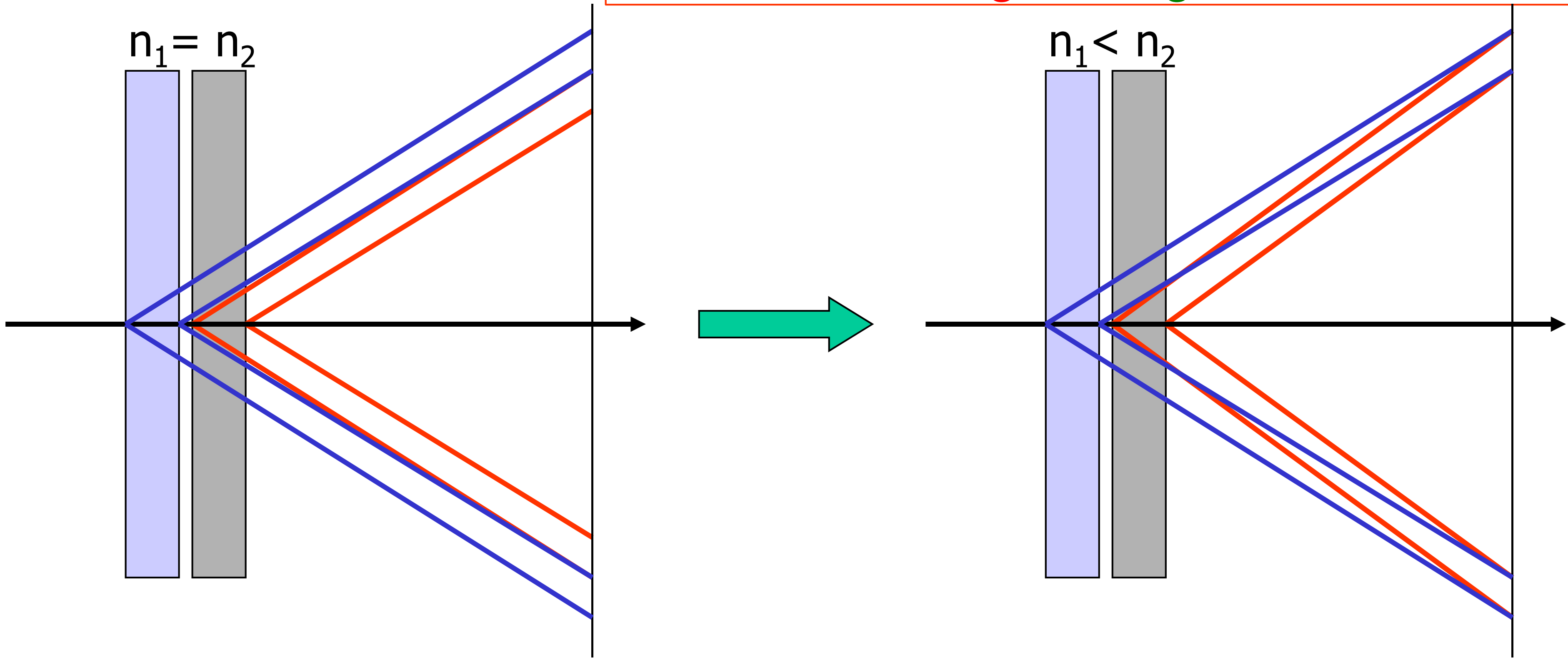

→ focusing radiator

Focusing configuration – data

4cm aerogel single index

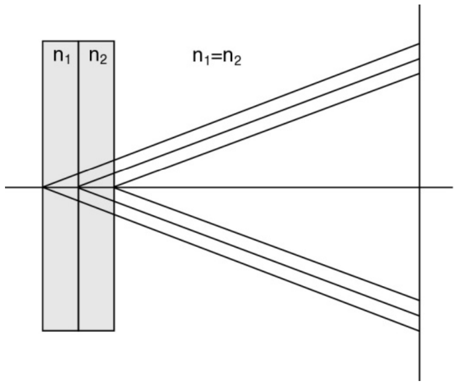

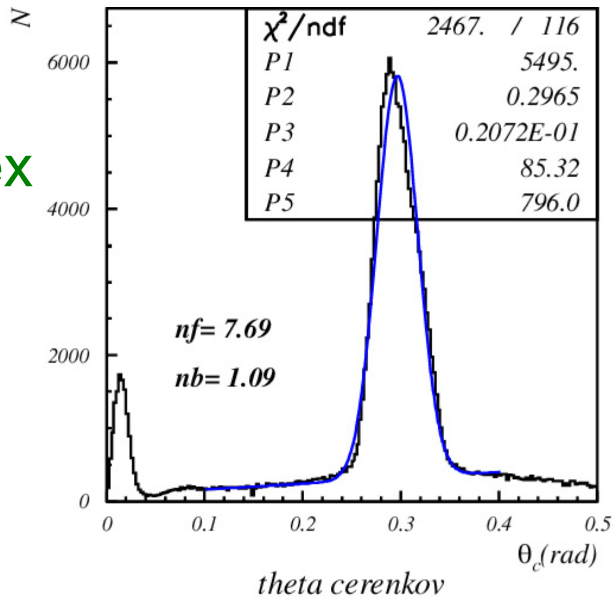

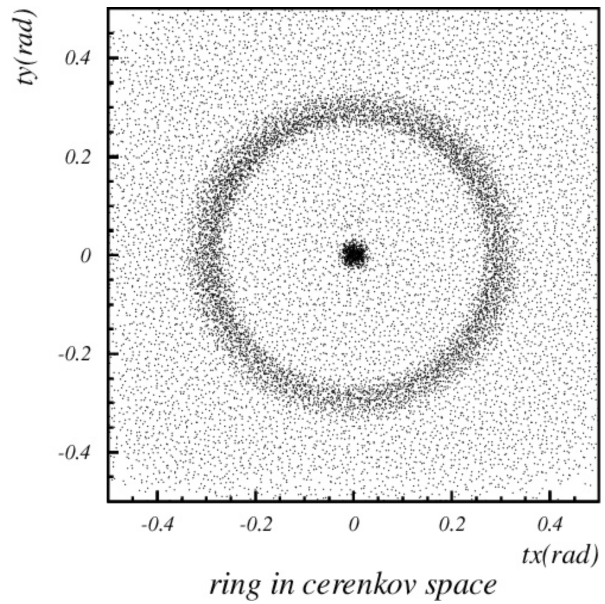

2+2cm aerogel

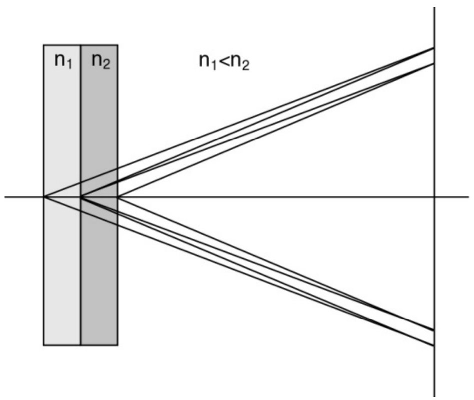

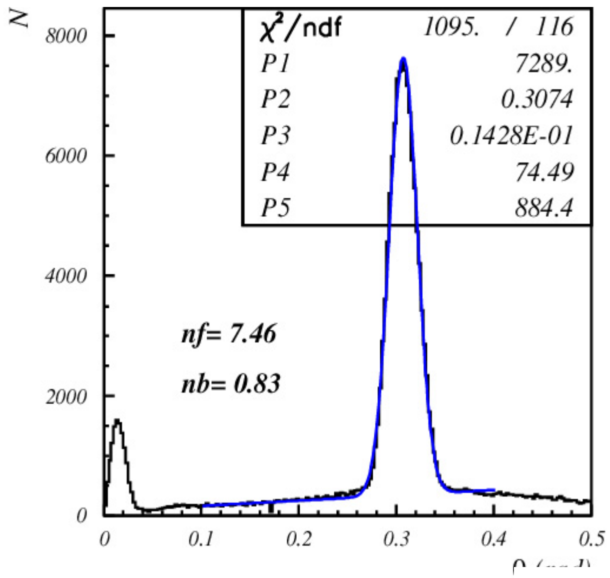

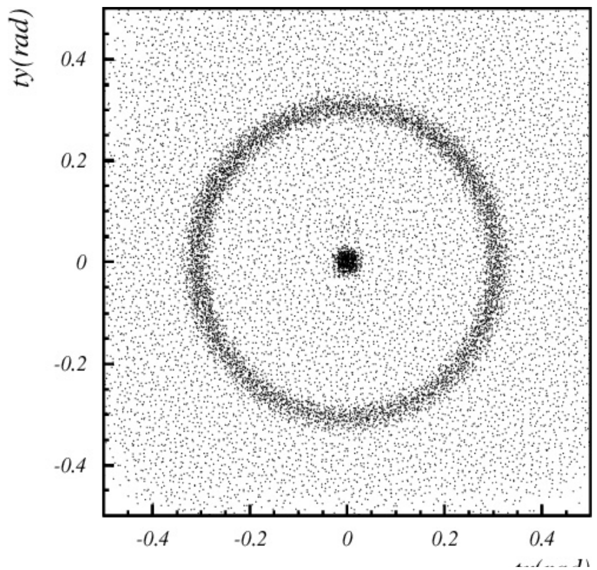

→NIM A548 (2005) 383

Radiator with multiple refractive indices

Such a configuration is only possible with aerogel (a form of Si_xO_y) – material with a tunable refractive index between 1.01 and 1.13.

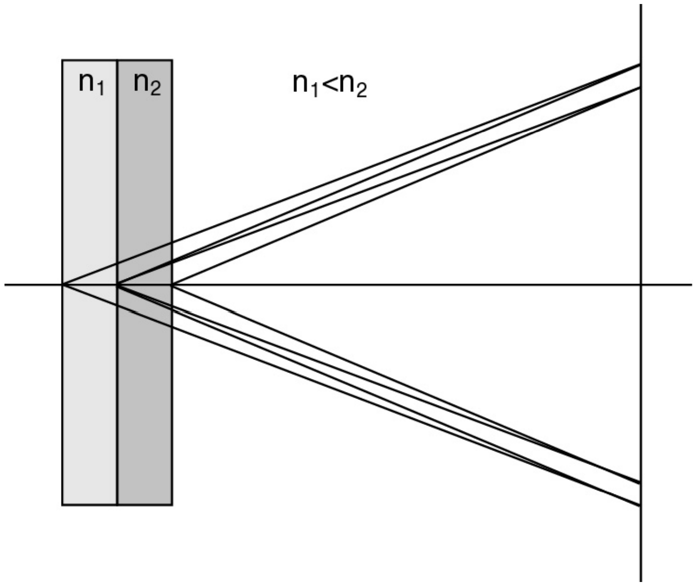

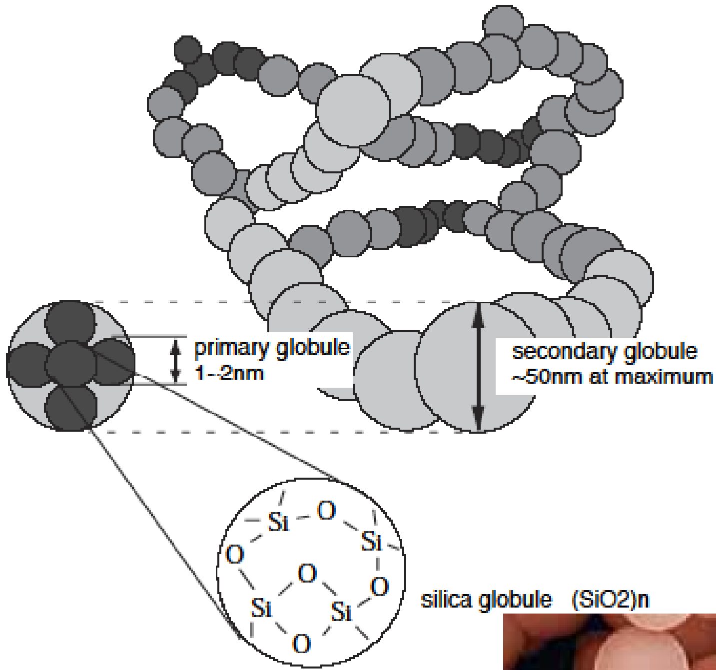

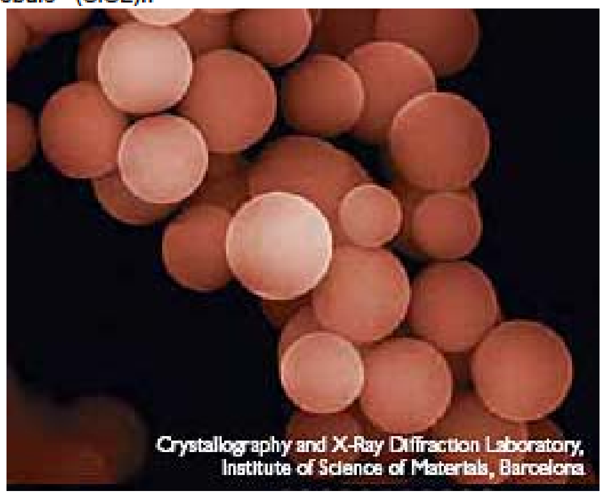

Aerogel production

Two production centers: Boreskov Institute of Catalysis, Novisibirsk, and KEK+Matsushita

Considerable improvement in aerogel production methods:

- Better transmission (>4cm for hydrophobic and ~8cm for hydrophylic)
- Larger tiles (LHCb: 20cmx20cmx5cm)
- Tiles with multiple refractive index

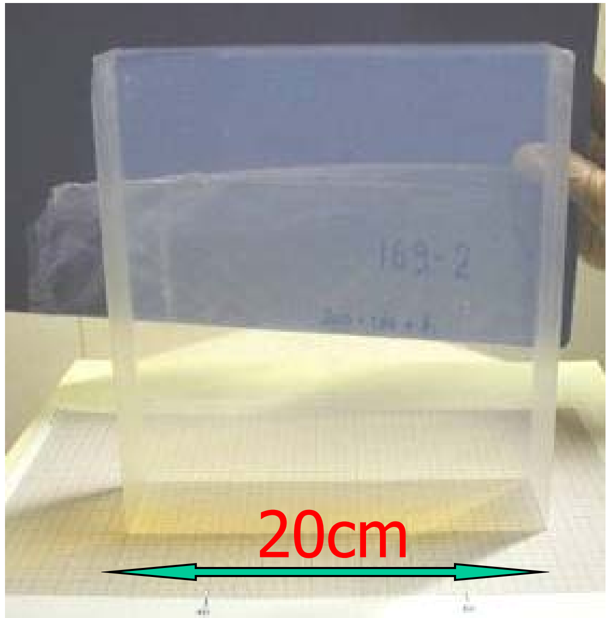

n1=1.046

n2=1.041

n3=1.037

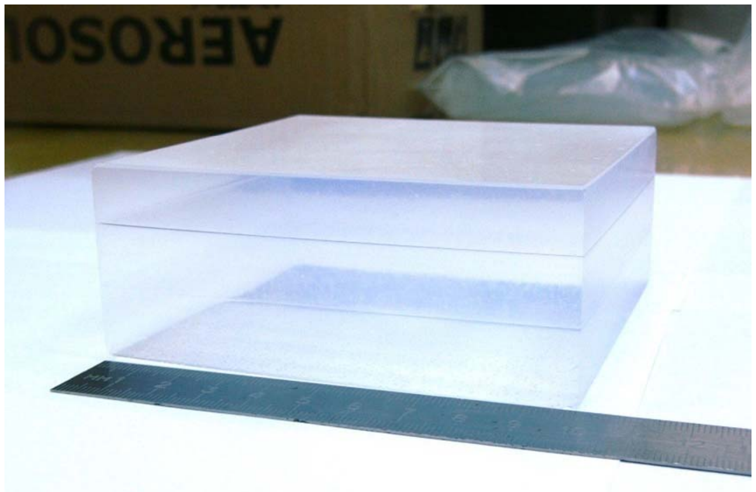

Proximity focusing RICH 2

Problem with perpendicular incidence in case of n> √2: tilt the radiator or form it as a sawtooth (CLEO).

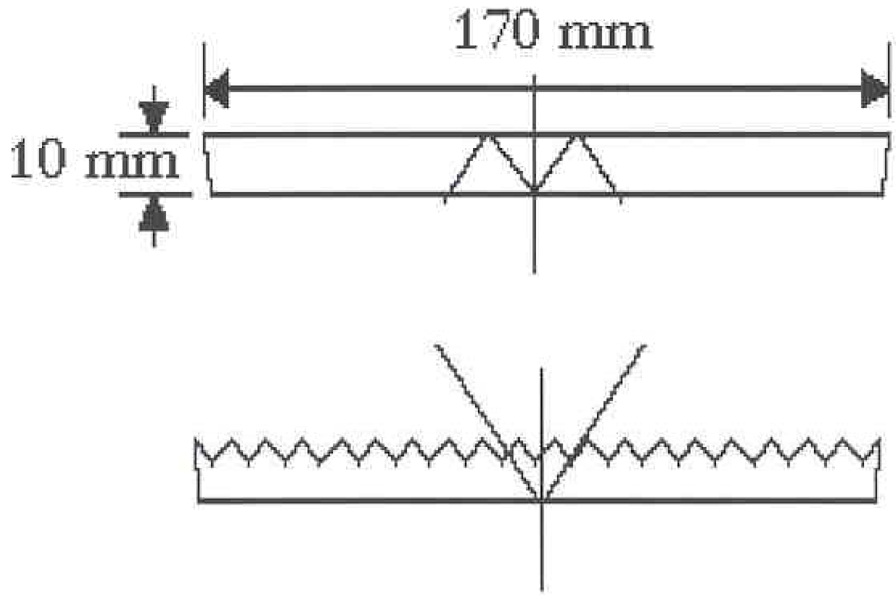

DIRC

Geometry variation: photons trapped in a solid radiator are propagated along the radiator bar to the side, and detected as they exit and traverse a gap.

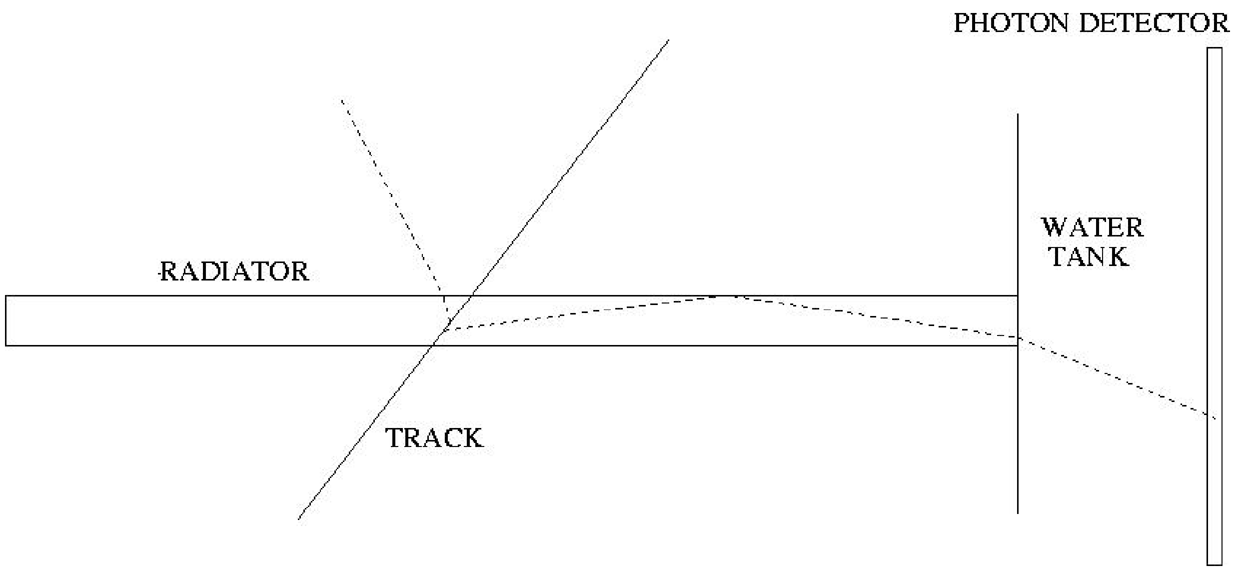

DIRC Layout

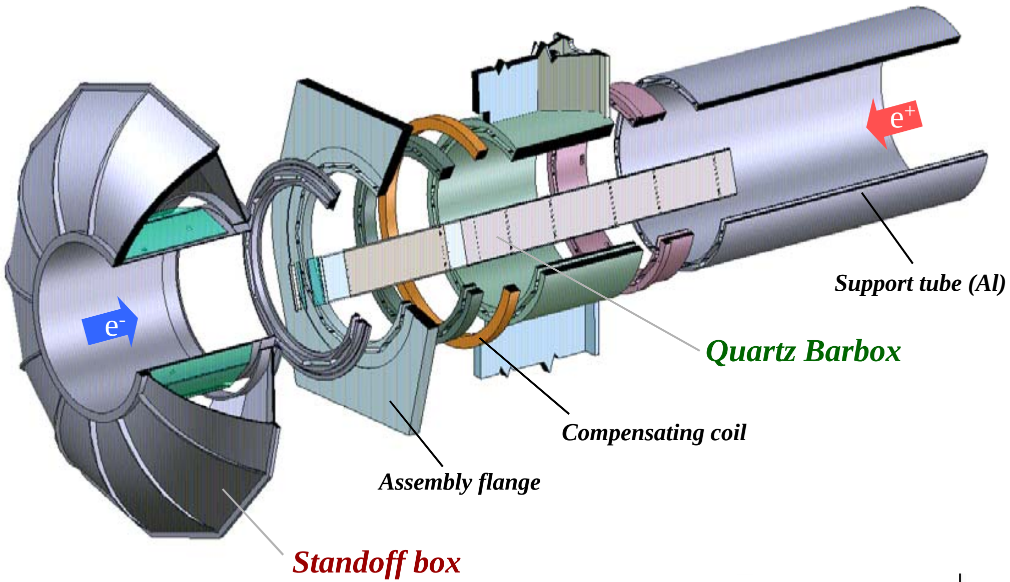

e+
e-
Support tube (Al)
Quartz Barbox
Compensating coil
Assembly flange
Standoff box

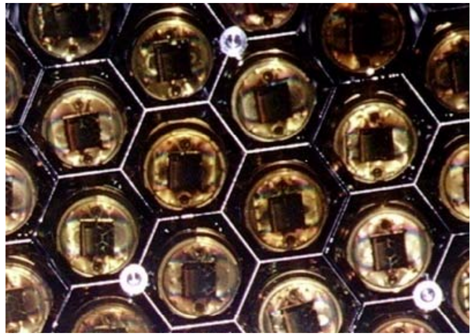

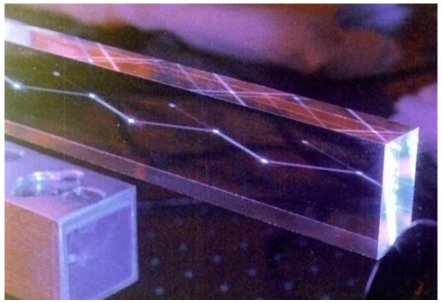

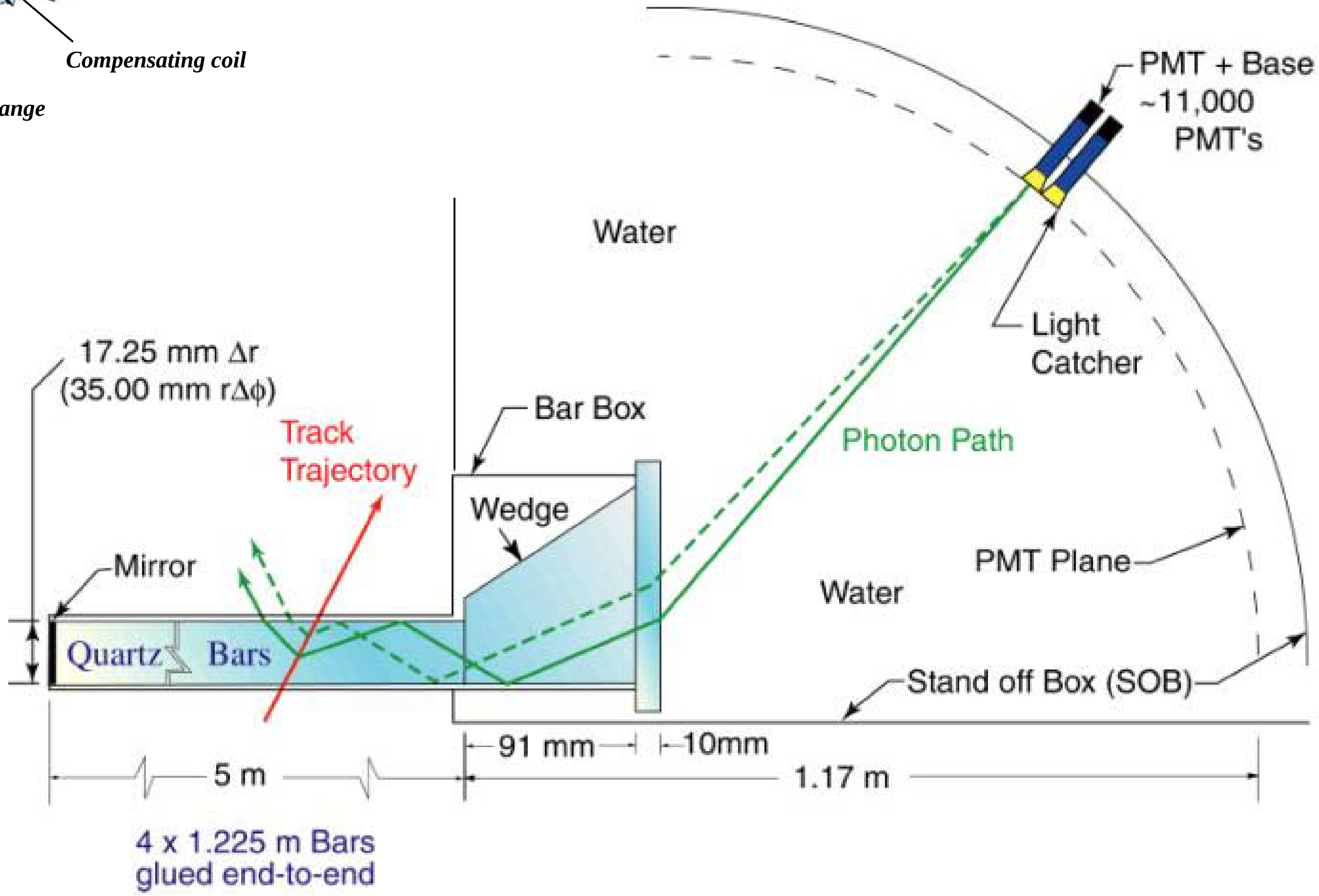

PMT + Base
~11,000
PMT's
Water
Light
Catcher
17.25 mm Δr
(35.00 mm rΔφ)
Track
Trajectory
Bar Box
Photon Path
Wedge
Mirror
PMT Plane
Water
Quartz Bars
Stand off Box (SOB)
91 mm
10mm
5 m
1.17 m
4 x 1.225 m Bars
glued end-to-end

DIRC

Babar DIRC: a Bhabha event $e^+ e^- \rightarrow e^+ e^-$

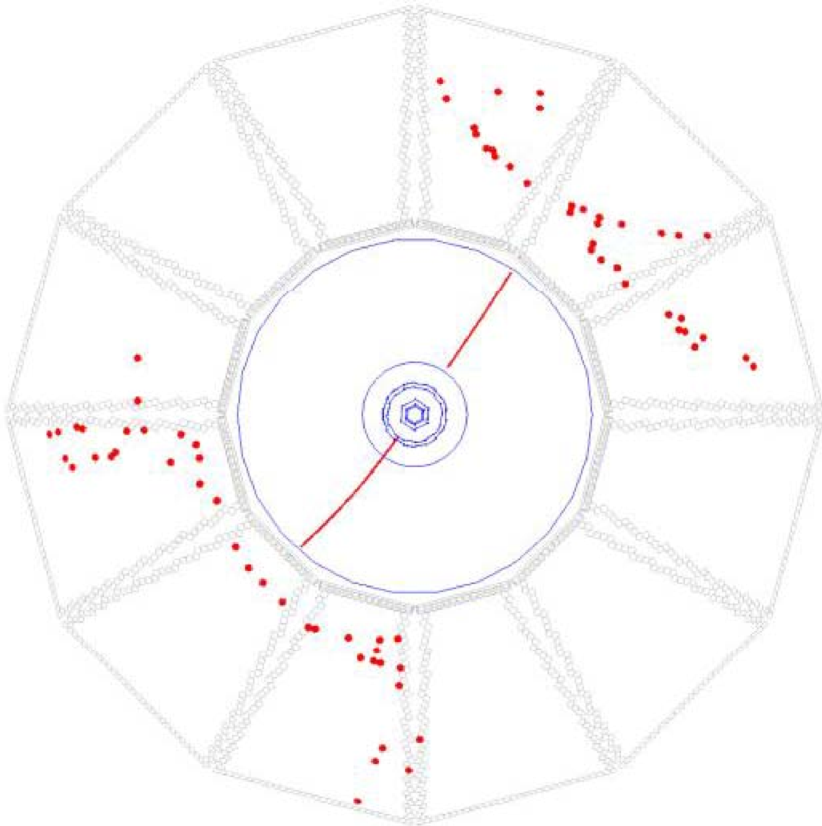

DIRC

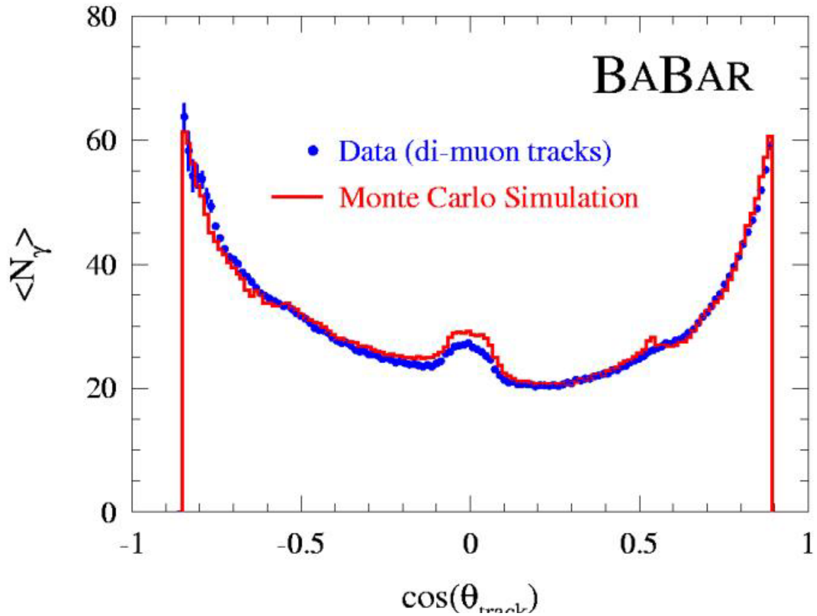

Performance

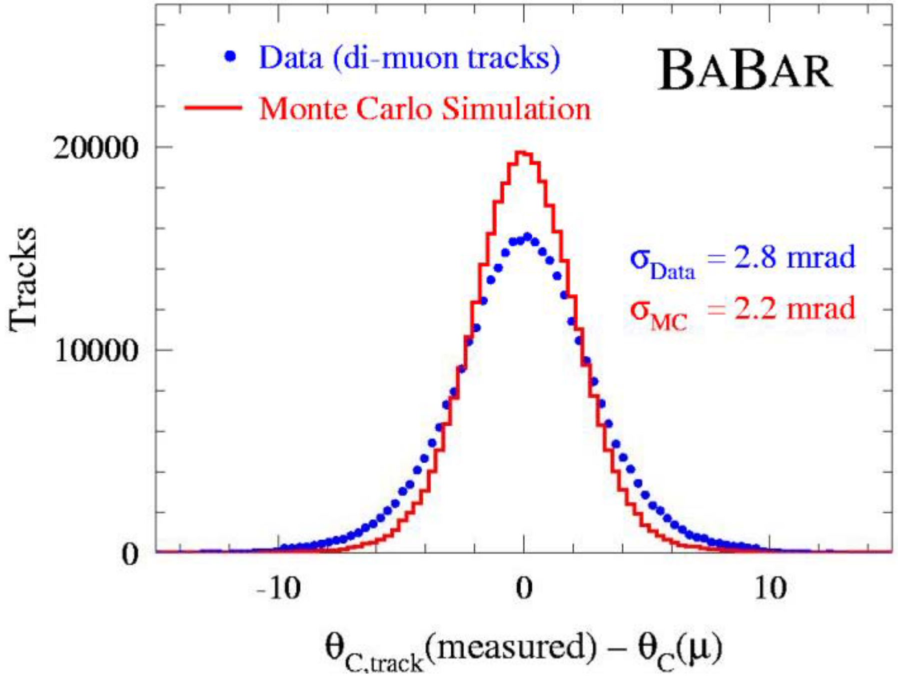

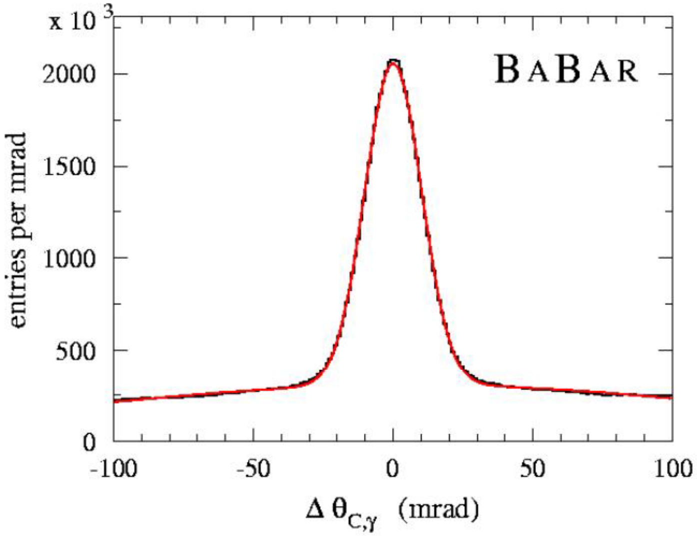

DIRC

Performance

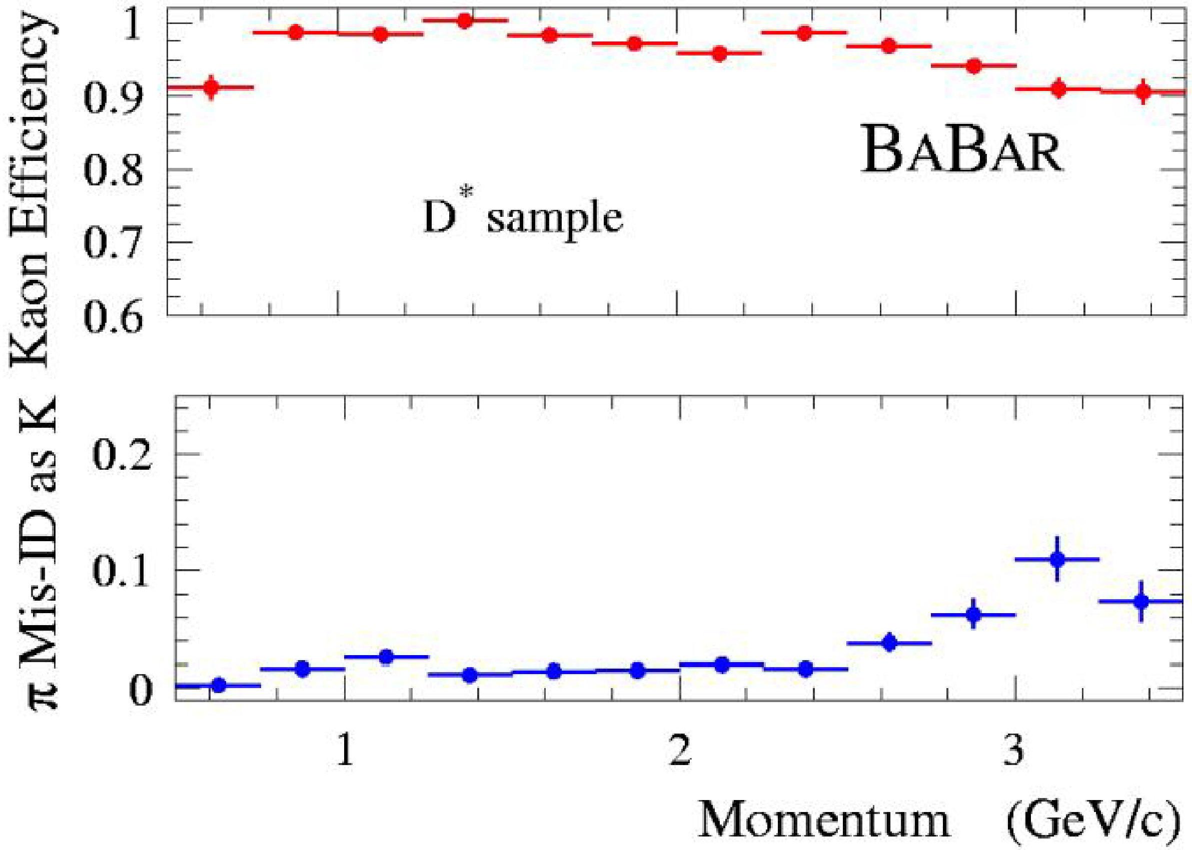

Time-Of-Propagation (TOP) counter

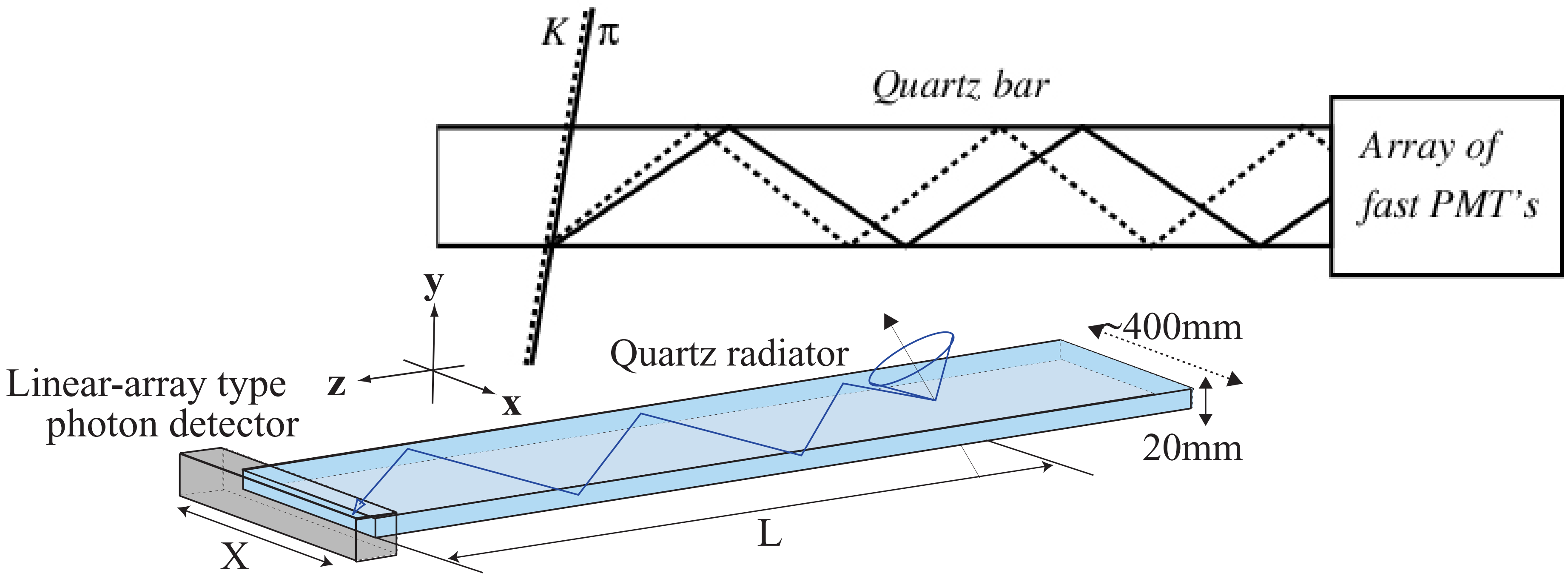

Similar to DIRC, but instead of two coordinates measure:

- One (or two coordinates) with a few mm precision
- Time-of-arrival

→ Excellent time resolution < ~40ps
required for single photons in 1.5T B field

TOP image

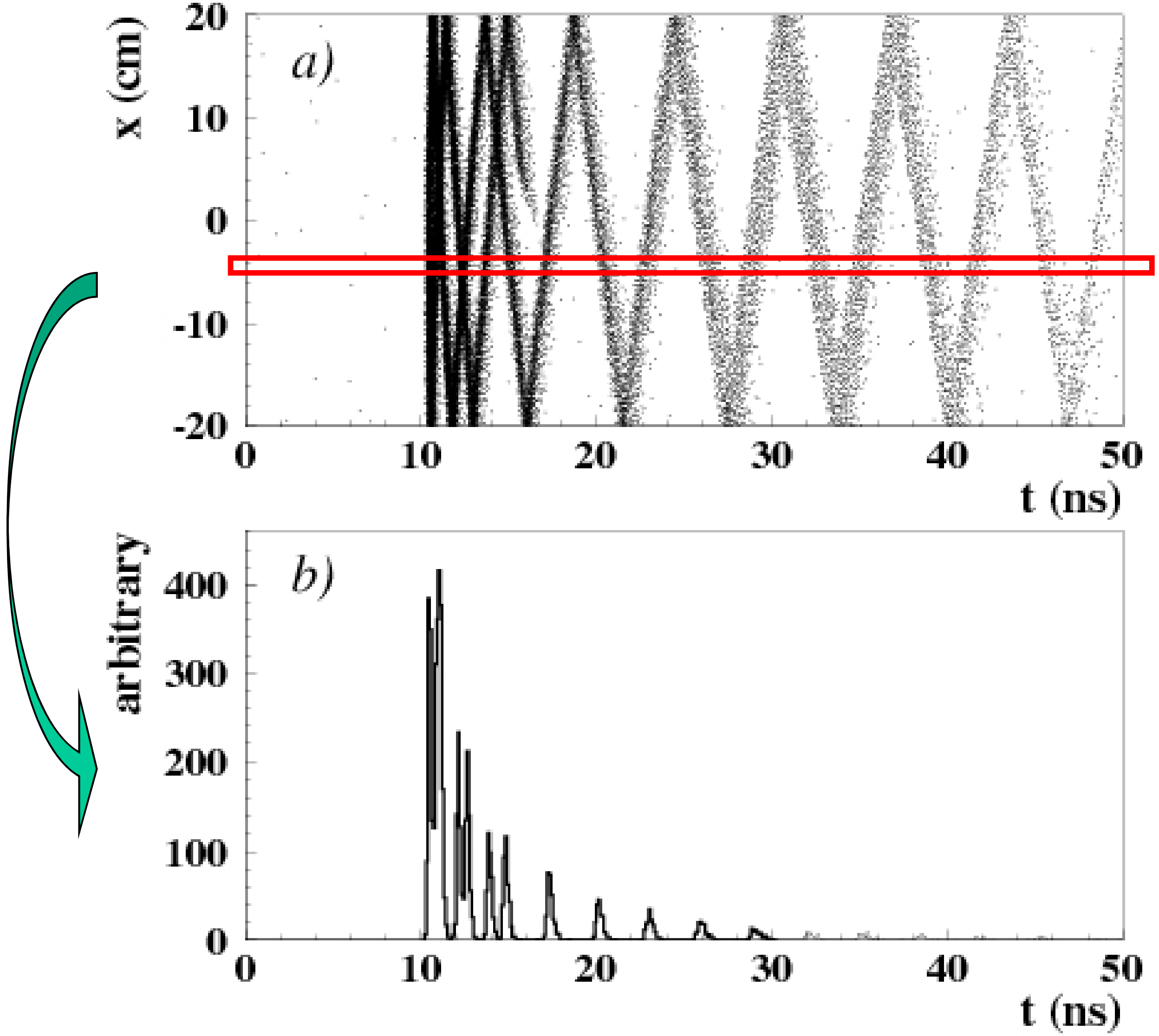

Pattern in the coordinate-time space ('ring') of a pion hitting a quartz bar with ~80 MAPMT channels

Time distribution of signals recorded by one of the PMT channels: different for π and K

Limits of the RICH technique

The choice of RICH radiator medium in case of a specific experiment depends on the particles we would like to identify, and their kinematics:

- the threshold momentum for the lighter of the two particles we want to separate: $\mathbf{p_t = \beta_t \gamma_t m c}$, $\mathbf{\beta_t = 1/n}$ should coincide with the lower limit of momentum spectrum p_{min}. Typically

$$\mathbf{p_{min} = \sqrt{2}\, p_t}$$

- the resolution in Čerenkov angle should allow for a separation up to the upper limits of kinematically allowed momenta $\mathbf{p_{max}}$

π/K separation example:

Limiting performance at the high momentum side: irreducible contribution to the resolution - dispersion.

radiator	LiF solid	C_6F_{14} liquid	C_5F_{12} gas	N_2 gas	He gas
σ_θ (mrad)	7.0	3.9	0.45	0.40	0.13
σ_N (mrad)	2.2	1.2	0.14	0.13	0.04
p_{max} (GeV/c) for 3σ π/K	3.5	6.9	50	100	330
p_{min} (GeV/c)	0.6	0.9	11	28	83

photon detector: TMAE, 10 det. photons assumed

Summary:

$$\mathbf{p_{max} / p_{min} \sim 4\text{-}7}$$

for a 3σ separation between the two particles

For a larger kinematic region **2 radiators are needed!**

RICHes with several radiators

- --> DELPHI, SLD (liquid+gas)
- --> HERMES (aerogel+gas)

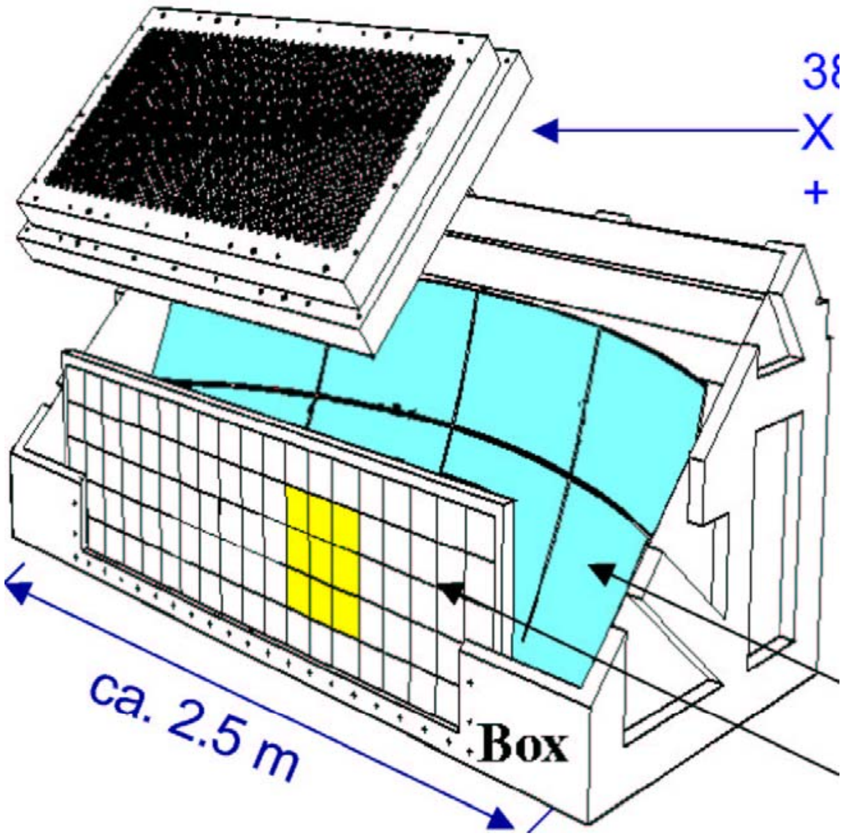

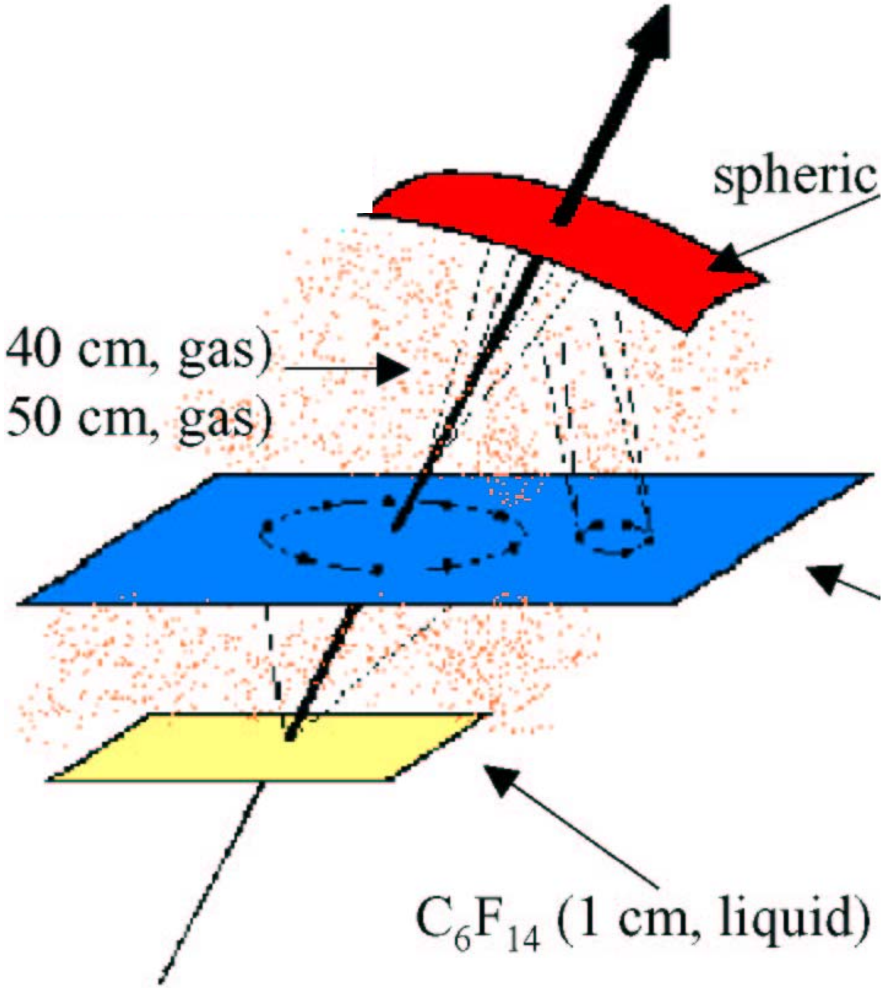

RICHes with several radiators 2

- --> LHC-b (aerogel+2 gases)

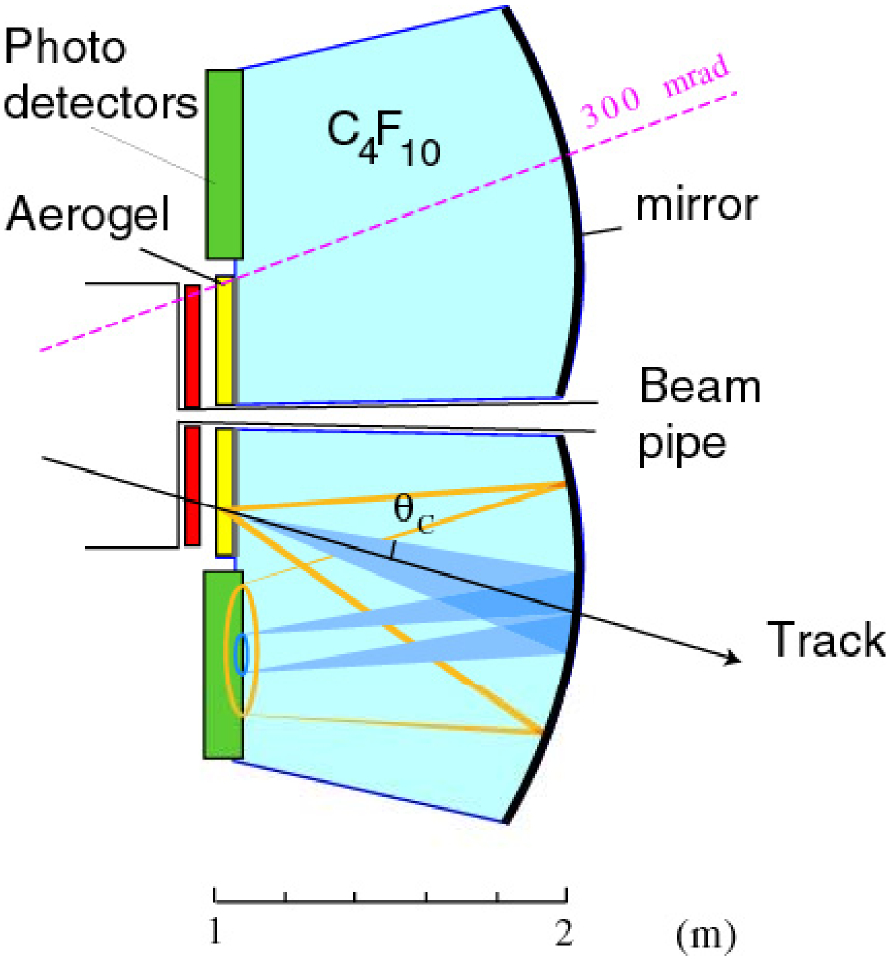

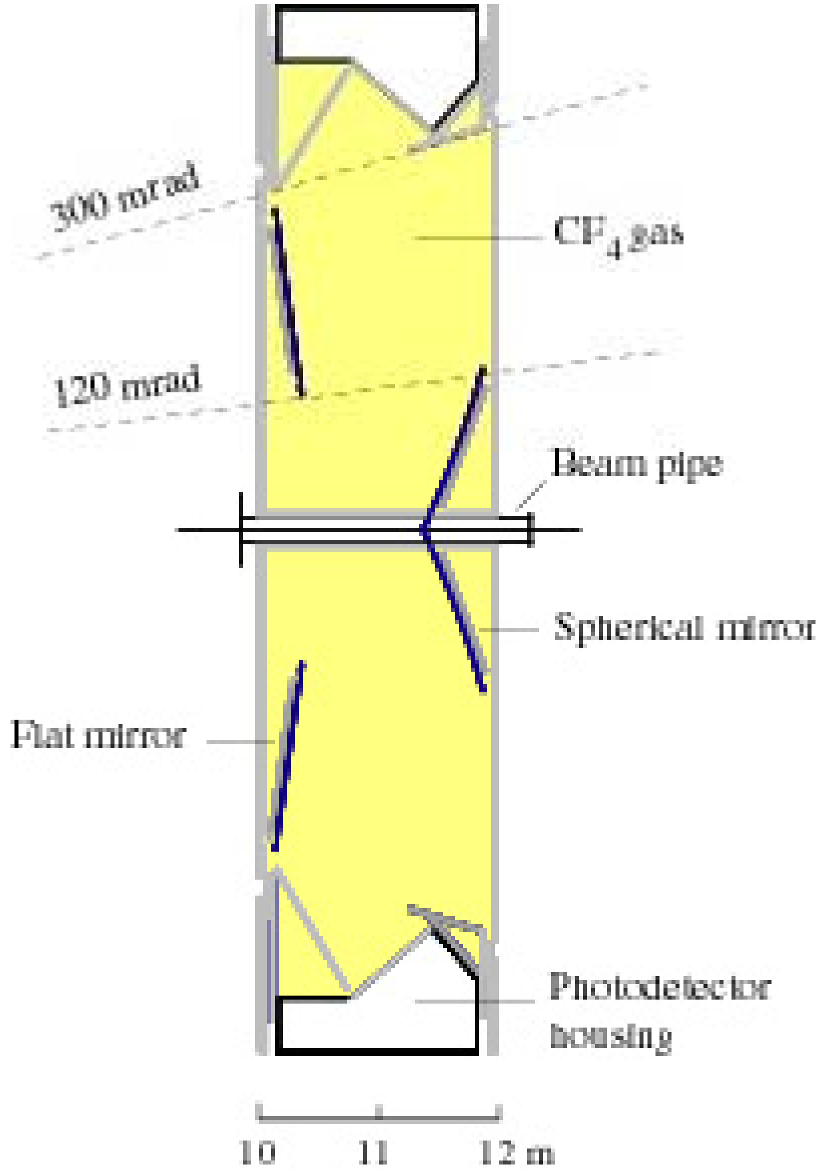

High occupancies

In case of a sizeable background under the Čerenkov angle peak:

effective resolution for N detected photons

$\sigma_N > \sigma_1 / \sqrt{N}$

HERA-B case: for isolated rings a 3σ π/K separation should be possible up to p_{max} ~ 100 GeV/c.

At high track densities, however, we get p_{max} ~ 50 GeV/c.

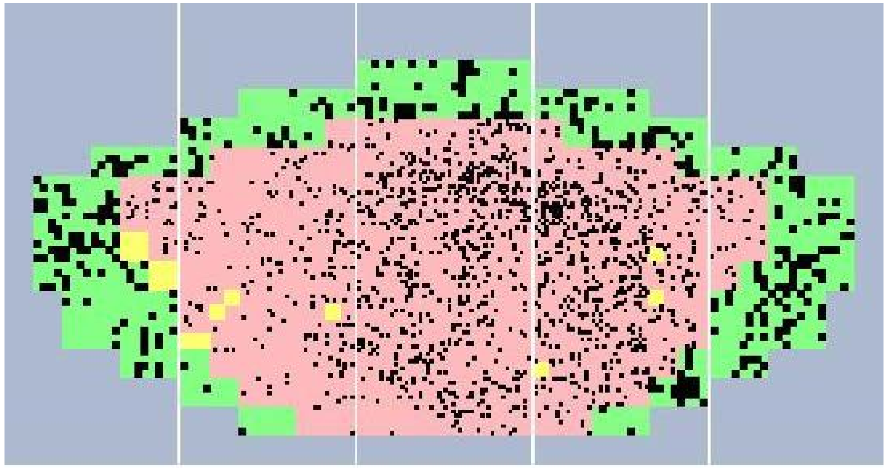

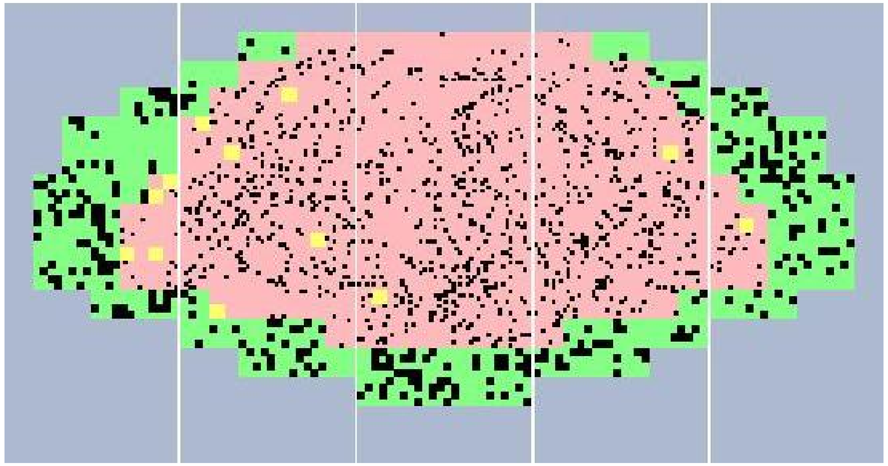

High occupancies

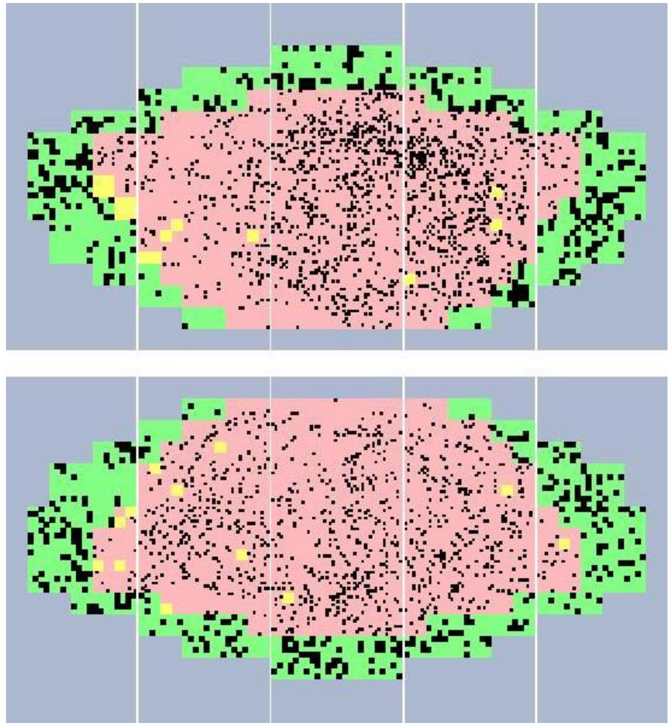

Still: it works actually very well!

Kaon efficiency and pion, proton fake probability

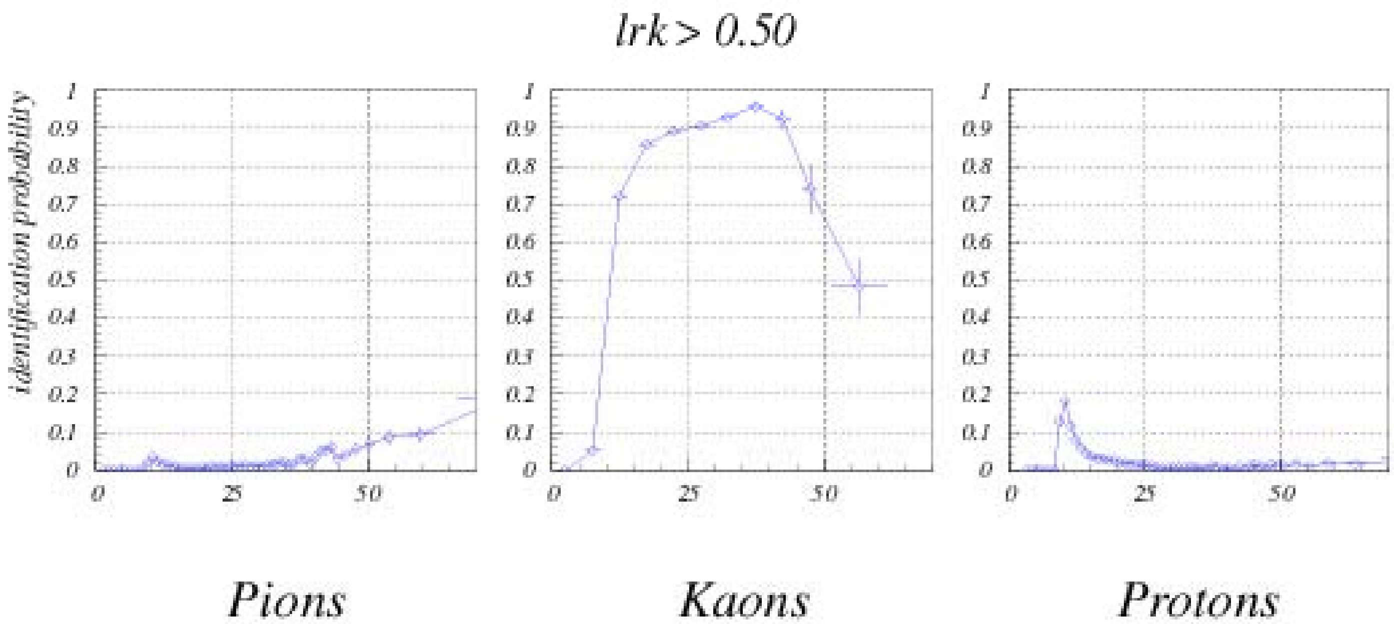

Overview: RICH Building Blocks

Need 10 - 20 detected photons and a good angular resolution:

How do we get there?

Very carefully design, build and run a RICH counter

RICH Building Blocks

- Radiators
- Photon detectors
- Light collectors
- Large system aspects

Radiators

Radiator length needed for **20** detected photons in case of beta=1 particles

Number of detected photons: $\mathbf{N = N_0\, L\, \sin^2\theta}$ with $\mathbf{N_0 = 50\text{-}100/cm}$

N =20:

- Solid radiators: example n=1.5, $\sin^2\theta = 1 - (\beta n)^{-2} = 0.55$
  ->L=0.7cm (for N_0 =50/cm)

- Gaseous radiators: example n=1.001, $\sin^2\theta = 1 - (\beta n)^{-2} \sim 2(n-1) = 0.002$
  ->L=200cm (for N_0 =50/cm)

- Aerogel radiator: example n=1.05, $\sin^2\theta = 1 - (\beta n)^{-2} \sim 2(n-1) = 0.1$
  ->L=4.3cm (for N_0 =50/cm)

Photon detectors

Need:

- photosensitive substance
- amplification/multiplication of the photoelectron

Photosensitive substances:

- solids (SbCs, Sb-K-Cs, CsI, ...)
- gases (TMAE, TEA)

Multiplication through:

- multiplication in a dynode structure in vacuum
- avalanche amplification in a gas
- avalanche amplification in silicon
- photoelectron acceleration in electric field in vacuum, detection in Si

Combined to

- gas based photon detectors (wire chambers with 2d read-out)
- vacuum based photon detectors (PMT, HPD)
- silicon based photon detectors (APD, VLPC)

Detection efficiency, radiator and window transmission.

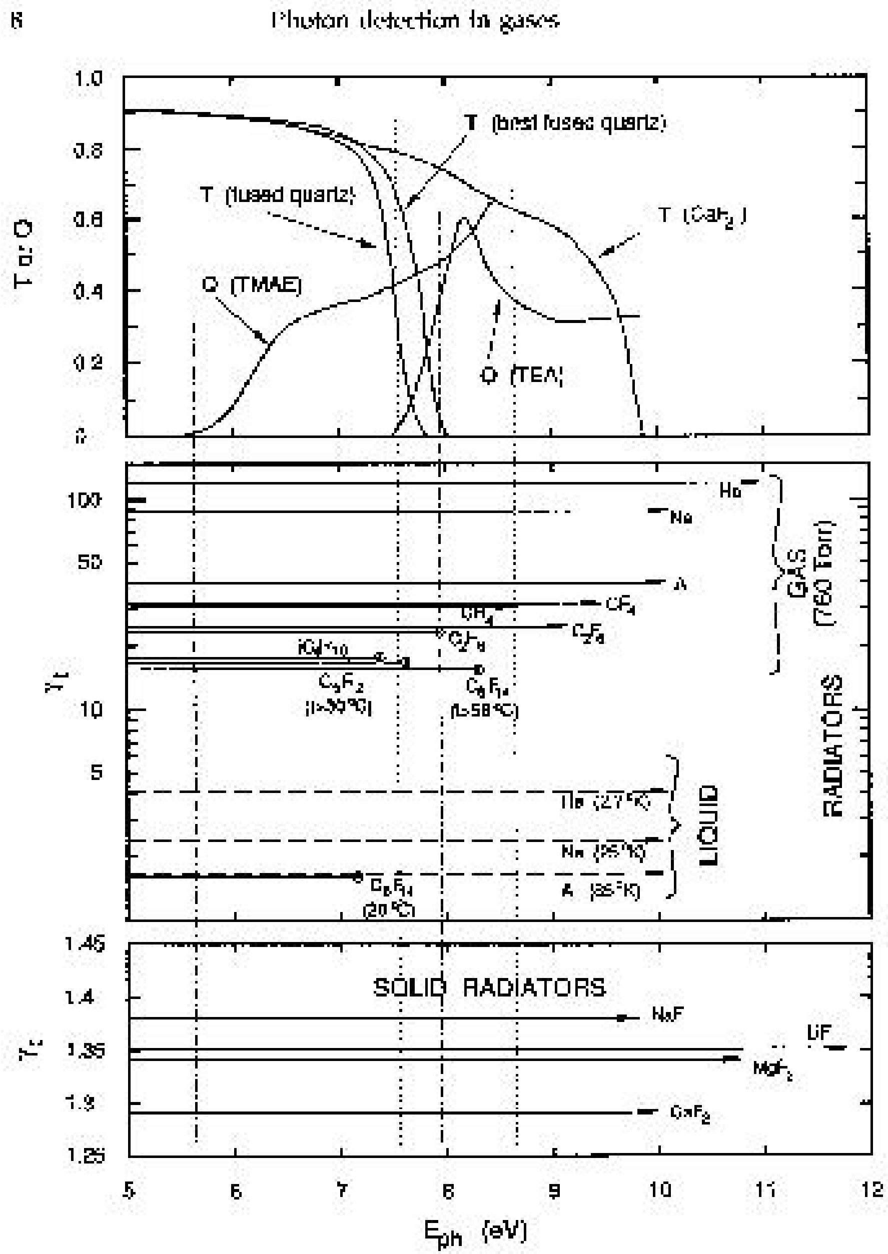

Mirrors

Good reflectivity in UV: not trivial to produce and maintain (water!).

But: was done and worked very well (DELPHI RICH, SLD CRID) for years

DELPHI mirror system →

HERA-B mirror system →

Typically: 0.5-1 cm of glass, coated with Al, and a protective layer (MgF_2 etc).

Light mirrors: on composite substrate (expensive!)

Sistem of mirrors of the HERA-B RICH

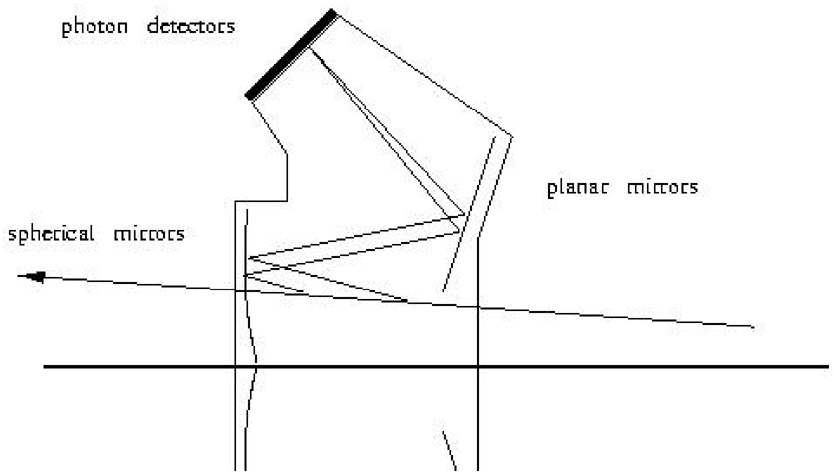

Mirrors 2

Sistem of mirrors of the DELPHI RICH

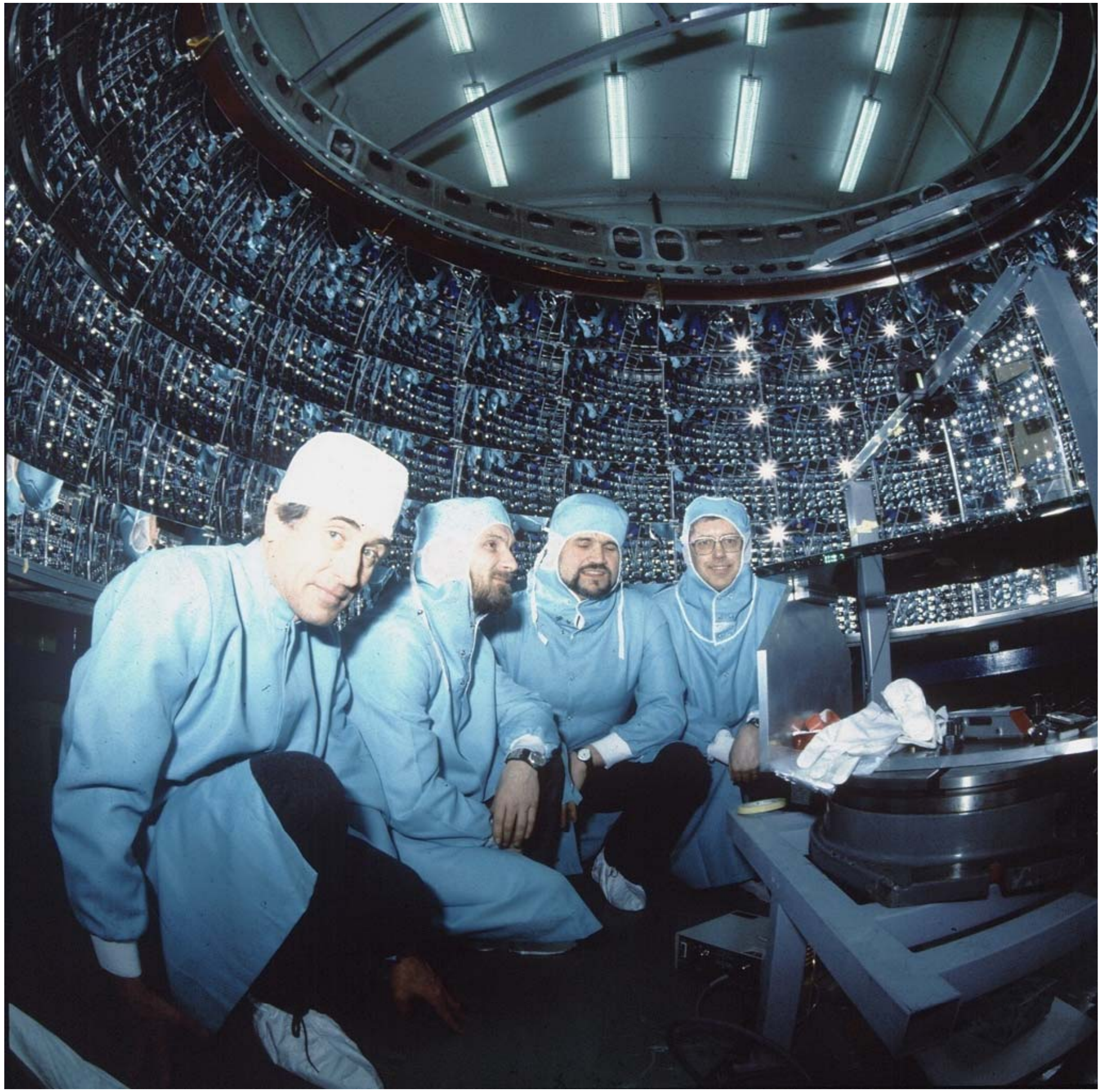

Windows

Transmission of radiator exit windows has to match the sensitivity of the photosensitive substance.

- quartz for TMAE, CsI,
- CaF_2 for TEA,
- UVT plexiglass for PMTs

For comparison: mylar is only transparent above ~ 400 nm, UVT plexiglass above 300 nm

Large system aspects

- Water and oxygen content in the radiator (order of one meter to a few meters of gas, or a centimeter of liquid) have to be kept very low in case of photon detectors for UV light.

Example: take a RICH with photon path of 7.5 m, plot the influence of 10 ppm of water or oxygen (or 100 ppm for 0.75 m).

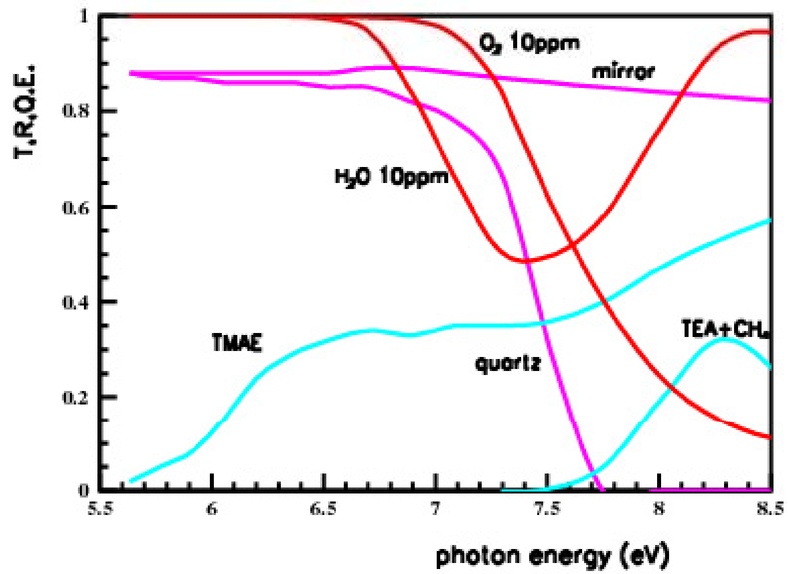

Gas based detectors (TMAE, TEA, CsI)

Why bother to develop gas chamber based light sensitive detectors instead of photomultiplier tubes?

Virtues:

- good spatial resolution (order few mm),
- coverage of large surfaces (square meters) with a large fraction of active area at reasonable cost,
- highly efficient single photon detection.

These virtues made gas based detectors boost the RICH identification method.

Example: metal surface

Note that a polished metal surface is sensitive to visual light, although with a very low efficiency.

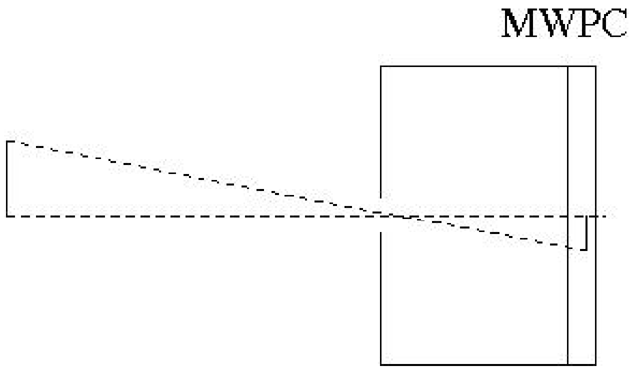

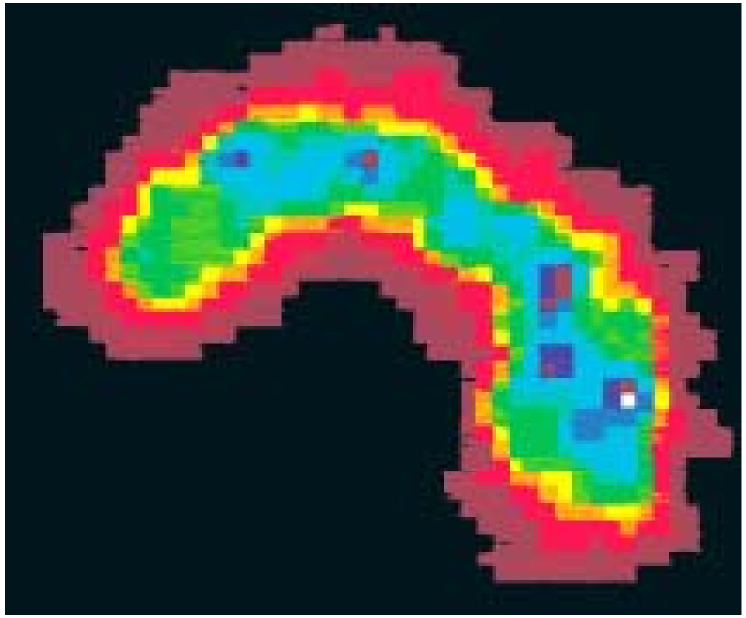

The 'photograph' of the tungsten filament in a light bulb was taken with a pinhole camera (a black box with a a small hole) equipped with a small 5cm x 5cm MWPC with a two dimensional delay line read-out.

UV photon detection in wire chambers: photosensitive materials

Either added to the gas mixture

- TMAE
- TEA

or a layer on one of the cathodes

- CsI on a Sn-Pb substrate

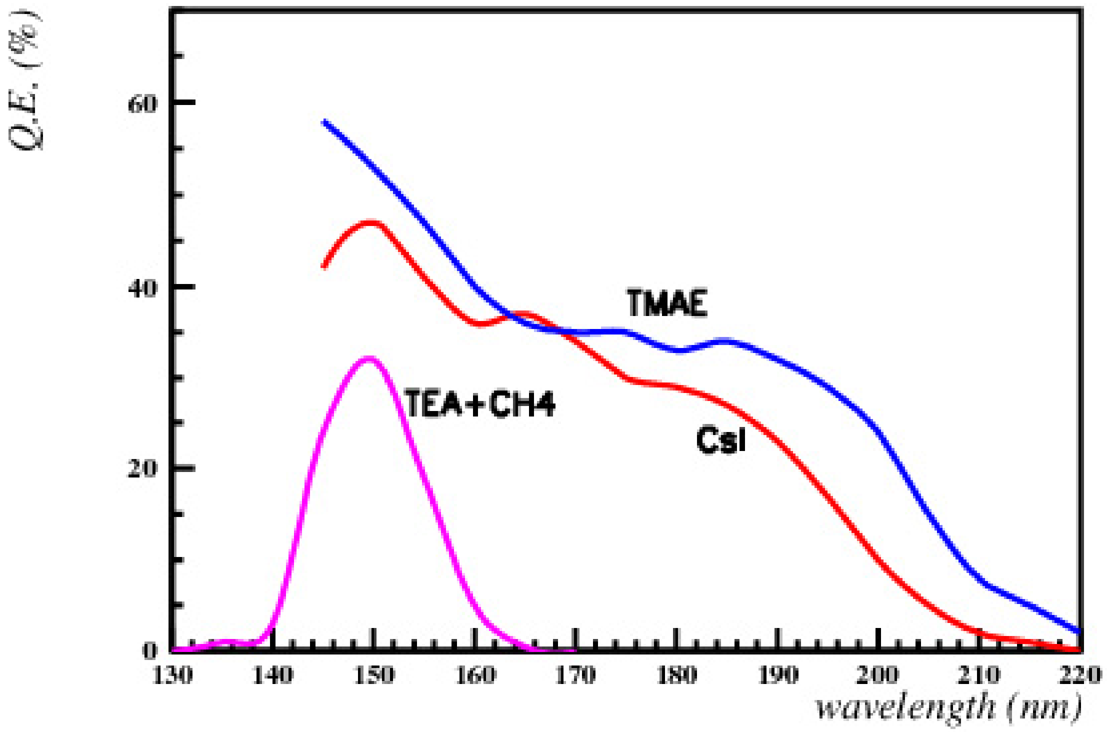

quantum efficiency vs λ

All chemically very active!

DELPHI RICH

Inside the DELPHI RICH:
segmented spherical mirror

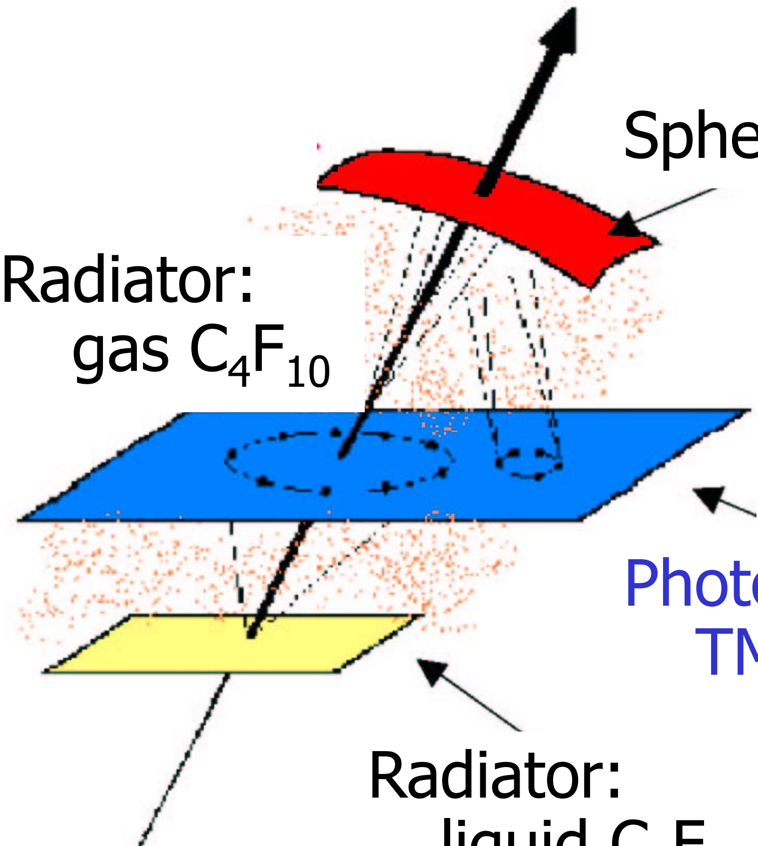

Spherical mirror

Radiator:
gas C_4F_{10}

Photon detector:
TMAE in methane

Radiator:
liquid C_6F_{14}

TMAE

A liquid at room temperature, with a vapour pressure of 0.30 torr (at 20 C)

Absorption length of about 3~cm at room temperature

Typical chamber: a thick conversion volume (~10cm is needed to enable an efficient absorption, usually combined with a TPC type chamber)

Gas purity and chamber materials : very clean system needed (TMAE reacts intensely with oxygen!), stainless steel pipes and valves, oxysorb

Examples:

TPC (Omega, DELPHI, SLD)

multiwire chamber with pad read-out (Caprice): two parallel plate stages, coupled to a multiwire chamber with pad read-out (CERES)

Higher rates: a different geometry is needed. An example is the JETSET/HERA-B prototype geometry with anode wires embedded in an egg-crate structure.

Photons enter the chamber from the left side.

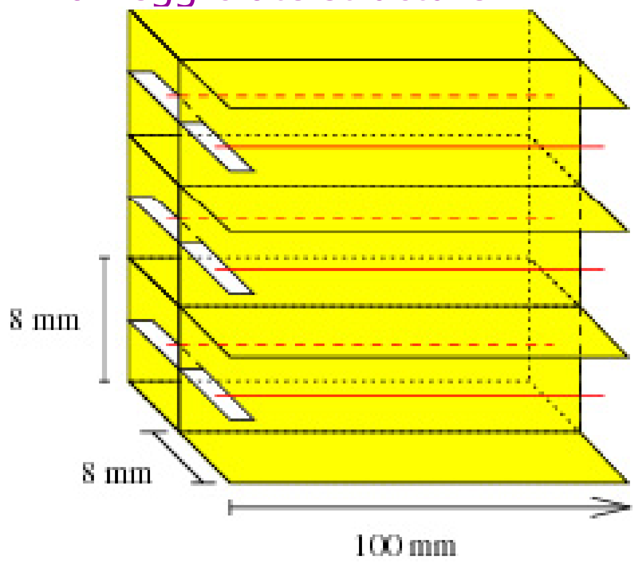

TEA

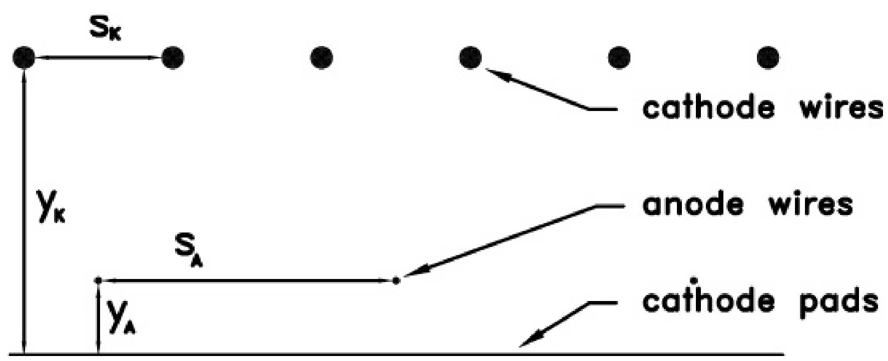

- A liquid at room temperature, with a vapour pressure of 52 torr (at 20 C); added to methane by bubbling it through the liquid.
- Absorption length of 0.61mm (at 20 C).
- Typical chamber: a multiwire chamber with pad read-out.
- Typical dimensions: few mm thick.
- First used in the pioneering RICH experiment E605.
- Examples: CL

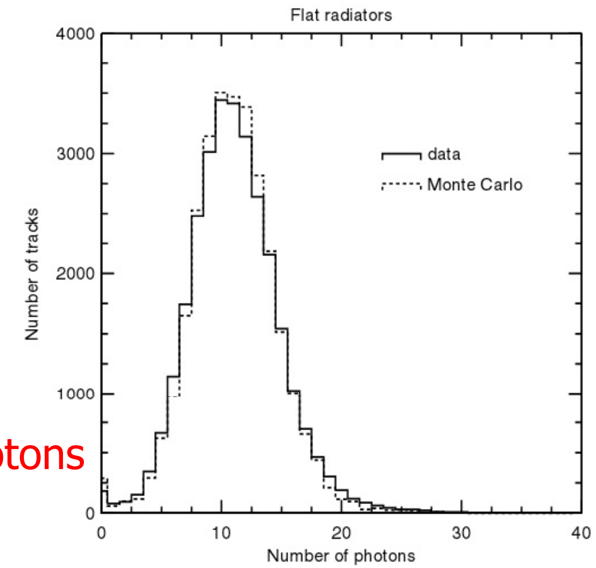

Number of detected photons

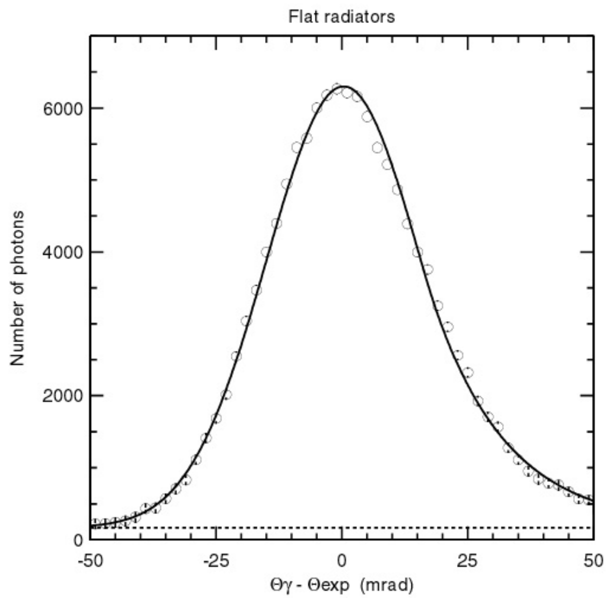

Resolution

CsI

A solid layer, 100nm – 1000nm thick, evaporated in vacuum on one of the cathodes (or on the entrance window)

Needs a high purity chamber gas, usually methane with a water and oxygen content of order ppm.

Typical chamber: a multiwire chamber with pad read-out, reflective photocathode.

Electric field: voltage on cathode wires has to be adjusted to guarantee a uniform amplification around the anode wire.

Chamber variation: photocathode evaporated on the entry window, chamber can then be a MSGC, MGC, can also have a GEM amplification structure and multiwire chamber with pad read-out.

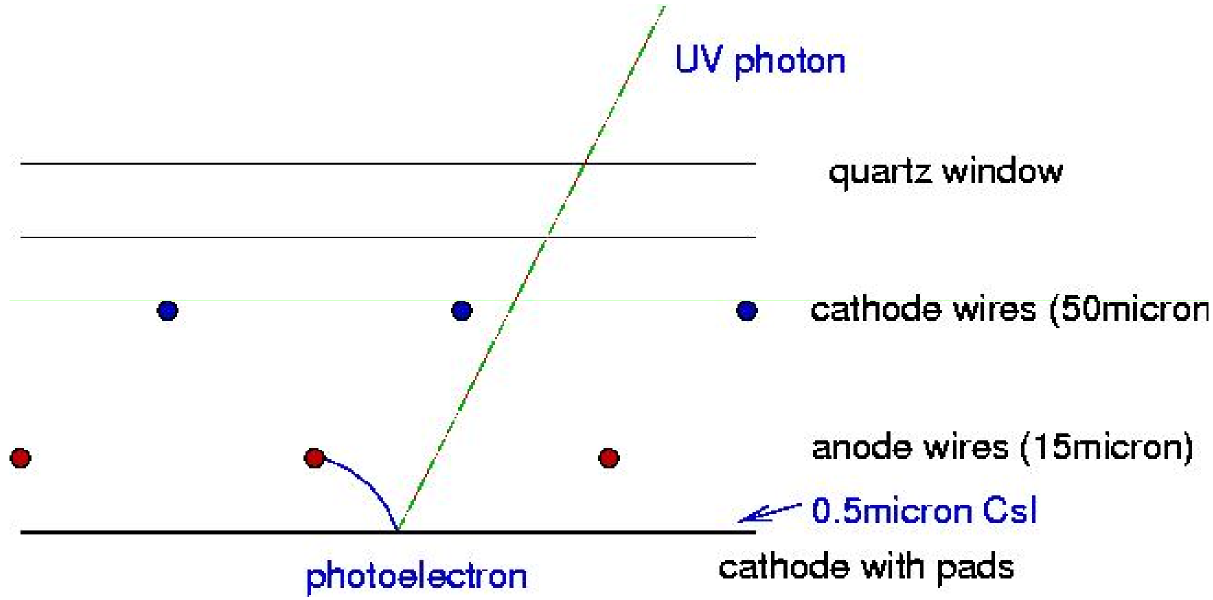

UV photon detection in wire chambers: photo-electron detection

Distribution of pulse heights due to individual photoelectrons is exponential!

Dramatic consequence for photo-electron detection probability (=efficiency). For a given electronics threshold U_{th} the efficiency is

$$\varepsilon = \int_{U_{th}}^{\infty} \frac{1}{\bar{\bar{U}}} e^{-\frac{U}{\bar{\bar{U}}}} dU = e^{-\frac{U_{th}}{\bar{\bar{U}}}}$$

-> efficient detection of single photons is only possible with a low noise electronics!

How low is low? The visual charge is about 20% (for integration times of order τ=20ns) of the avalanche charge, i.e. at a gas amplification of 2 10^5 the average detected signal corresponds to 4 10^4 electrons.

If we want to cut noise at 4σ, and keep a 90% efficiency (U_{th} = 0.1 U), the electronics noise has to be kept at 4x10^4x0.1/4 = 1000 e- ENC

Problems of wire chamber based photon detectors 1

Feedback photons: Avalanche photons cause emission of secondary photons (feedback photons). The process is enhanced because chamber is light sensitive no or little quenching gas is used. The result is more background (best case) or chamber instability (in particular in cases when a lot of primary electrons are liberated by a charged track which passed the chamber).

- Solution: use isolated cell geometry or isolate anode wires from each other by using blinds, or work at low gain, preferably in a region with no charged tracks

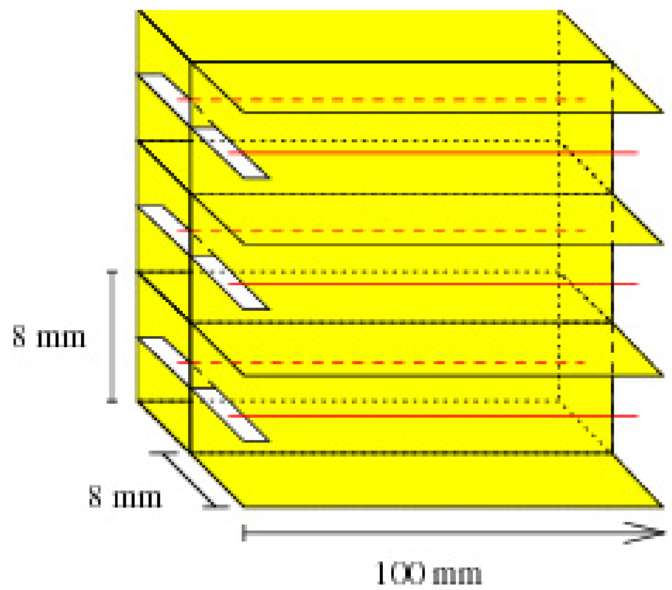

Problems of wire chamber based photon detectors 2

Anode related effects: ageing due to accumulation of polymerisation deposits on the anode wires, particularly in TMAE loaded gases. Consequence: gas amplification drops as a function of deposited charge. A drop of amplification exponentially decreases the efficiency.

- Recovery: Remove deposits by washing the wires with alcohols, or heating. Attractive: in situ heatable anode wires for high rate applications.

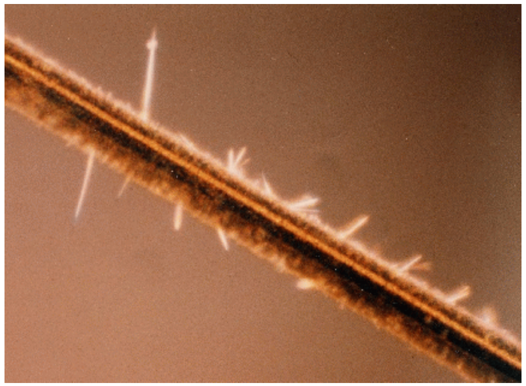

Cathode related effects: Accumulation of polymerisation deposits on the cathode planes (good insulators) can cause a large electric field after enough charge has accumulated, emission of electrons from the cathode - Malter effect.

Summary on RICHes with wire chamber based photon detectors.

- Only UV photons can be detected, their detection is not trivial.
- However: large system have been successfully operated for years.
- Visual photon detection in gas chambers: still being developed.
- High rate operation: problematic, in particular if long term stability is required – much more R+D would be needed to become competitive with PMTs

Vaccuum base photon detectors

Vaccum operation: a large variety of photosensitive material in visible.

RICH counters: preferably highest sensitivity in blue.

Low wavelength cut-off: defined by the window.

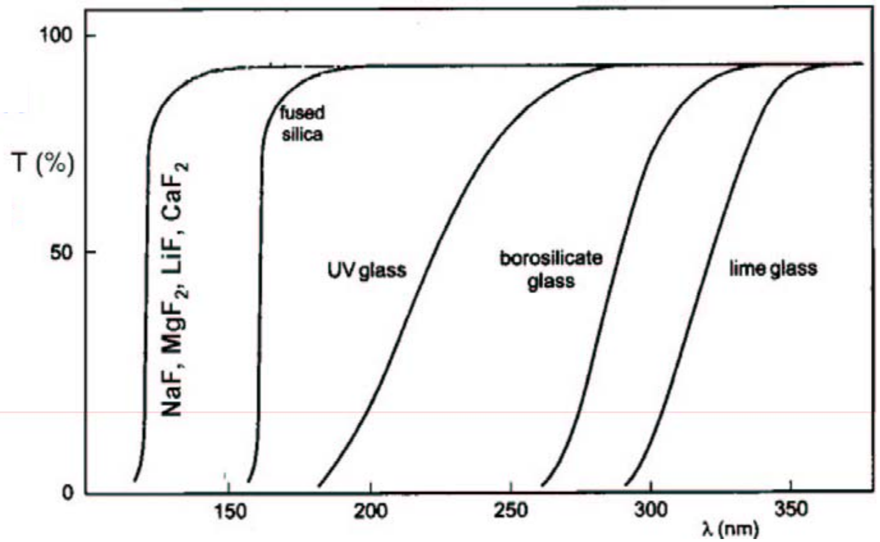

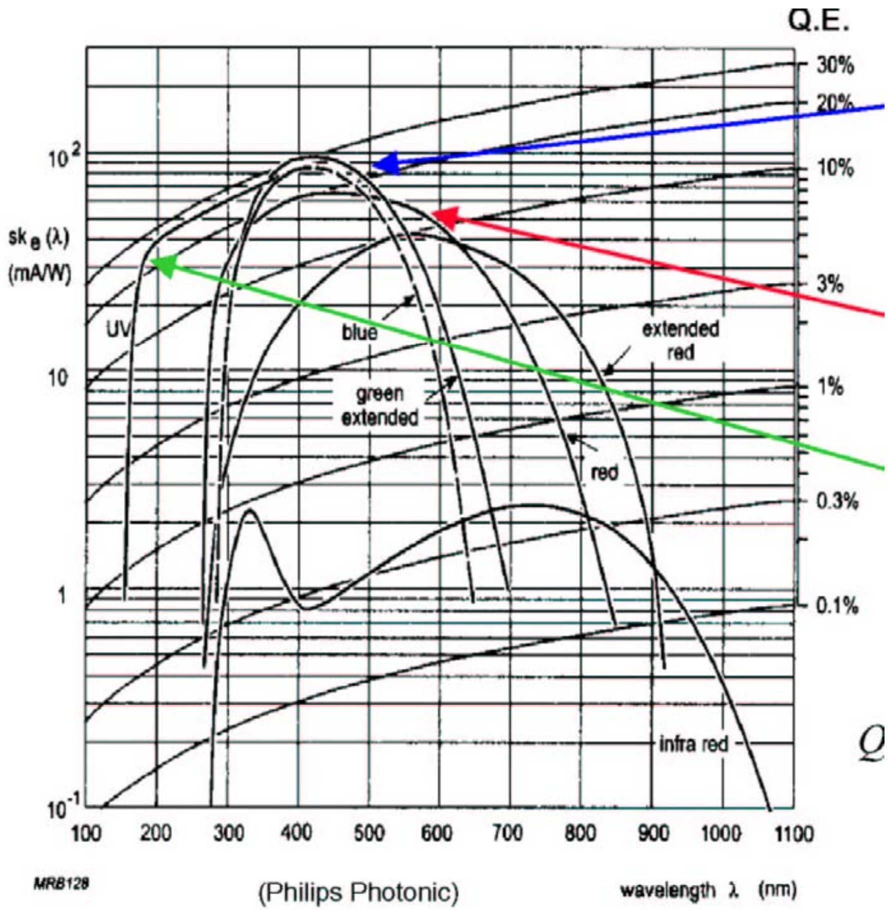

Photomultiplier tubes (PMTs)

Photoelectron signal is amplified by the multiplication at each dynode stage.

Several issues:

- Single photon response
- More than one channel per tube
- Low dead area fraction

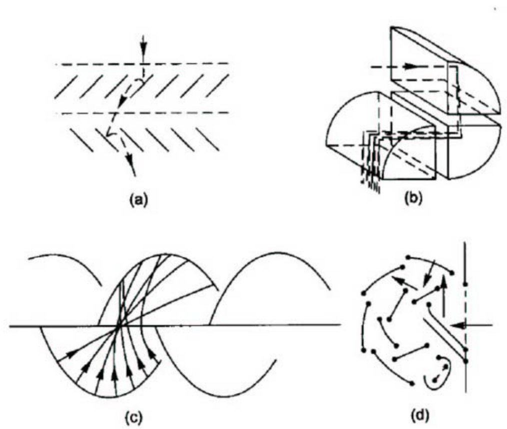

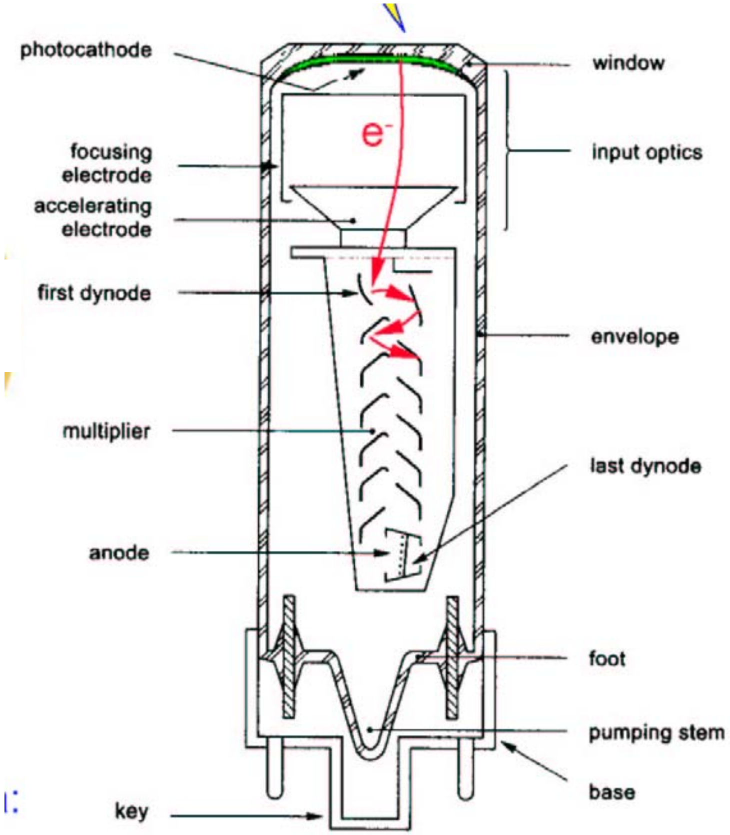

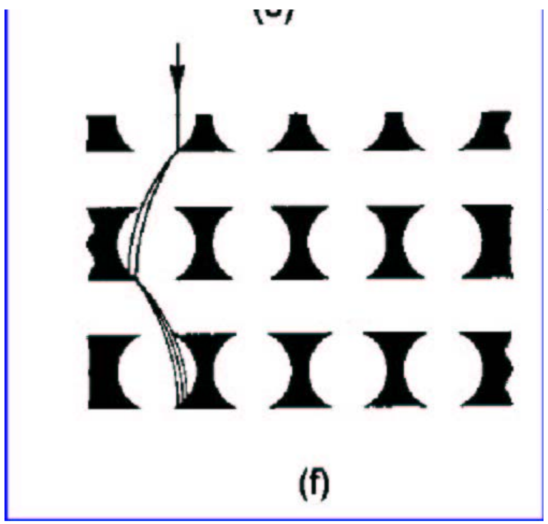

Best structure to implement many anodes with very little cross-talk

Single photon response

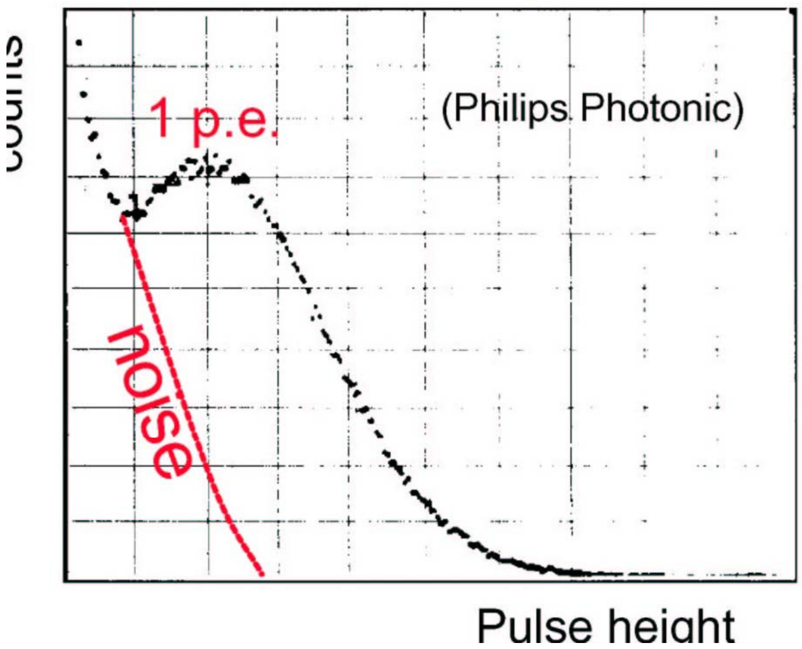

Not trivial to detect single photons in PMTs, most do not have that capability

<- not bad on that scale

Multianode Hamamatsu R5900-M16 PMT: excellent

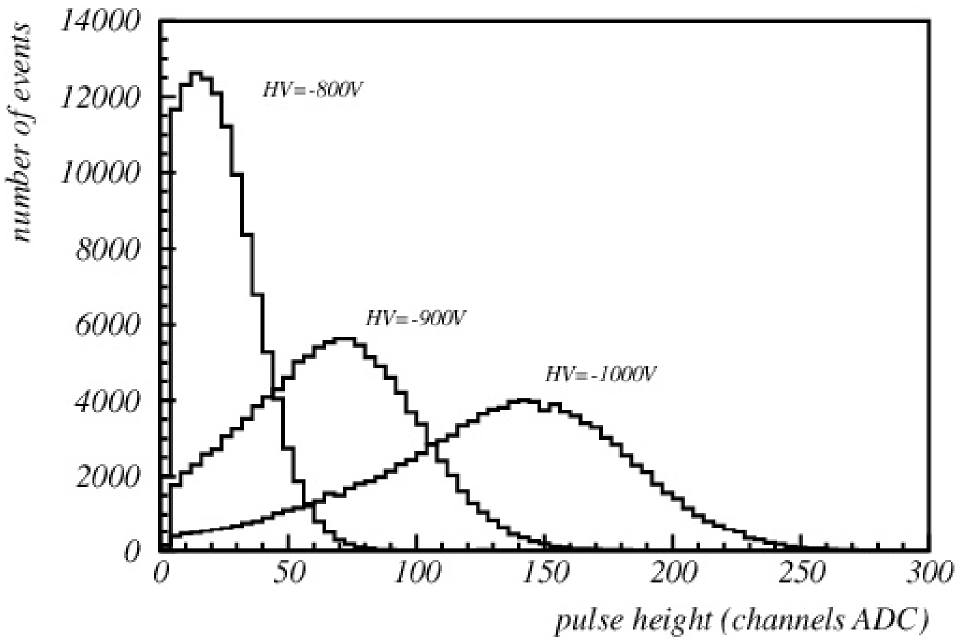

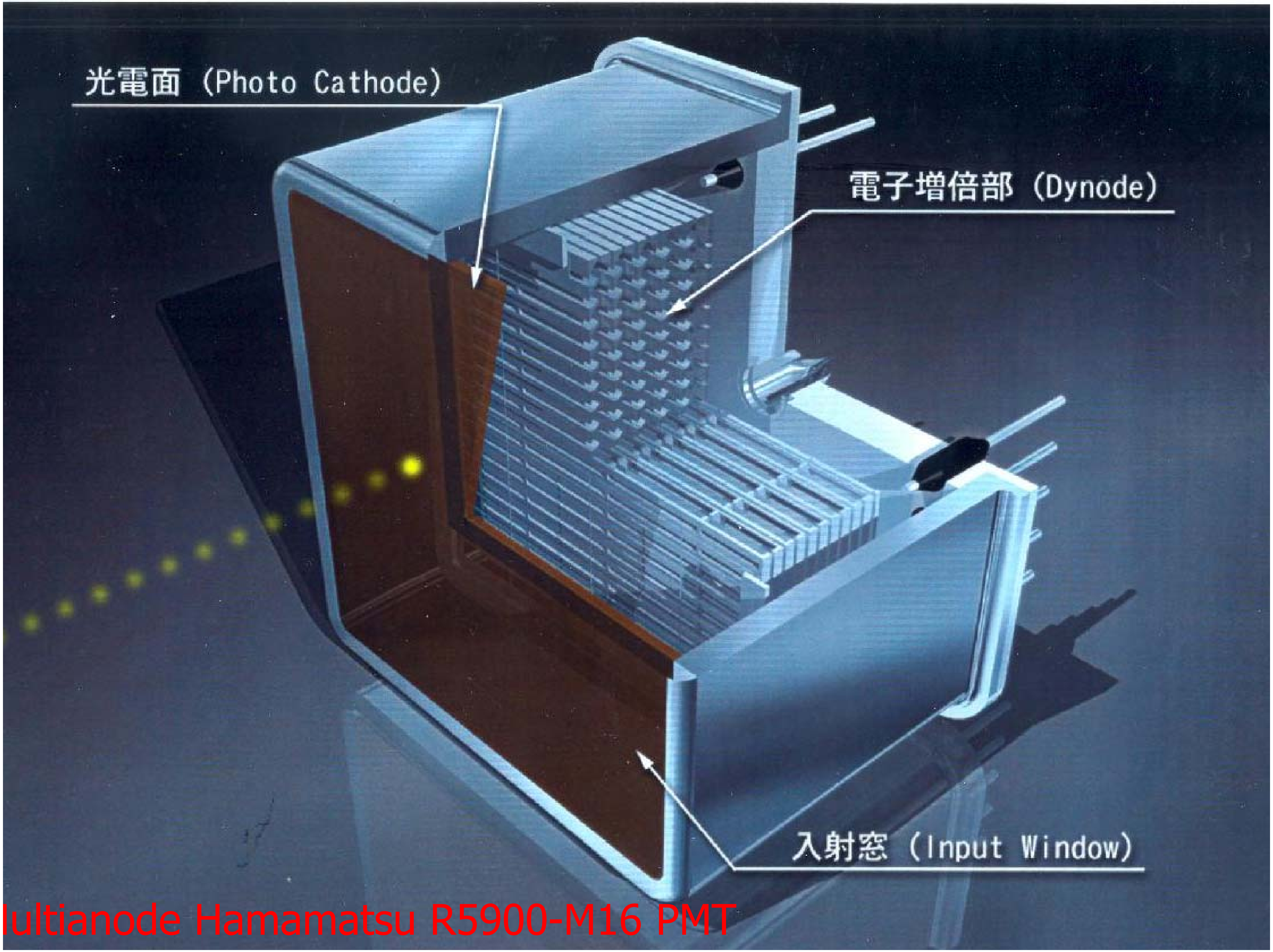

lultianode Hamamatsu R5900-M16 PMT

Light collectors

Used to reduce the dead area between photon detector segments (in particular in the case of PMTs), or to adapt the required photon detector granularity to the PMT (pad) size

- Winston cones
- Reflectors
- Lens combinations

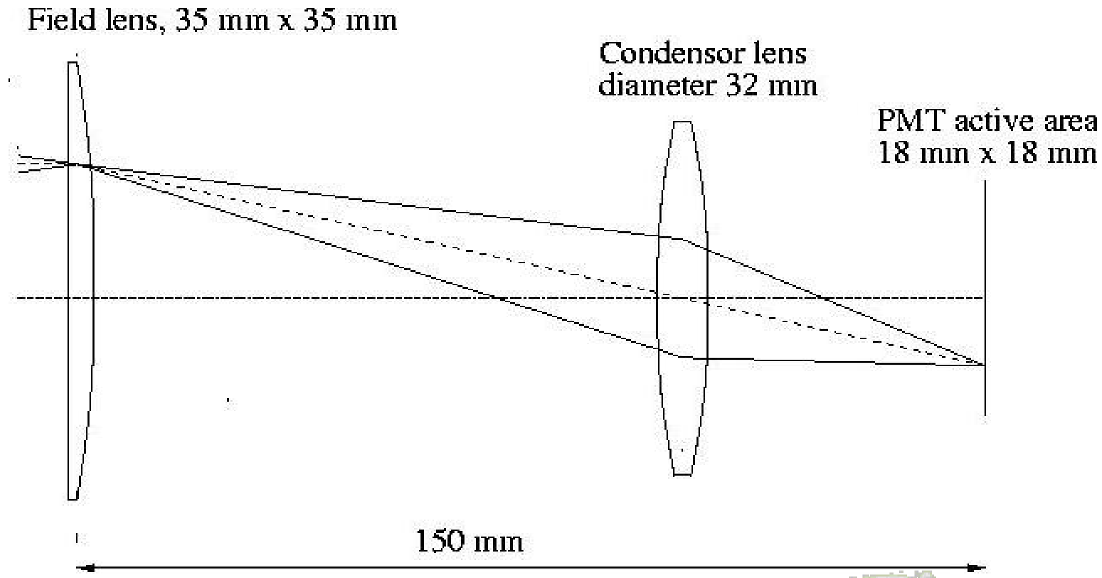

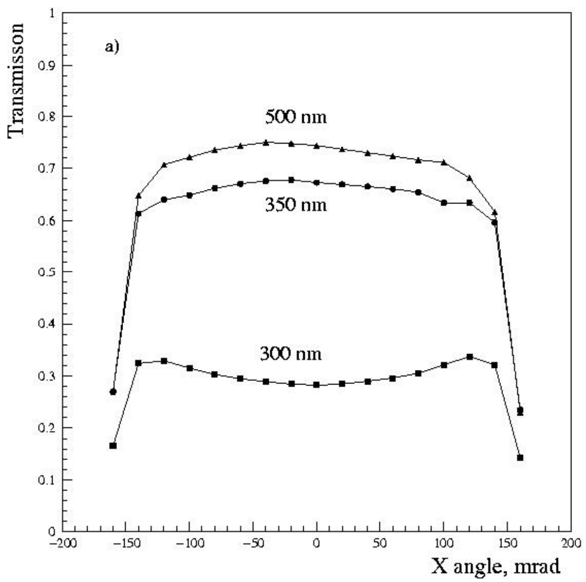

Example: Optical system for light collection and demagnification of the HERA-B RICH.

→ angular acceptance, material transmission

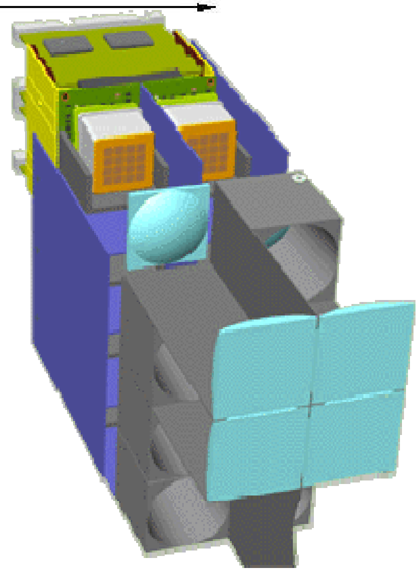

RICH photon detector with multi-anode PMTs: HERA-B

2300 PMT, 16 and 4 channel type, 30.000 electronic channels

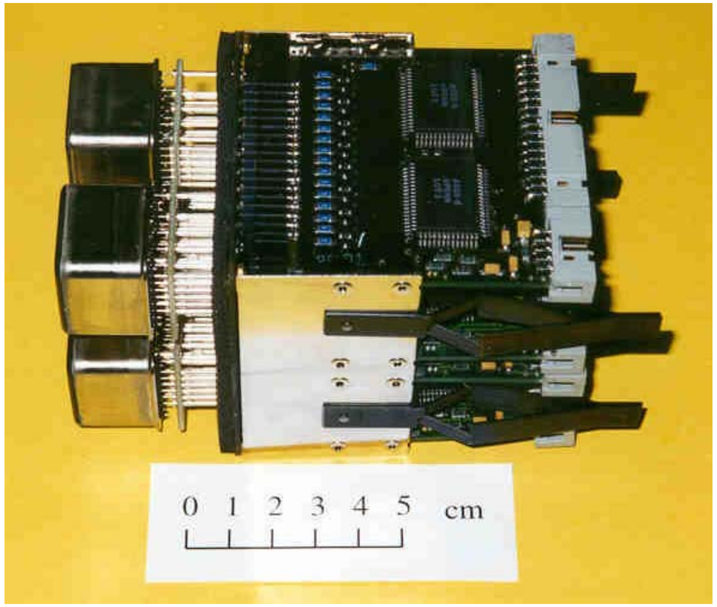

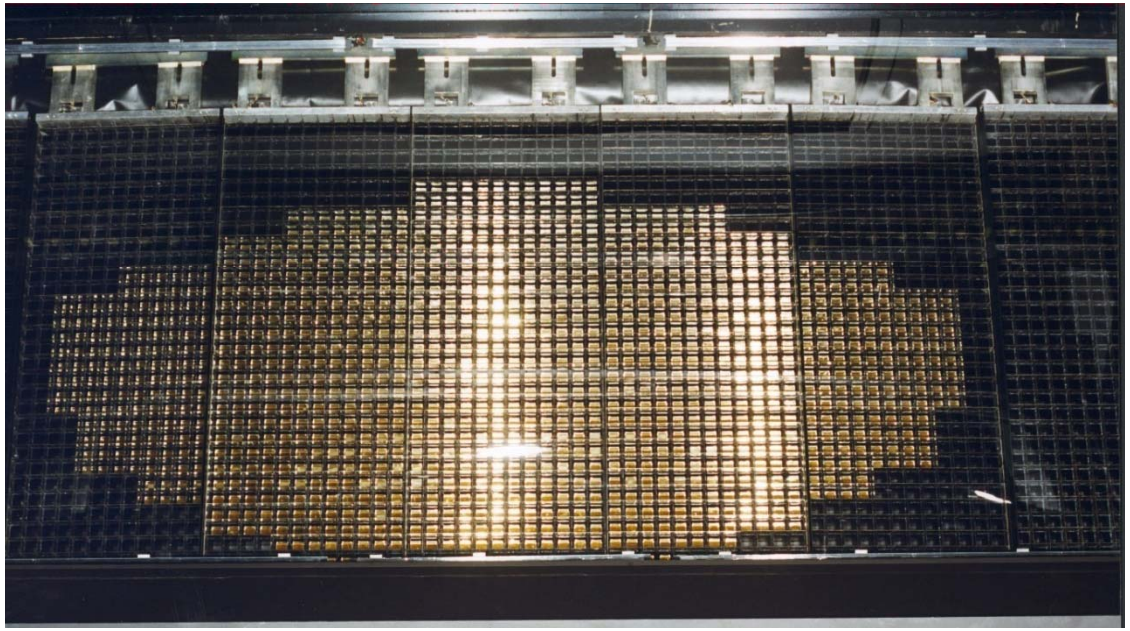

Detect photolectron in silicon: hybrid photon detector - HPD

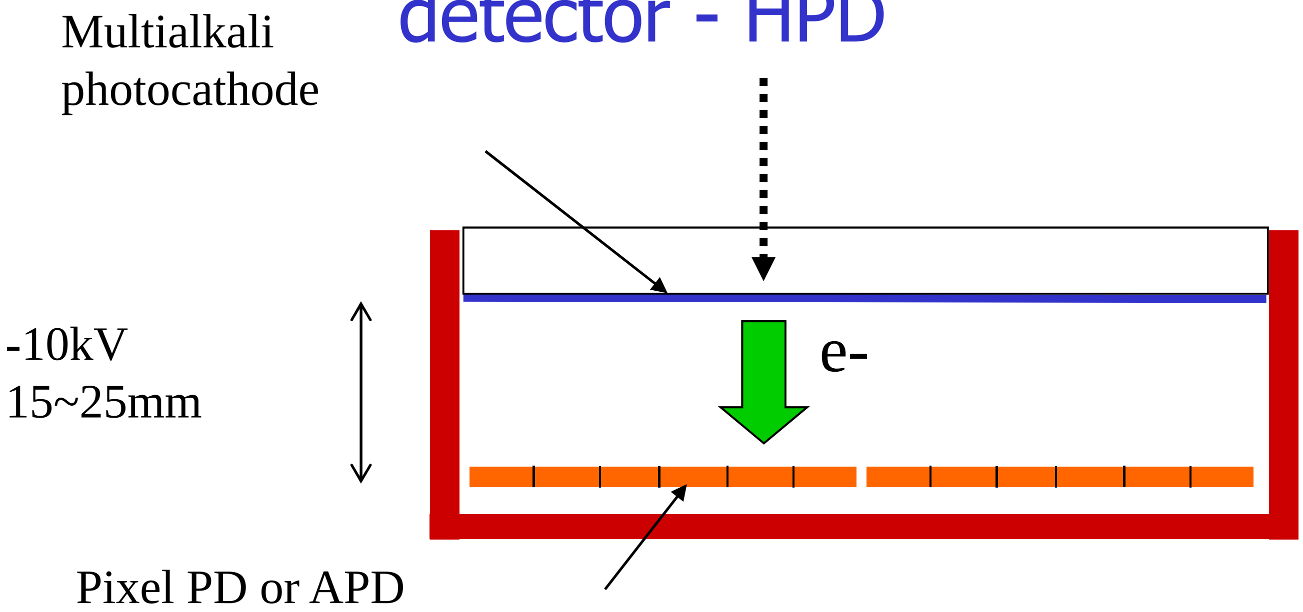

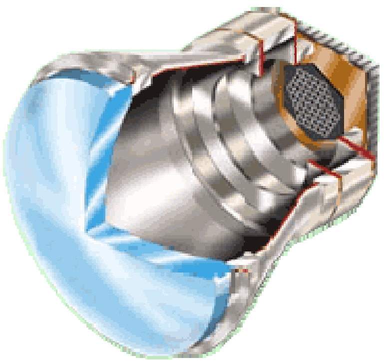

Focusing in E field with additional electrodes

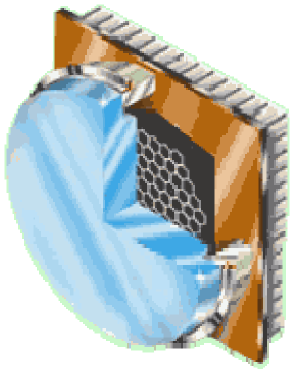

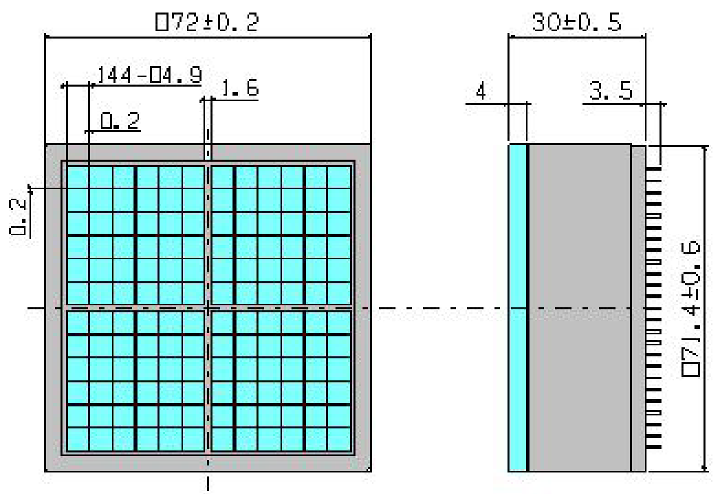

No focusing in E field

Hybrid photon detector – focusing type

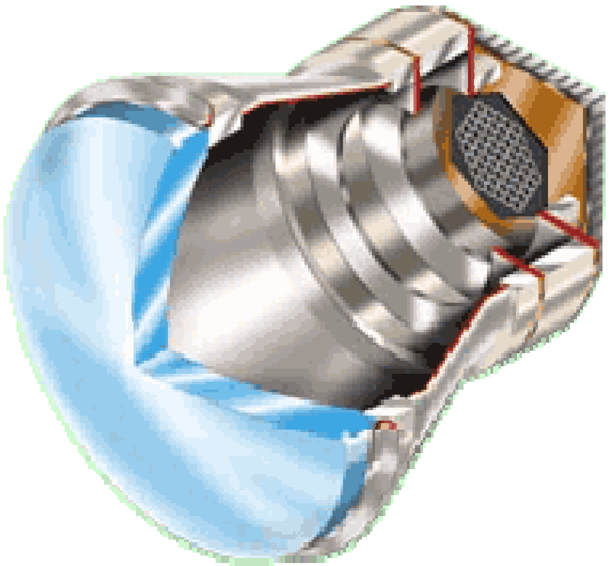

Focusing in E field with additional electrodes

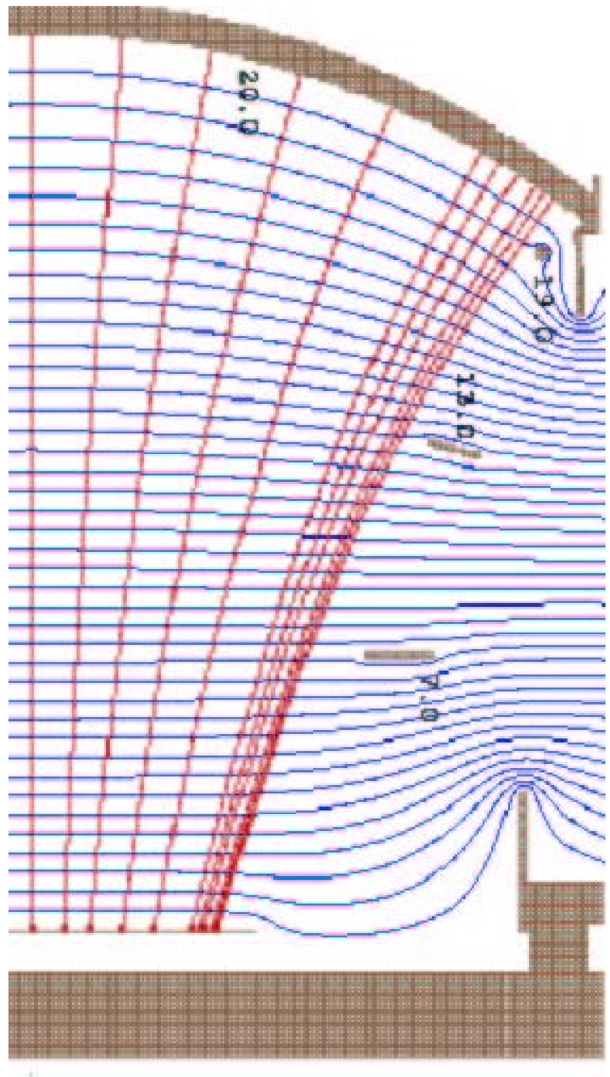

Visual photon detection in silicon

Need a very low noise device – one possibility: run at liquid He temperatures

VLPC: visual light photon counter

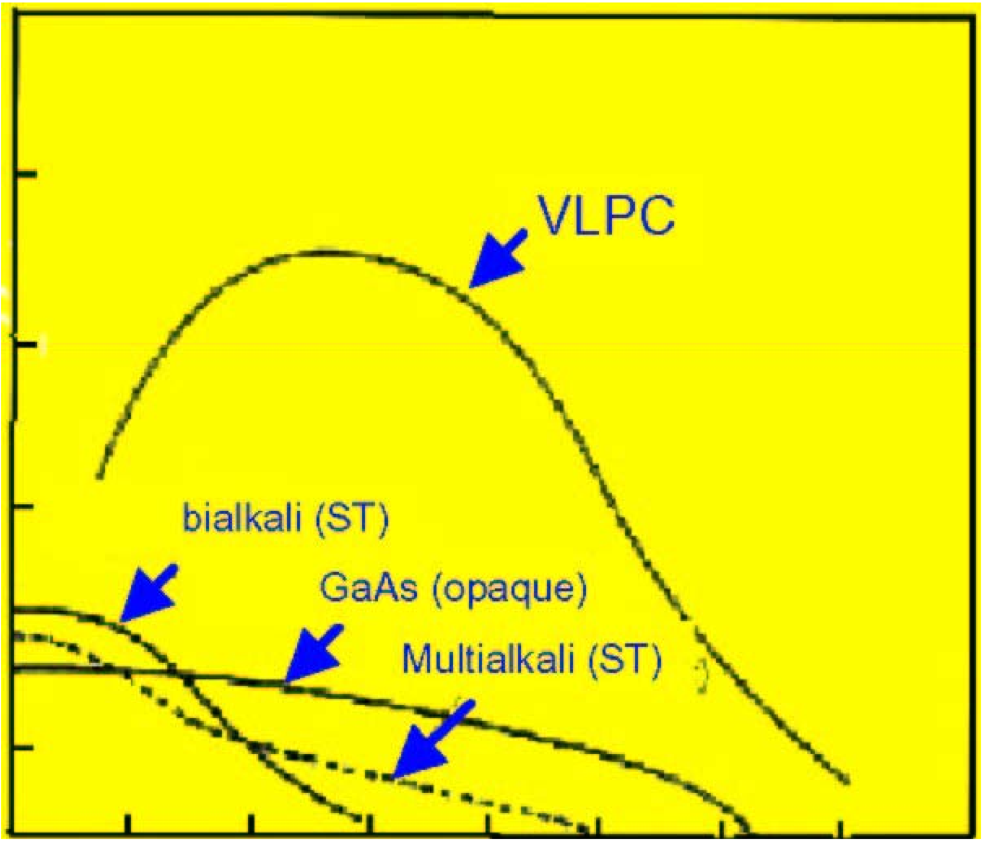

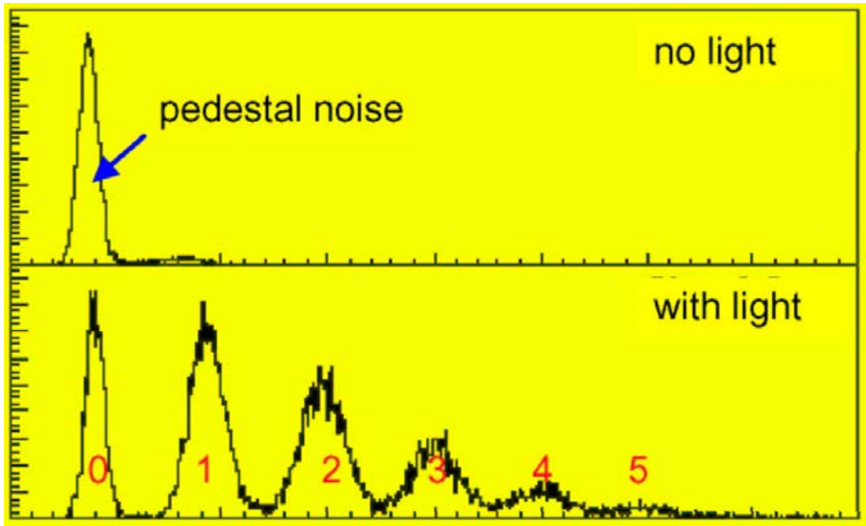

Polprevodniški detektorji

Kako se polvod. detektorji kvalificirajo za detekcijo posameznih (ali malega števila) fotonov?

- PIN diode: standardne (n.pr. CsI kalorimetri: CLEO, Belle, BaBar), prag ~100 fotonov
- APD: prag ~20 fotonov, prvi večji eksperiment: elektromagnetni kalorimeter EMC v CMS.
- SiPM (GAPD): v principu lahko z njimi zaznavamo posamezne fotone

Avalanche Photodiodes or Geiger-mode Avalanche Photodiodes

Avalanche photodiodes (APDs) have internal gain which improves the signal to noise ratio compared to normal photodiodes but still some 20 photons are needed for a detectable signal. The excess noise, the fluctuations of the avalanche multiplication, limits the useful range of gain.

Geiger-mode Avalanche photodiodes (G-APDs or SiPMs) can detect single photons and the gain is in the range of 10^5 to 10^7 and no (or at most a simple) amplifier is needed. Pickup noise is no more a concern (no shielding). The excess noise factor can be close to 1 (APDs >2, PMTs: 1.2).

SiPMs as photon detectors for RICH

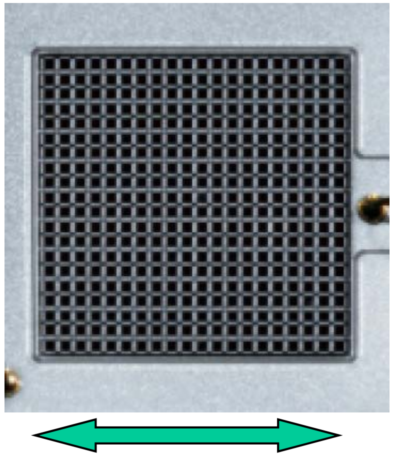

SiPM is an array of APDs operating in Geiger mode. Characteristics:

- low operation voltage ~ 10-100 V
- gain ~ 10^6
- peak PDE up to 65%(@400nm)

  $PDE = QE \times \varepsilon_{geiger} \times \varepsilon_{geo}$
- ε_{geo} – dead space between the cells
- time resolution ~ 100 ps
- works in high magnetic field
- dark counts ~ few 100 kHz/mm^2
- radiation damage (p,n)

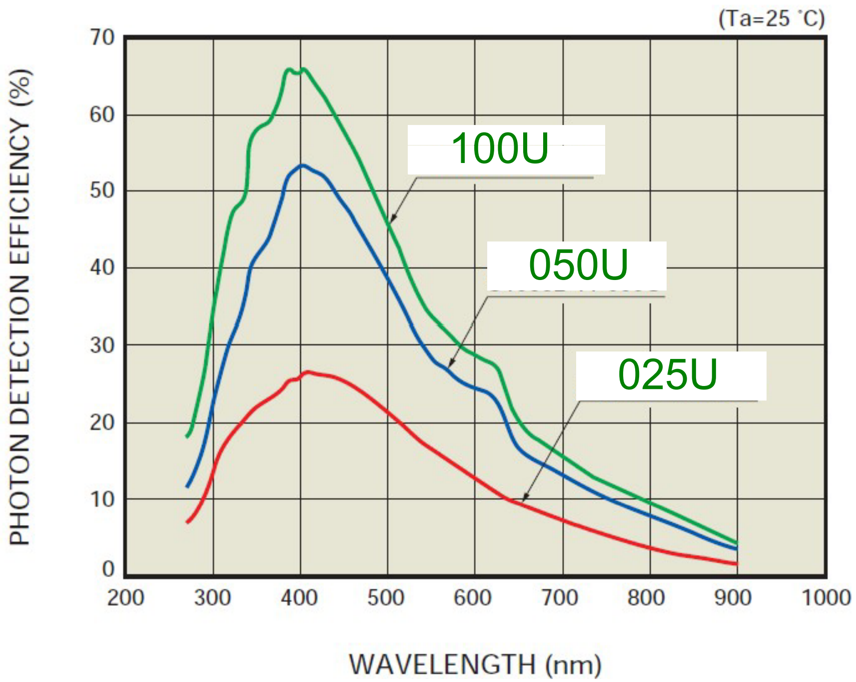

Hamamatsu MPPC: S10362-11

Surface sensitivity for single photons 4

Hamamatsu MPPCs

H100C

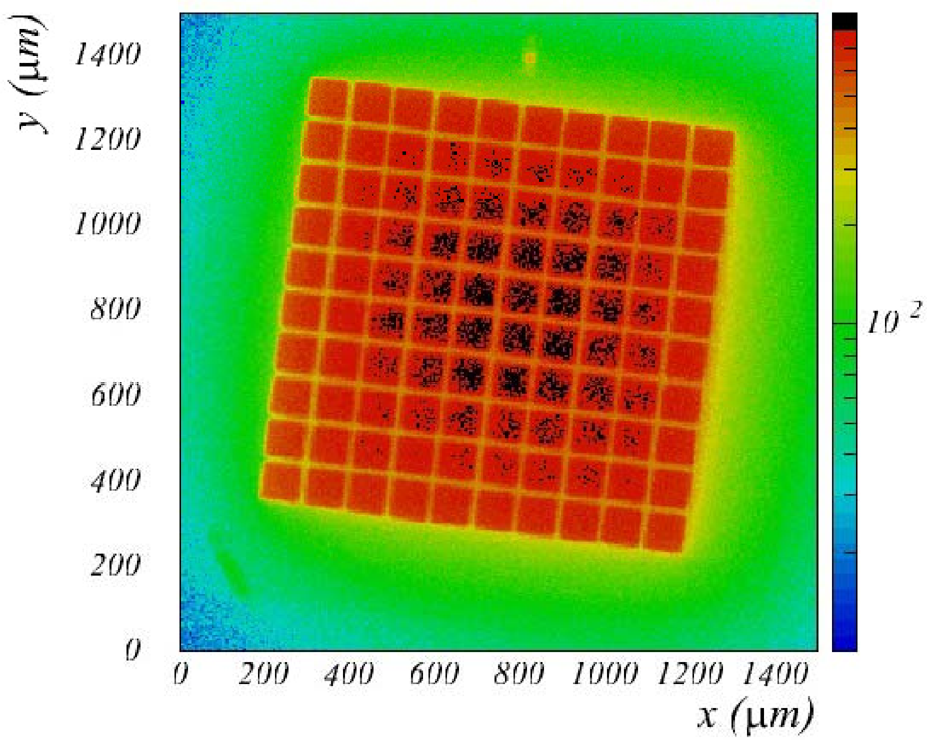

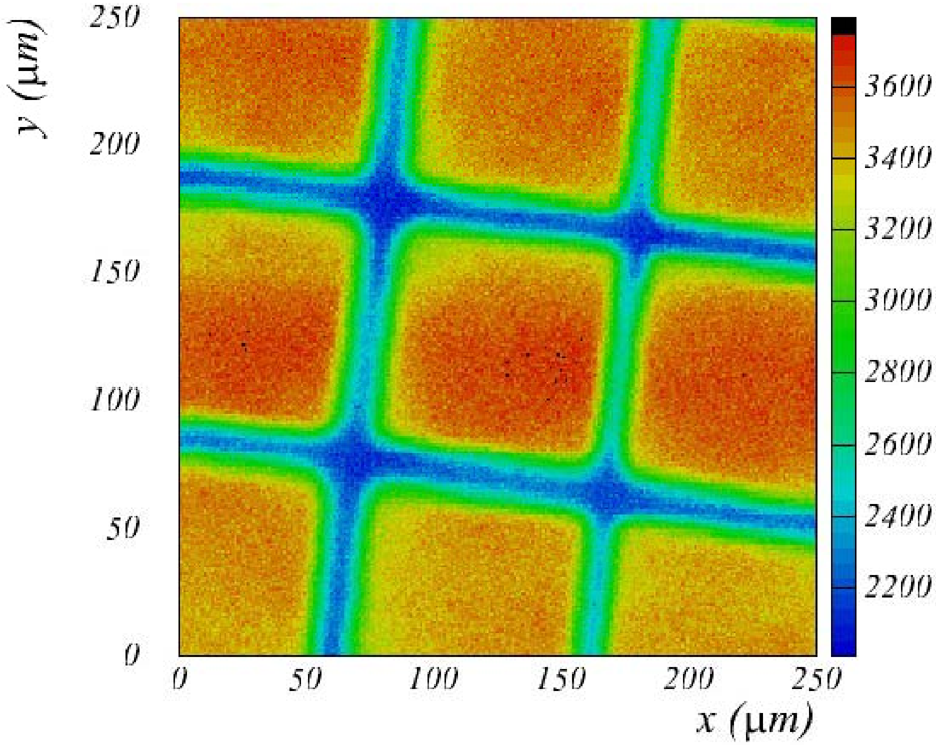

Time resolution: blue vs red

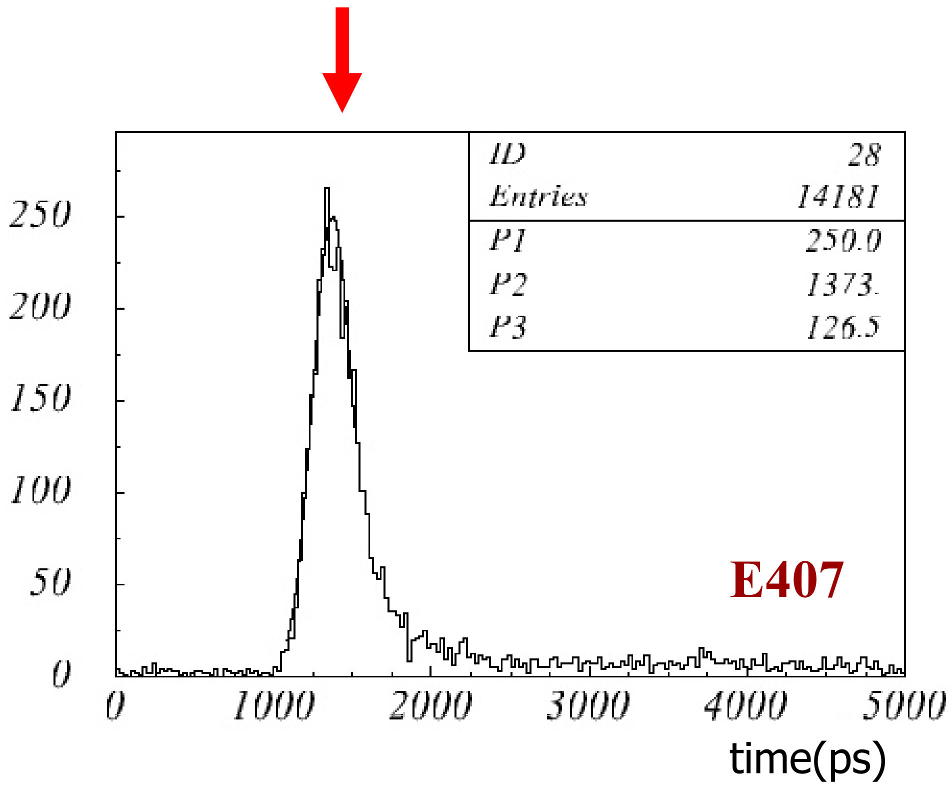

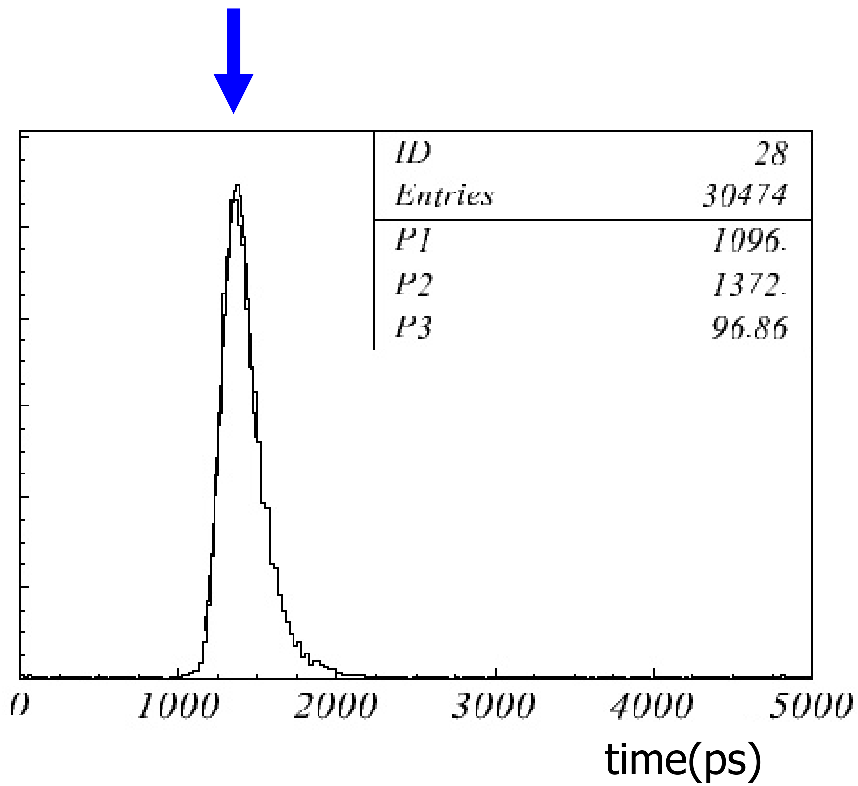

	E407	S137	H100C	H025C
σ_{red} (ps)	**127**	**182**	**145**	**154**
σ_{blue} (ps)	**97**	**151**	**136**	**135**

- $\sigma \approx 100$ ps

- $\sigma_{red} > \sigma_{blue}$

Expected number of photons for aerogel RICH

with multianode PMTs or SiPMs(100U), and
aerogel radiator: thickness 2.5 cm, n = 1.045
and transmission length (@400nm) 4 cm.

N_{SiPM}/N_{PMT}~5

Assuming 100% detector active area

Never before tested in a RICH where we have to detect single photons. ← Dark counts have single photon pulse heights (rate 0.1-1 MHz)

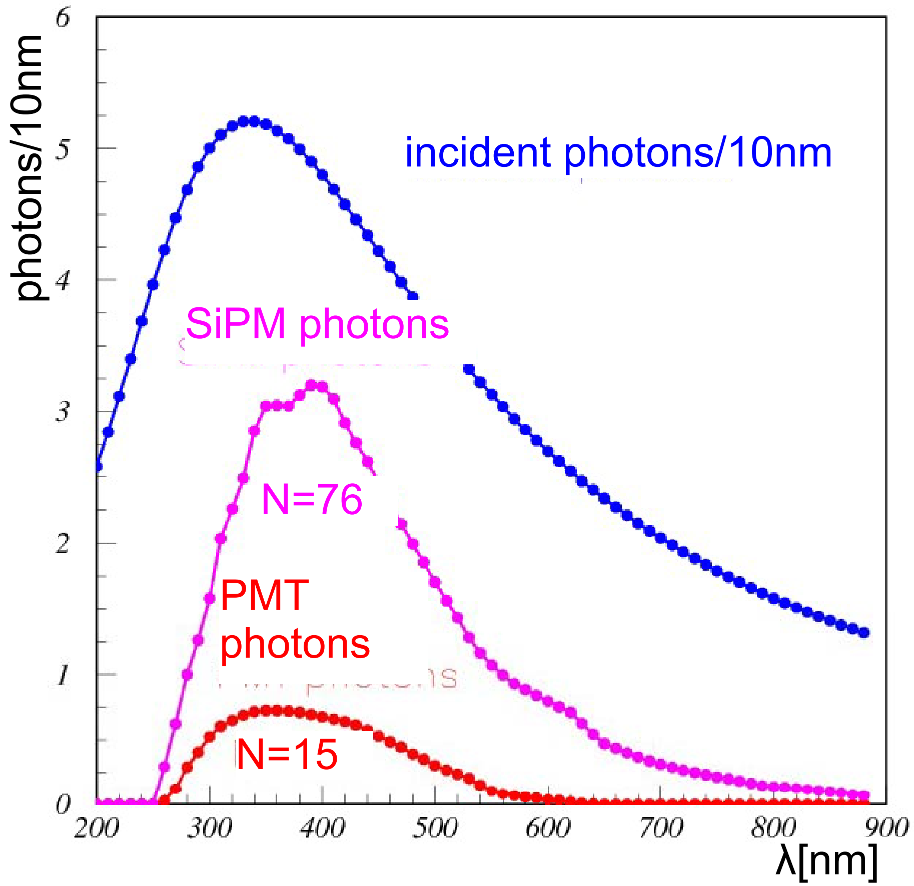

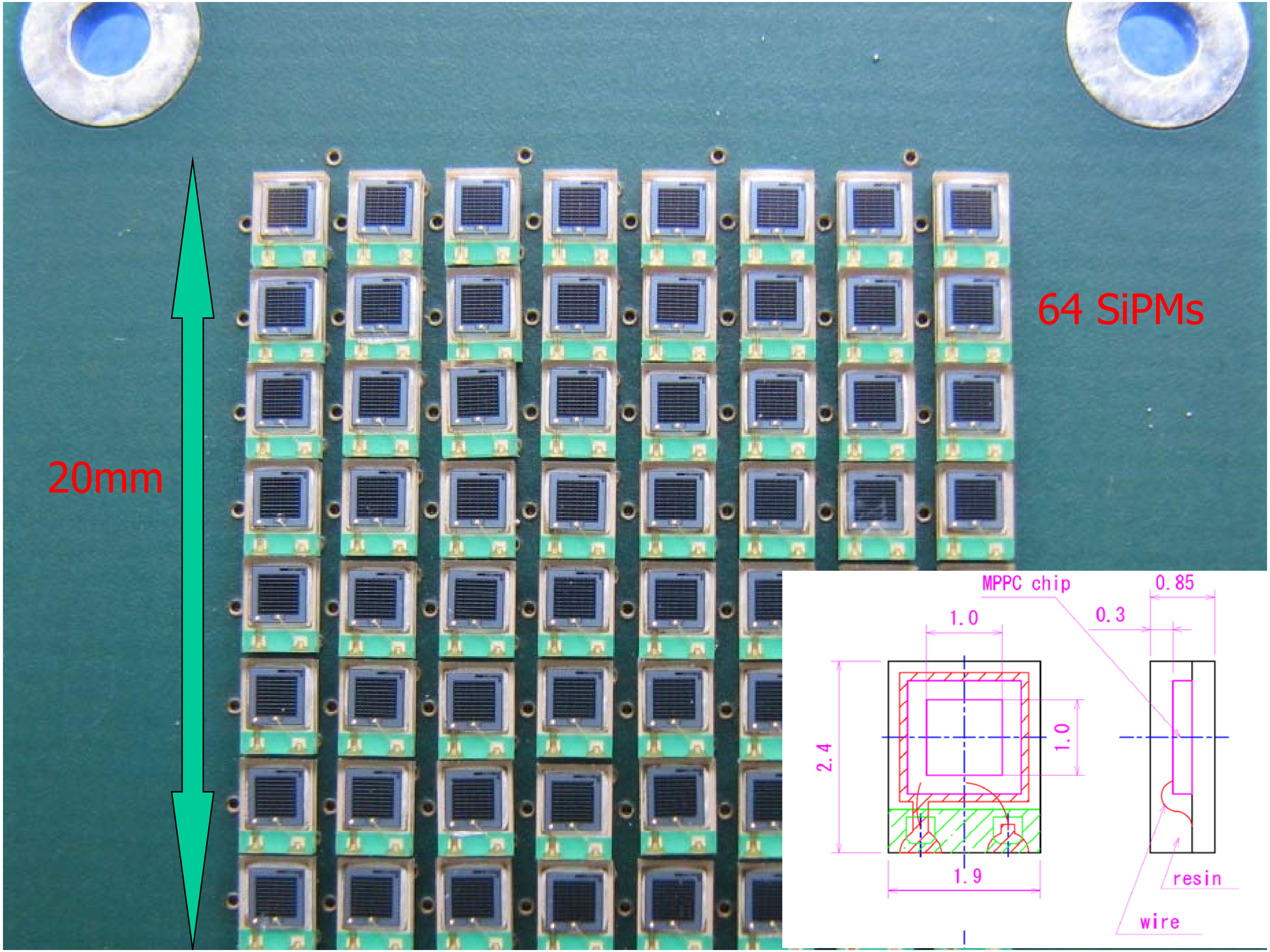
64 SiPMs
20mm
MPPC chip
0.85
1.0
0.3
2.4
1.0
1.9
resin
wire

Increase the active area: use light guides

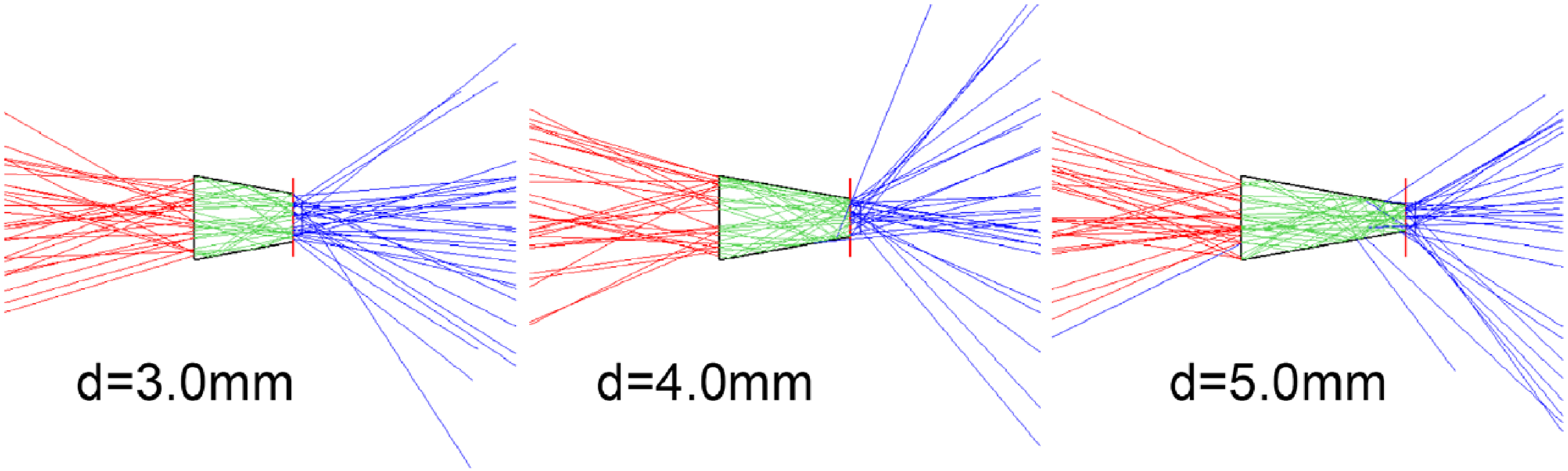

d (mm)	out (mm)	accept. (%)
3.0	1.48	51.6
3.1	1.45	54.0
3.2	1.41	55.7
3.3	1.38	57.8
3.4	1.34	59.2
3.5	1.31	61.0
3.6	1.27	62.6
3.7	1.24	63.1
3.8	1.20	64.4
3.9	1.16	64.4
4.0	**1.13**	**64.9**
4.1	1.09	64.3
4.2	1.06	63.8
4.3	1.02	62.8
4.4	0.99	61.8
4.5	0.95	60.5
4.6	0.92	58.5
4.7	0.88	56.4
4.8	0.85	54.6
4.9	0.81	51.9

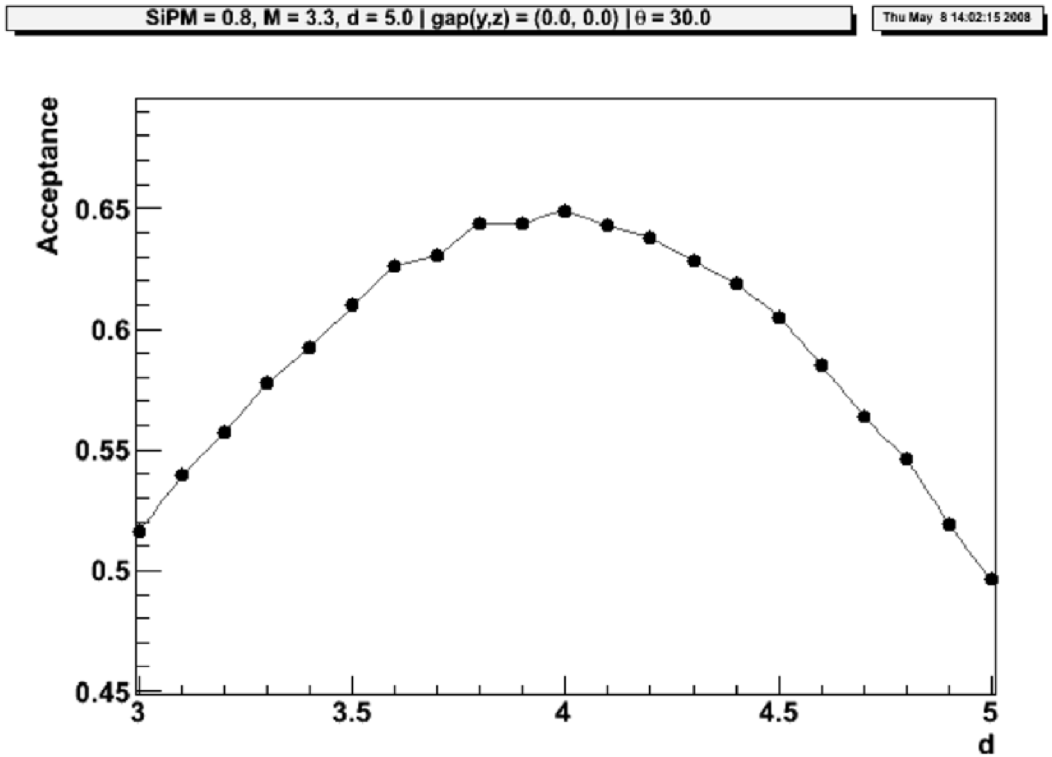

Detector module for beam tests at KEK

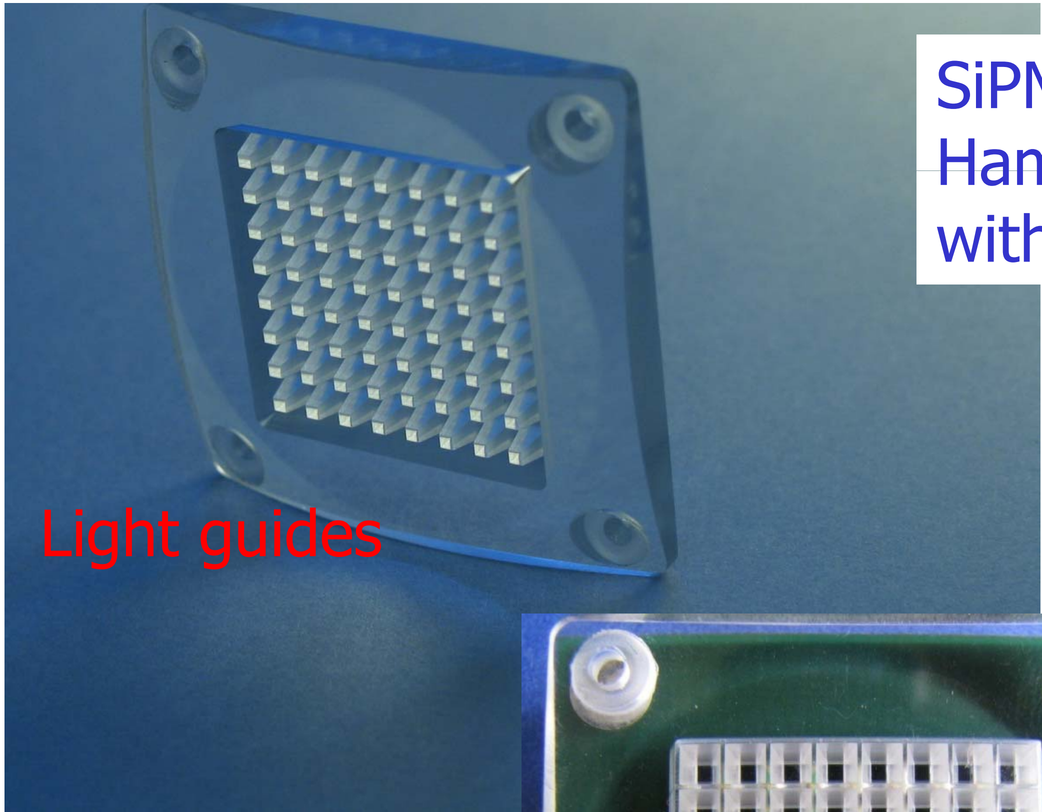

Light guides

SiPMs: array of 8x8 SMD mount Hamamatsu S10362-11-100P with 0.3mm protective layer

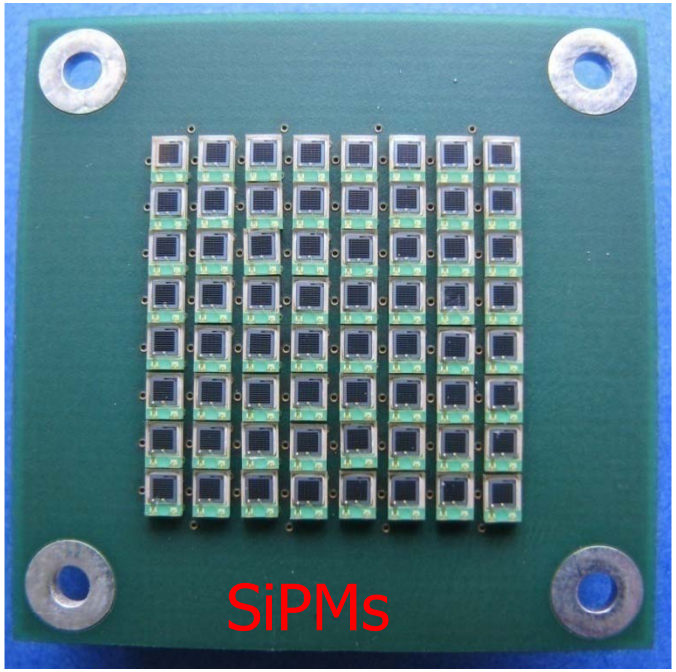

SiPMs

2cm

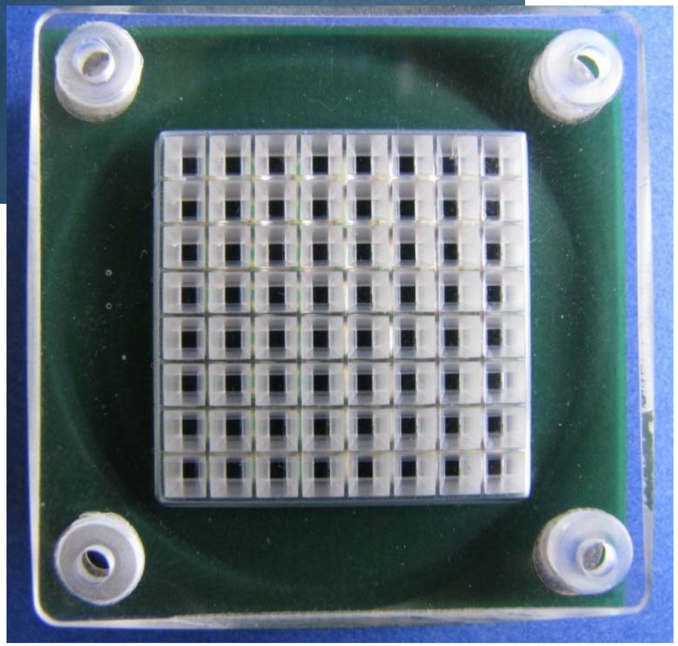

SiPMs + light guides

Cherenkov angle distributions

- background subtracted distributions
- ratio of detected photons w/ and w/o: ~ 2.3
- resolution within expectations (14.5mrad)

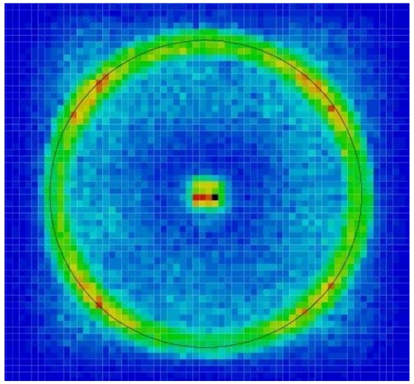

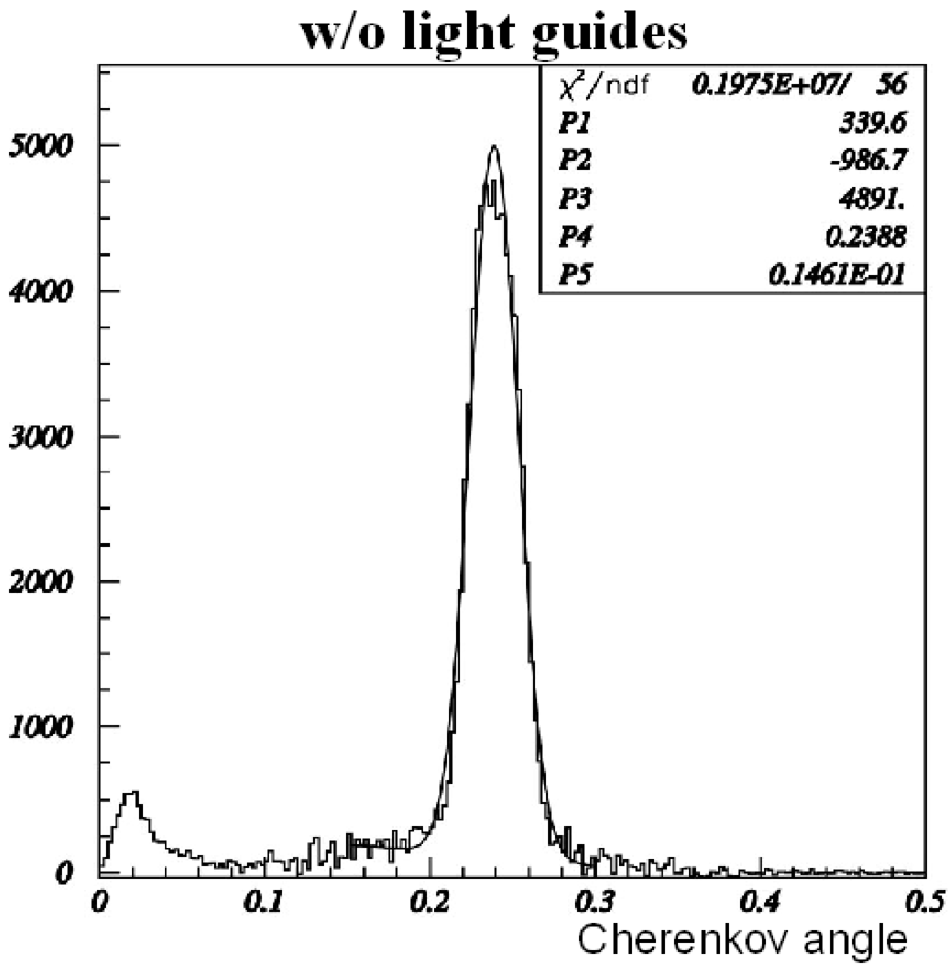

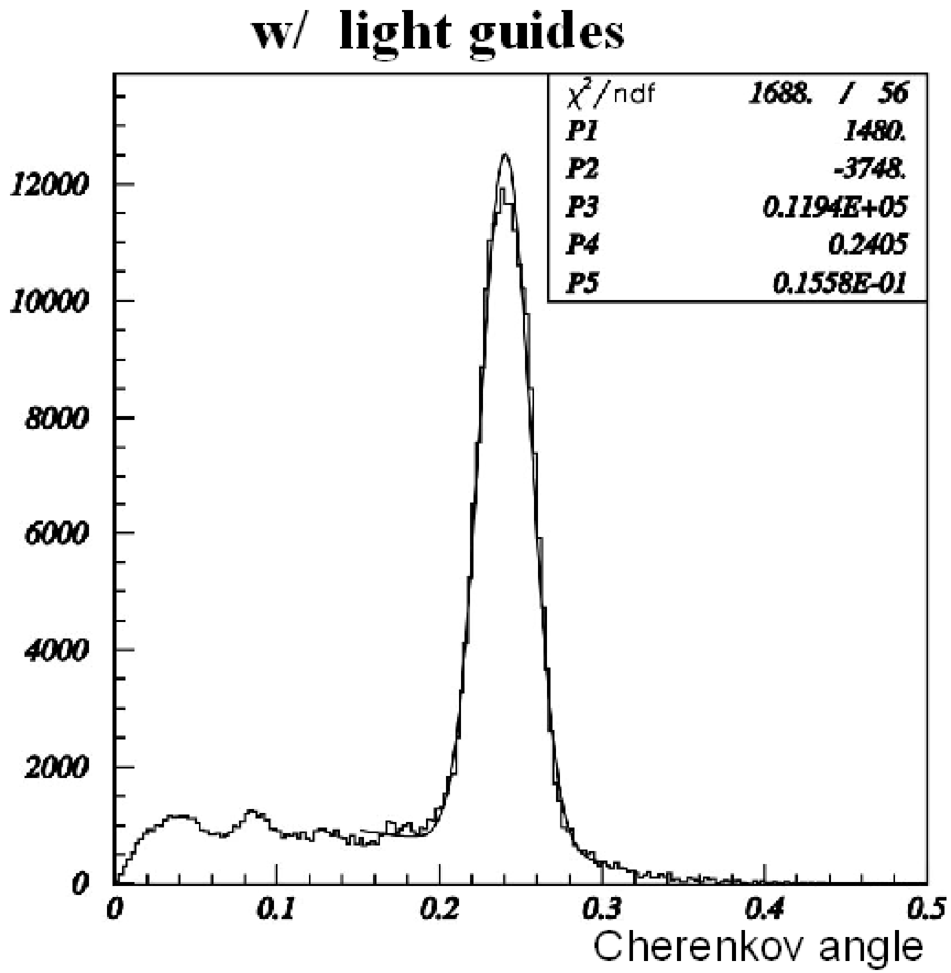

Transition radiation

X rays emitted at the boundary of two media with different refractive indices, emission angle ~1/γ

Emission rate depends on γ (Lorentz factor): becomes important at γ~1000

- Electrons at 0.5 GeV
- Pions, muons above 100 GeV

In between: discrimination e vs pions, mions

Detection of X rays: high Z gas – Xe

Few photons per boundary can be detected

Need many boundaries

- Stacks of thin foils or
- Porous materials – foam with many boundaries of individual ‘bubbles’

Transition radiation - 1

Separation of X ray detection – high energy deposit on one place – against ionisation losses

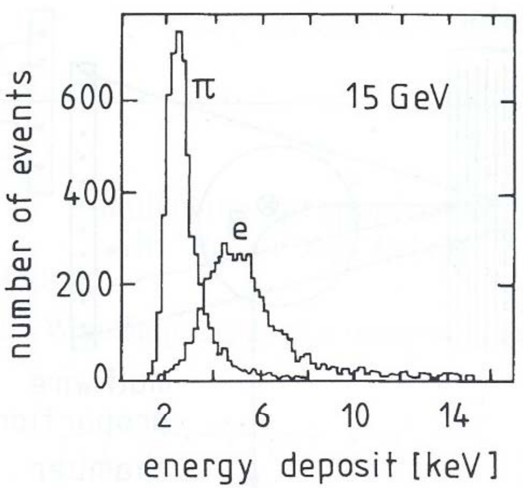

Fig. 6.25. Energy-loss distribution of 15 GeV electrons and pions in a transition radiation detector [467].

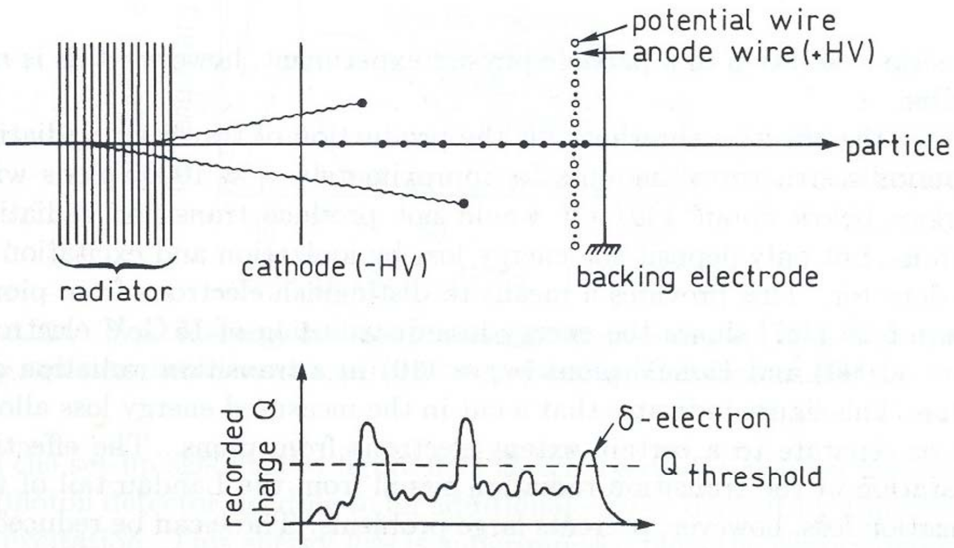

Fig. 6.26. Principle of separating ionization energy loss from the energy loss from emission of transition radiation photons.

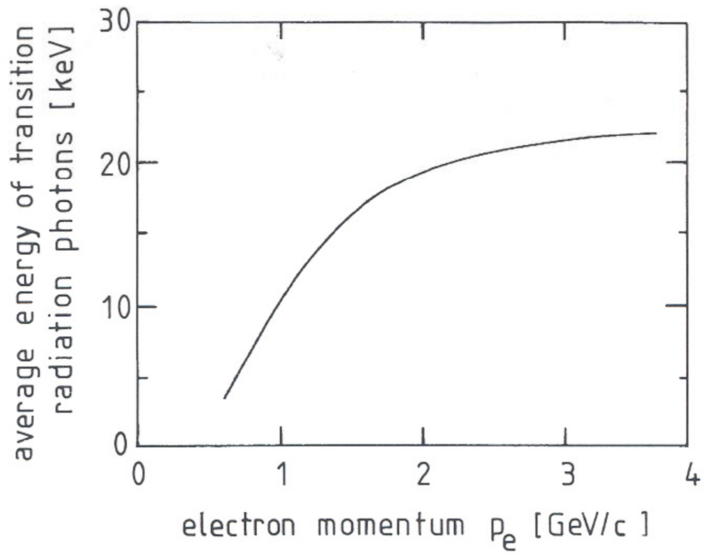

Transition radiation - 2

Example of performance –
NOMAD experiment

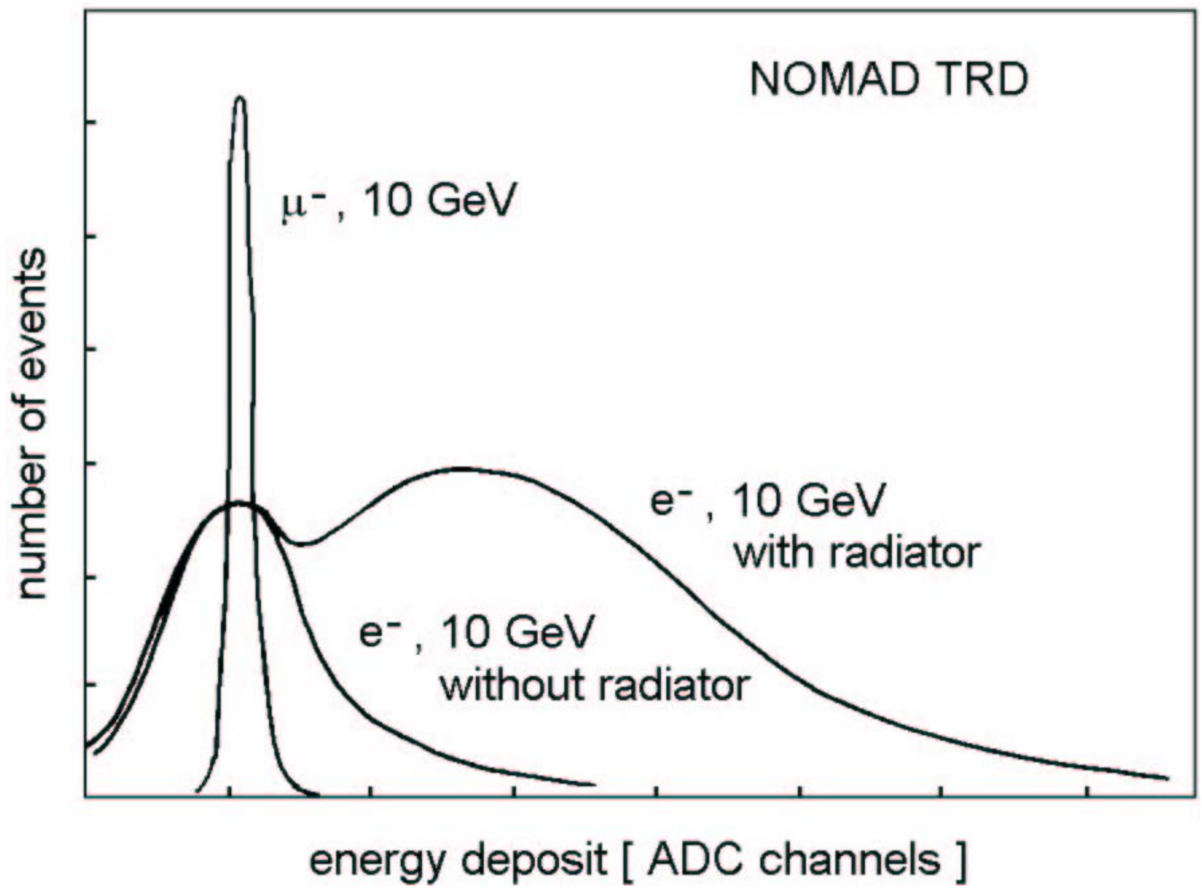

Transition radiation - 3

Example of performance 2

Radiator: organic foam
between the detector tubes
(straws made of capton
foil)

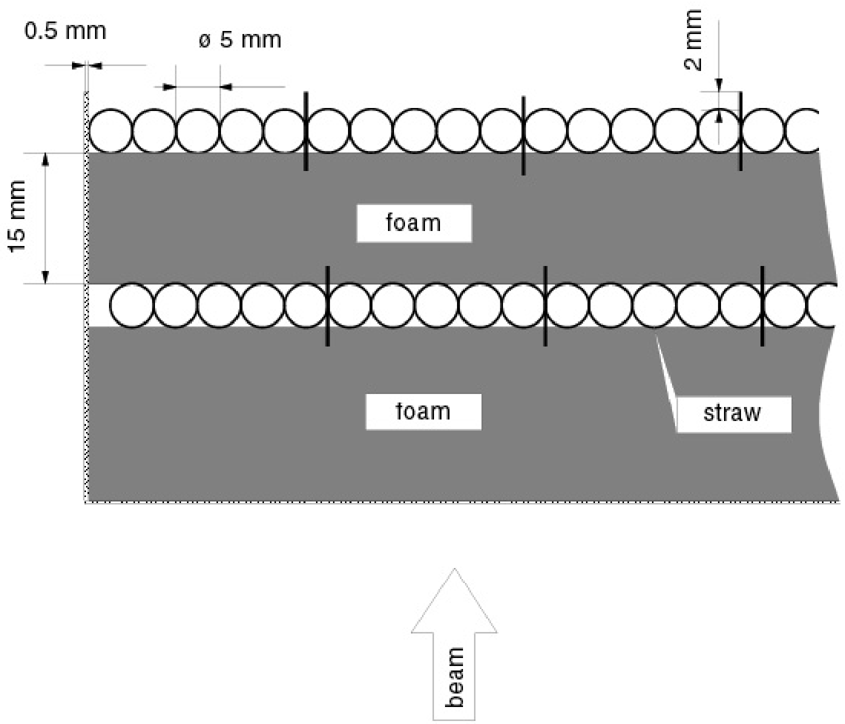

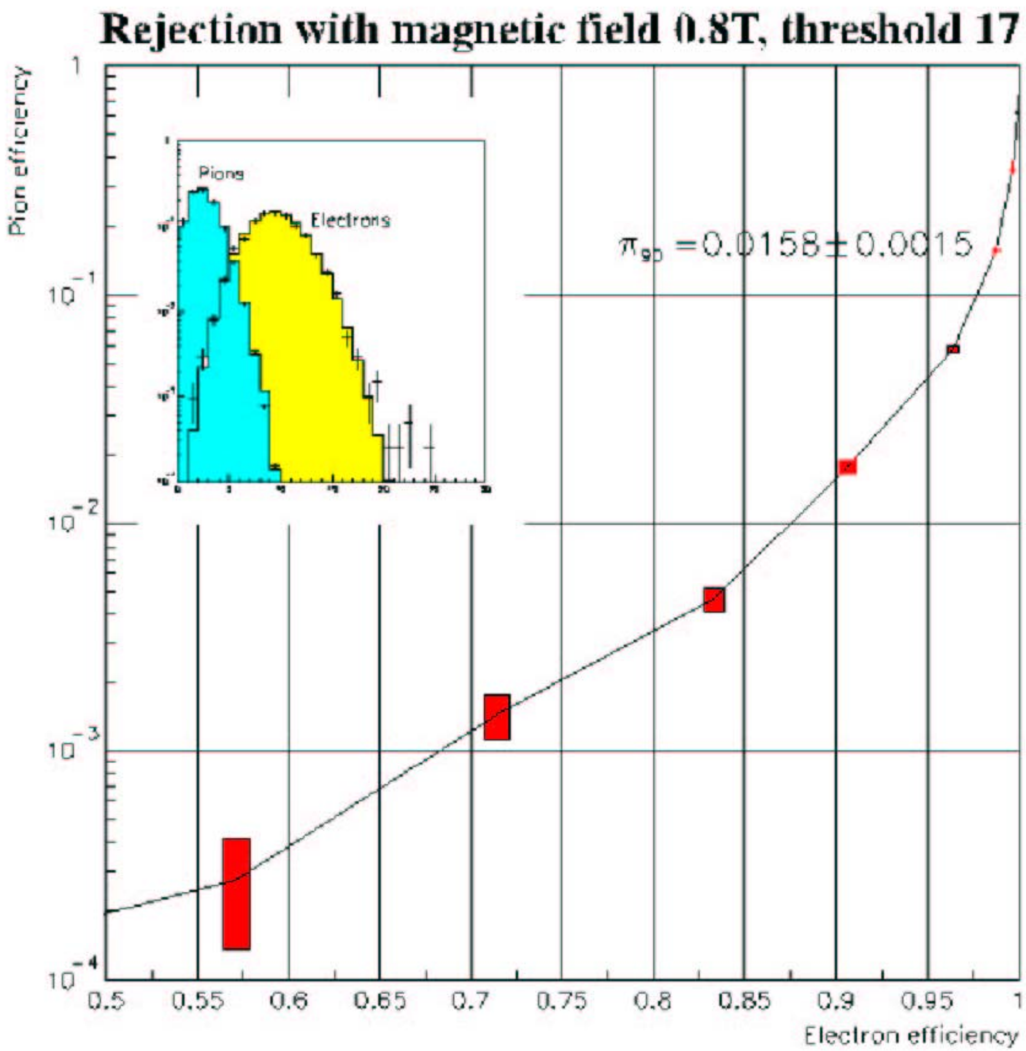

Transition radiation detector in ATLAS: combination of a tracker and a transition radiation detector

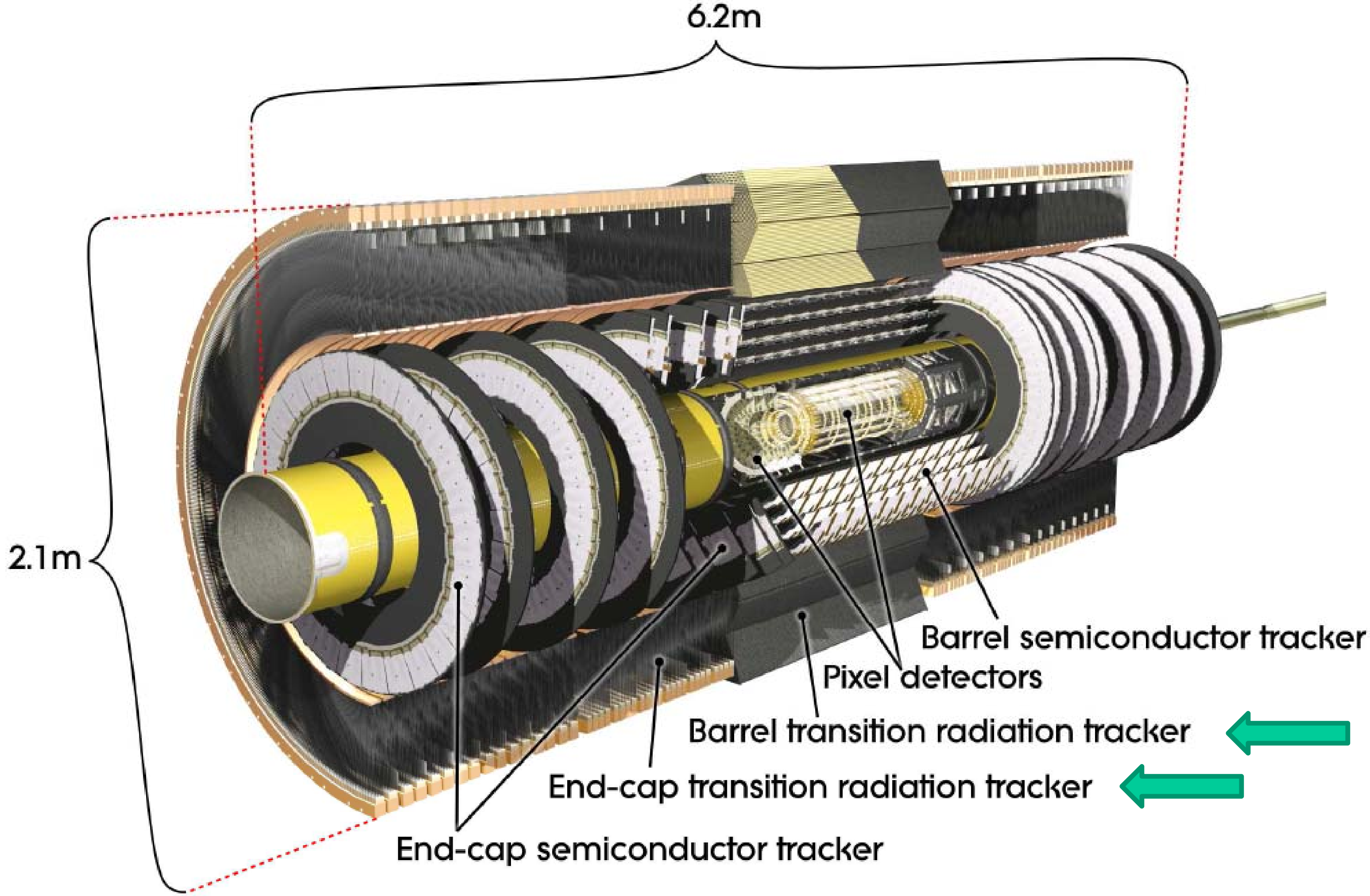

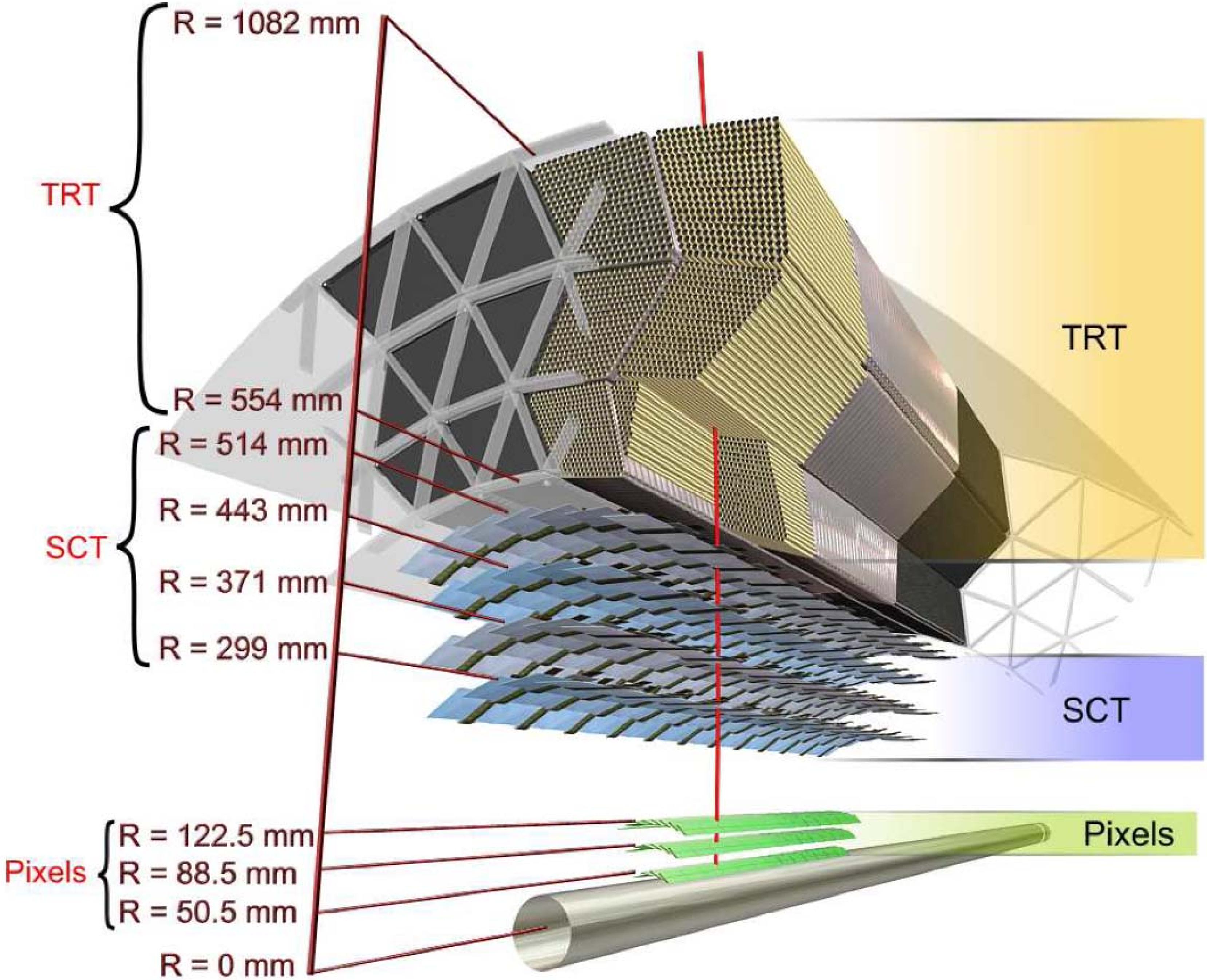

R = 1082 mm
TRT
R = 554 mm
R = 514 mm
R = 443 mm
SCT
R = 371 mm
R = 299 mm
R = 122.5 mm
Pixels
R = 88.5 mm
R = 50.5 mm
R = 0 mm
TRT
SCT
Pixels

ATLAS TRT: combination of Transition Radiation detector and a Tracker

Radiator: 3mm thick layers made of polypropylene-polyethylene fibers with ~19 micron diameter, density: 0.06 g/cm^3

Straw tubes: 4mm diameter with 31 micron diameter anode wires, gas: 70% Xe, 27% CO_2, 3% O_2.

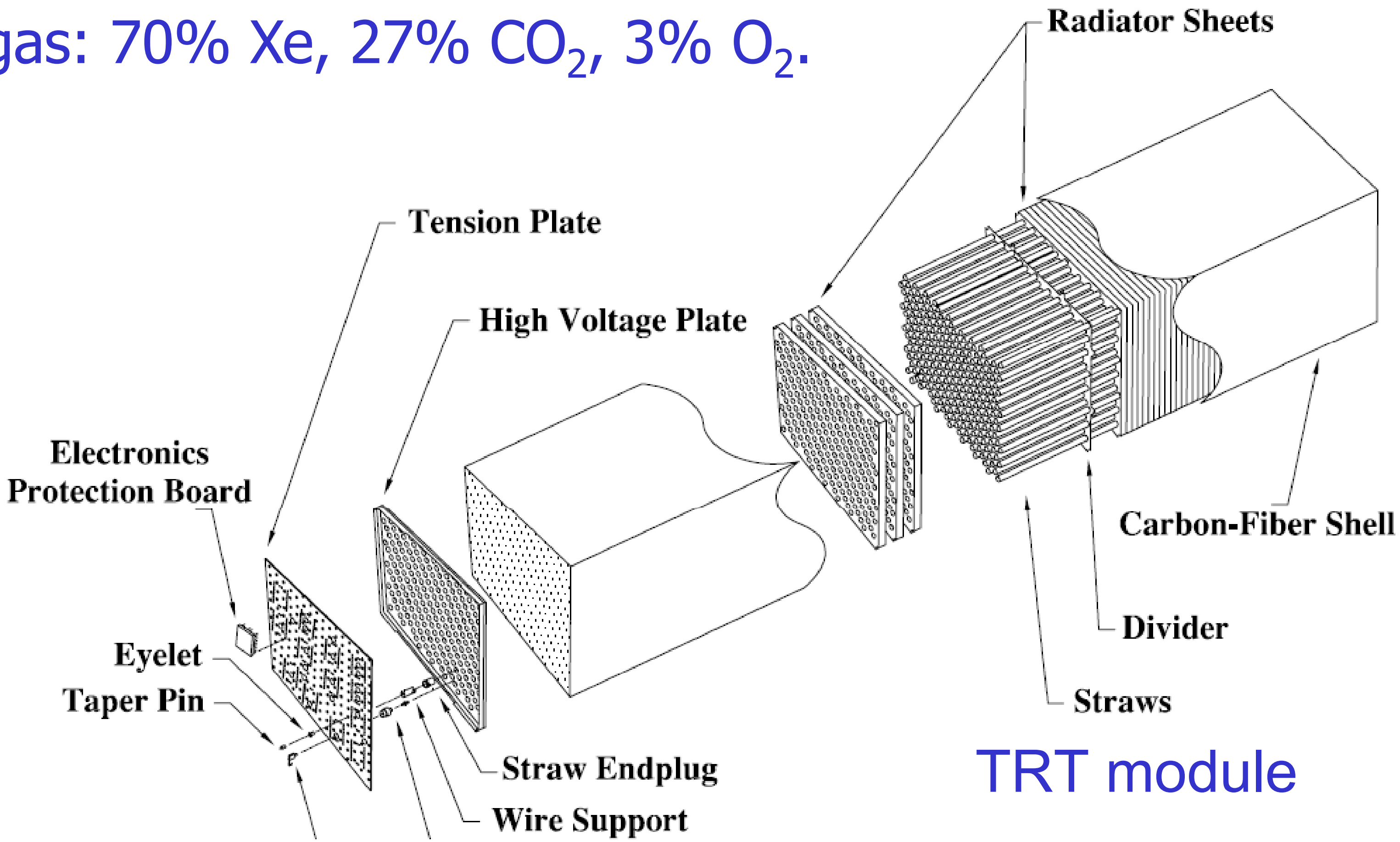

TRT module

TRT: pion-electron separation

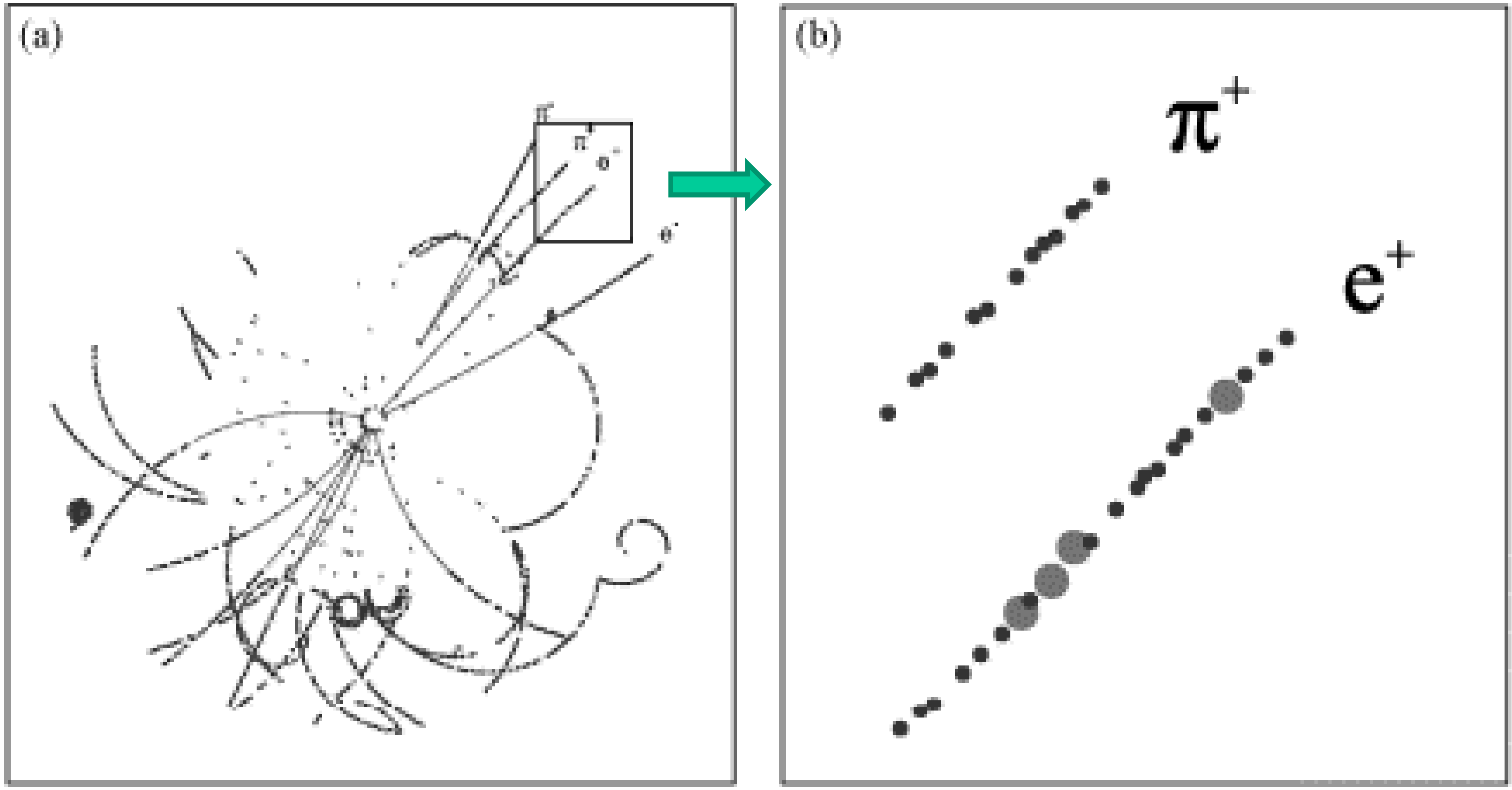

Small circles: low threshold (ionisation), big circles: high threshold (X ray detection)

TRT read-out electronics: two thresholds (low for tracking, high for X rays)

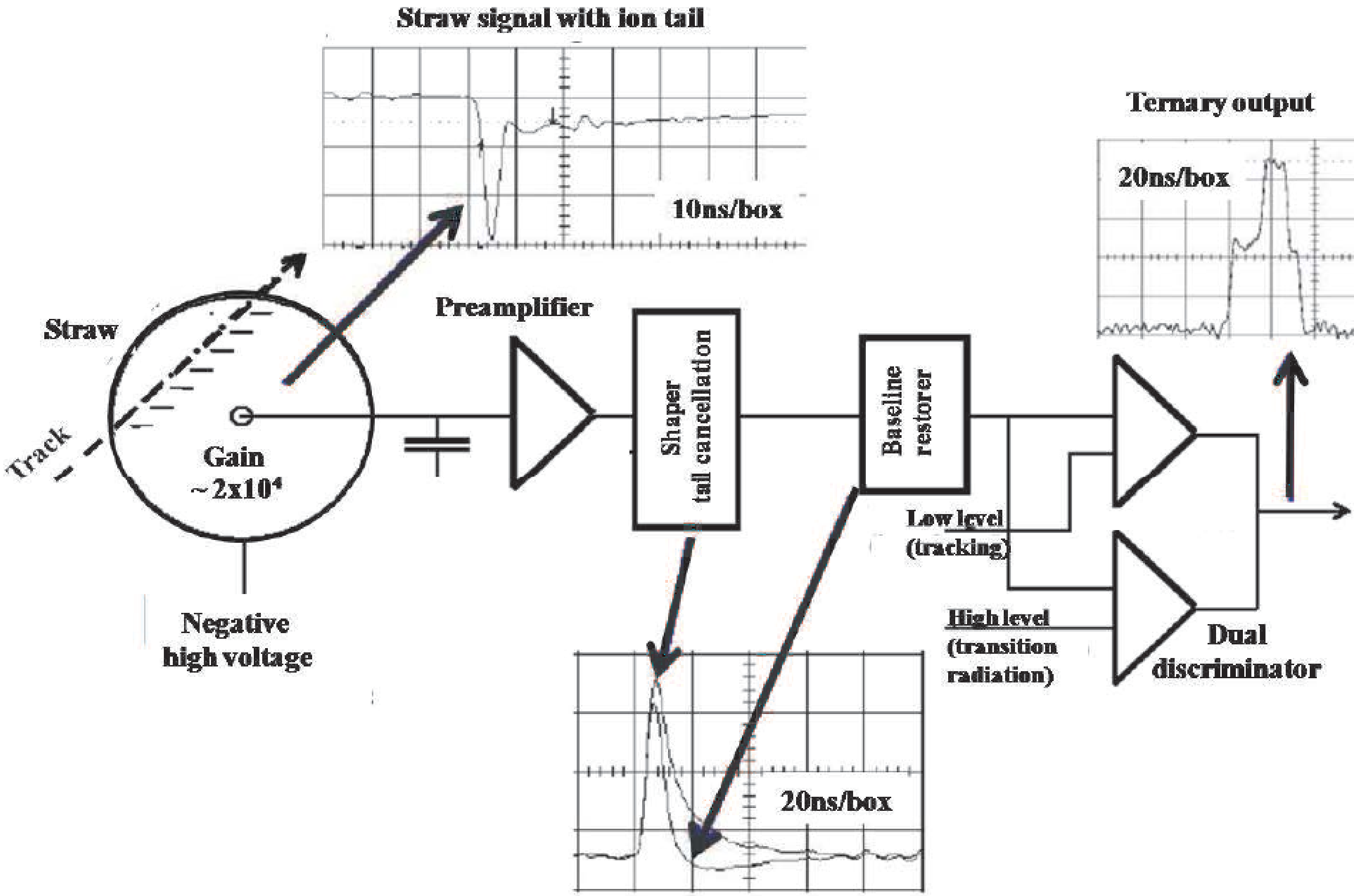

TRT performance

at 90% electron efficiency

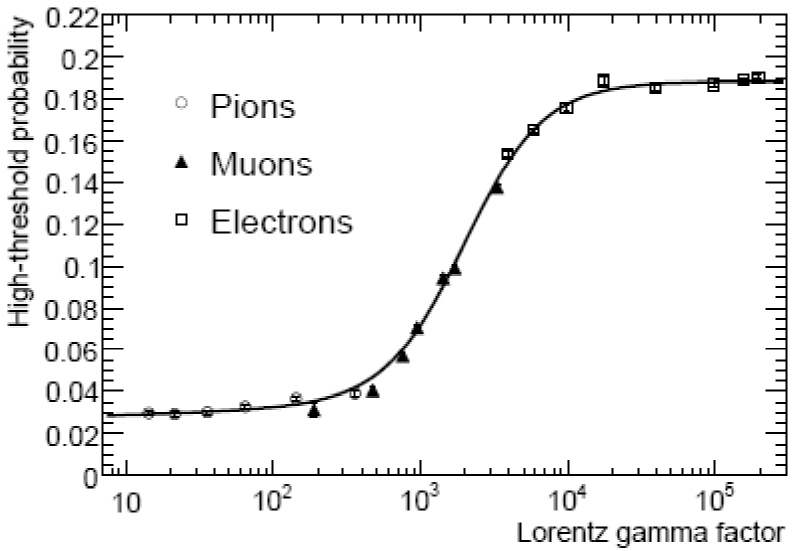

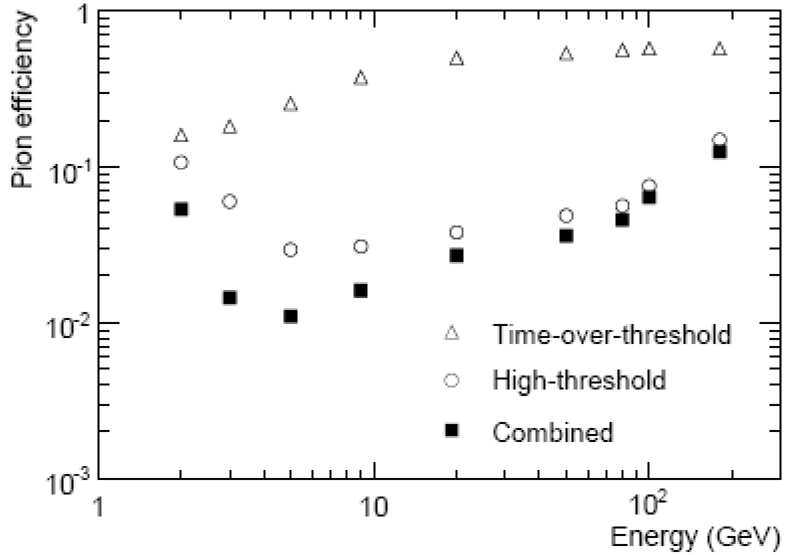

Figure 10.25: Average probability of a high-threshold hit in the barrel TRT as a function of the Lorentz γ-factor for electrons (open squares), muons (full triangles) and pions (open circles) in the energy range 2–350 GeV, as measured in the combined test-beam.

Figure 10.26: Pion efficiency shown as a function of the pion energy for 90% electron efficiency, using high-threshold hits (open circles), time-over-threshold (open triangles) and their combination (full squares), as measured in the combined test-beam.

TRT performance

Data form the first LHC collissions in Nov/Dec 2009

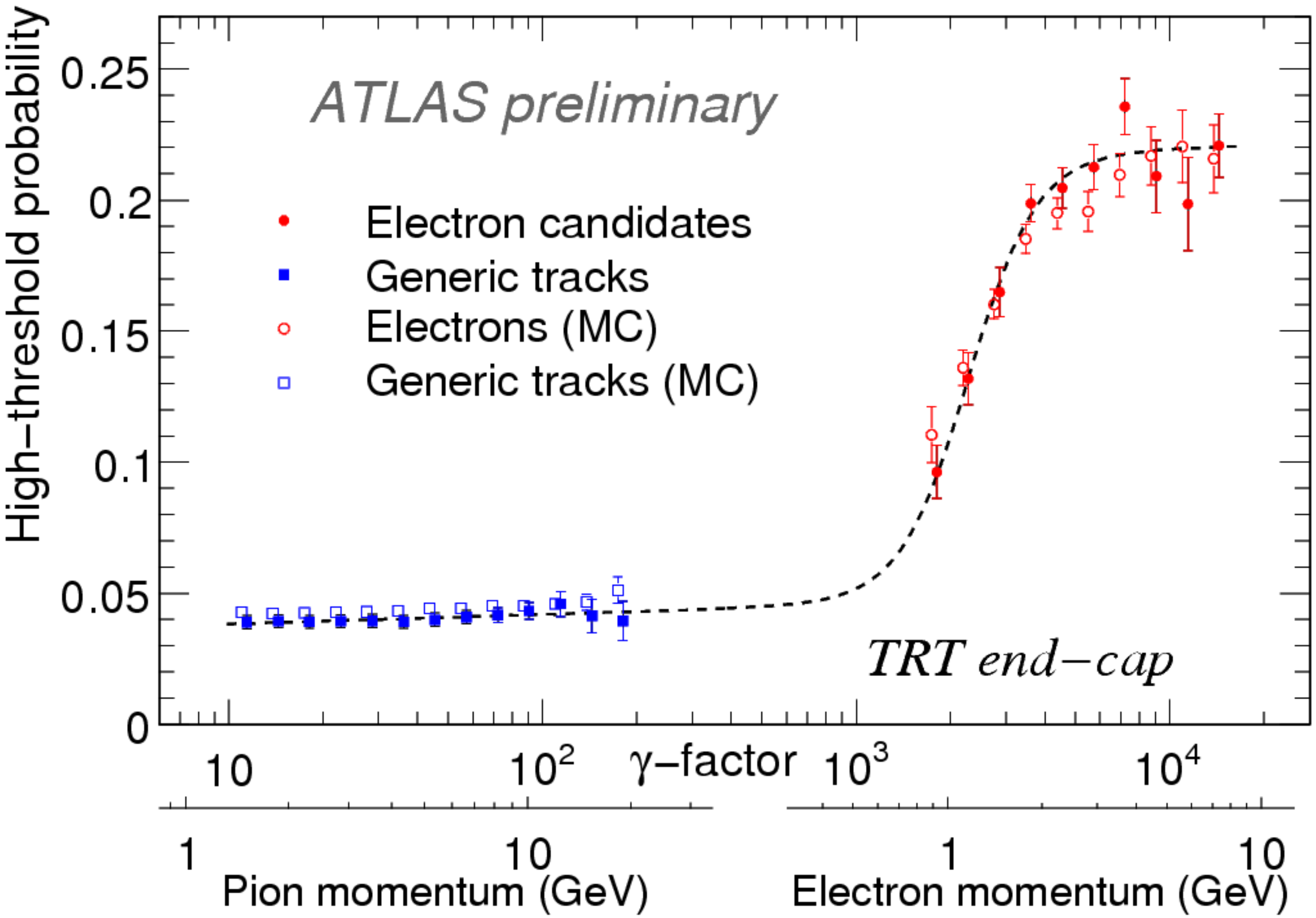

e/pion separation: high threshold hit probability per straw

TRT performance

Data form the first LHC collissions in Nov/Dec 2009

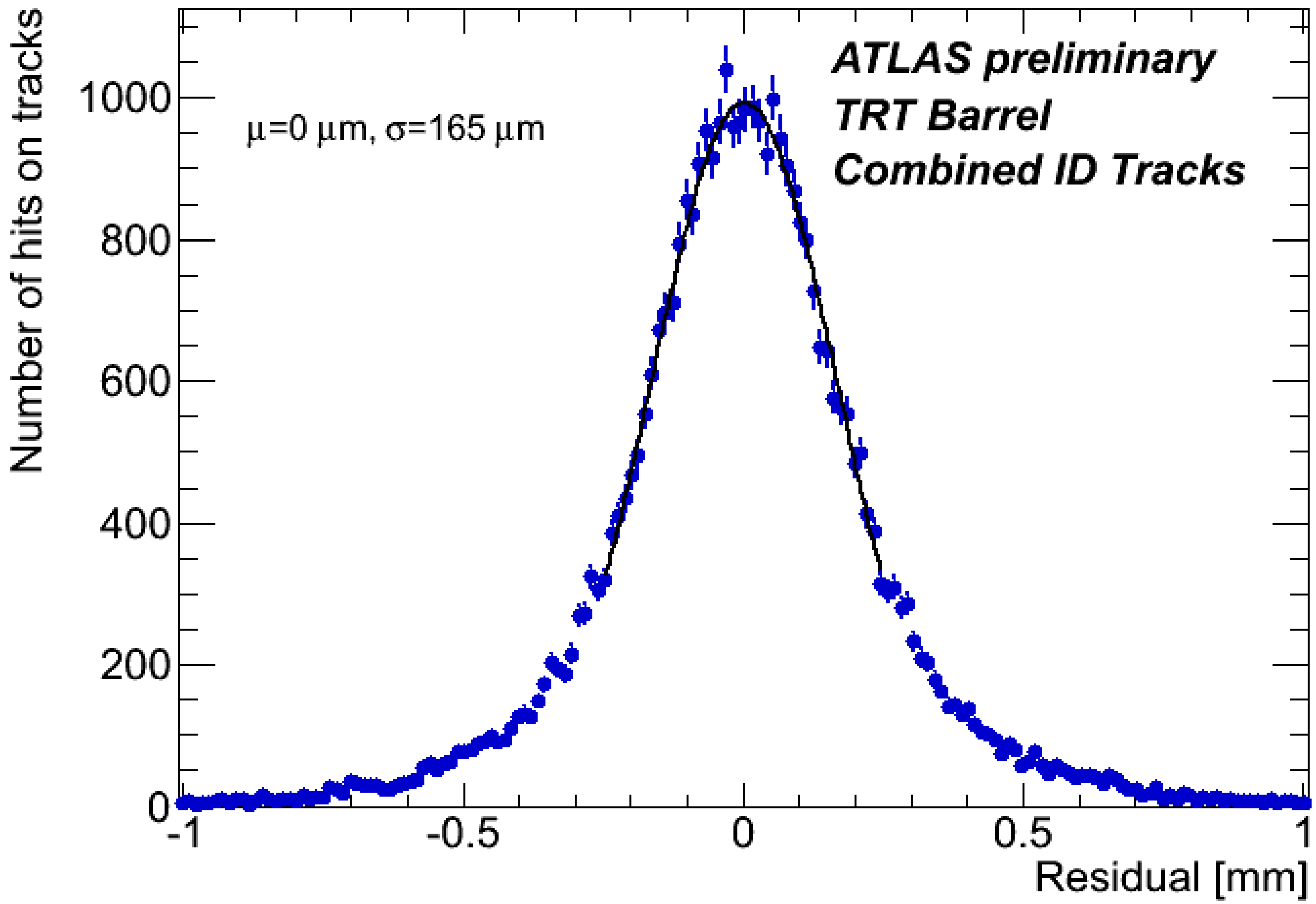

Resolution in coordinate for individual straws

Particle identification
Comparison of methods

Time-of-flight

dE/dx measurement

Čerenkov counters

Transition radiation counters

Compare by calculating the length of detector needed for a given separation (3σ)

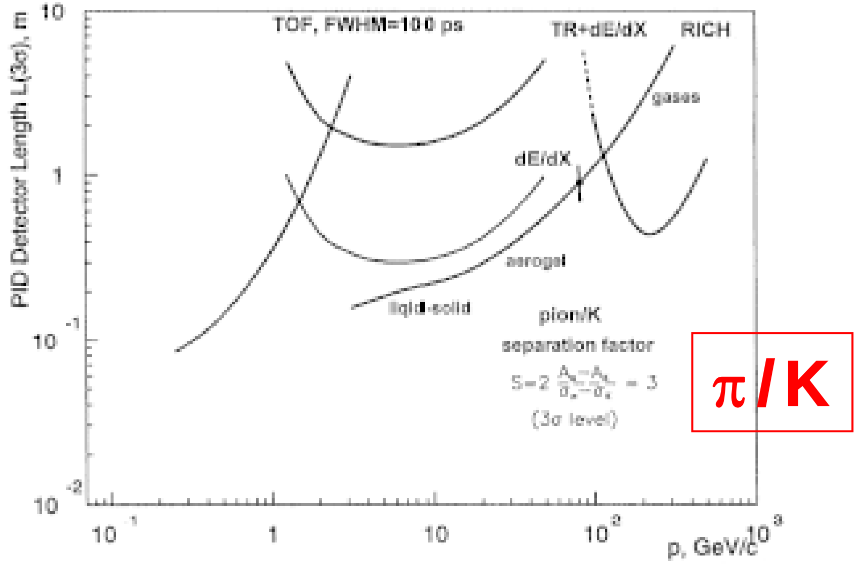

Fig. 14. Pion–kaon separation by different PID methods: the length of the detectors needed for 3 sigma separation.

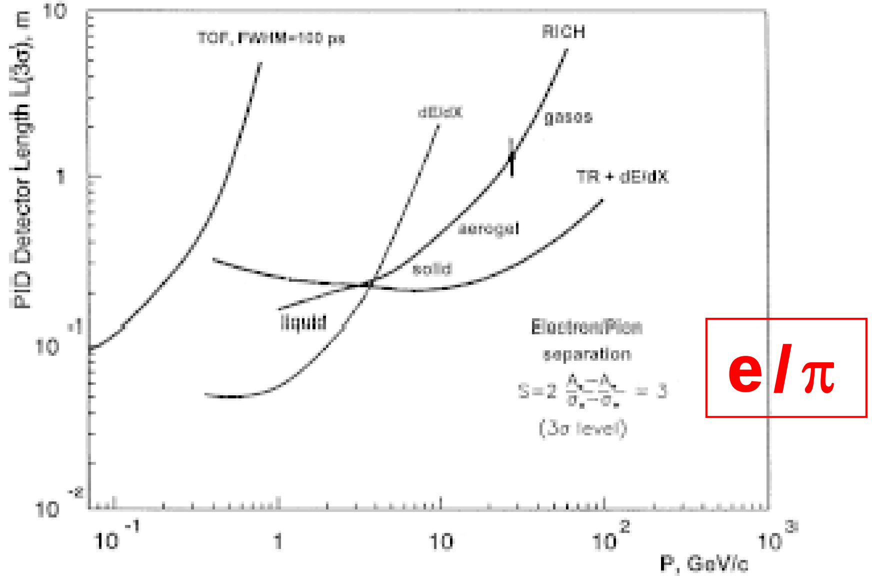

Fig. 15. The same as Fig. 14 for electron–pion separation.

Muon and K_L detector at B factories

Separate muons from hadrons (pions and kaons): exploit the fact that muons interact only electromag., while hadrons interact strongly → need a few interaction lengths to stop hadrons (interaction lengths = about 10x radiation length in iron, 20x in CsI). A particle is identified as muon if it penetrates the material.

Detect K_L interaction (cluster): again need a few interaction lengths.

Some numbers: 0.8 interaction length (CsI) + 3.9 interaction lengths (iron)

Interaction length: iron 132 g/cm^2, CsI 167 g/cm^2

$(dE/dx)_{min}$: iron 1.45 MeV/(g/cm^2), CsI 1.24 MeV/(g/cm^2)

→ ΔE_{min} = (0.36+0.11) GeV = 0.47 GeV → reliable identification of muons possible above ~600 MeV

Example: Muon and K_L detection at Belle

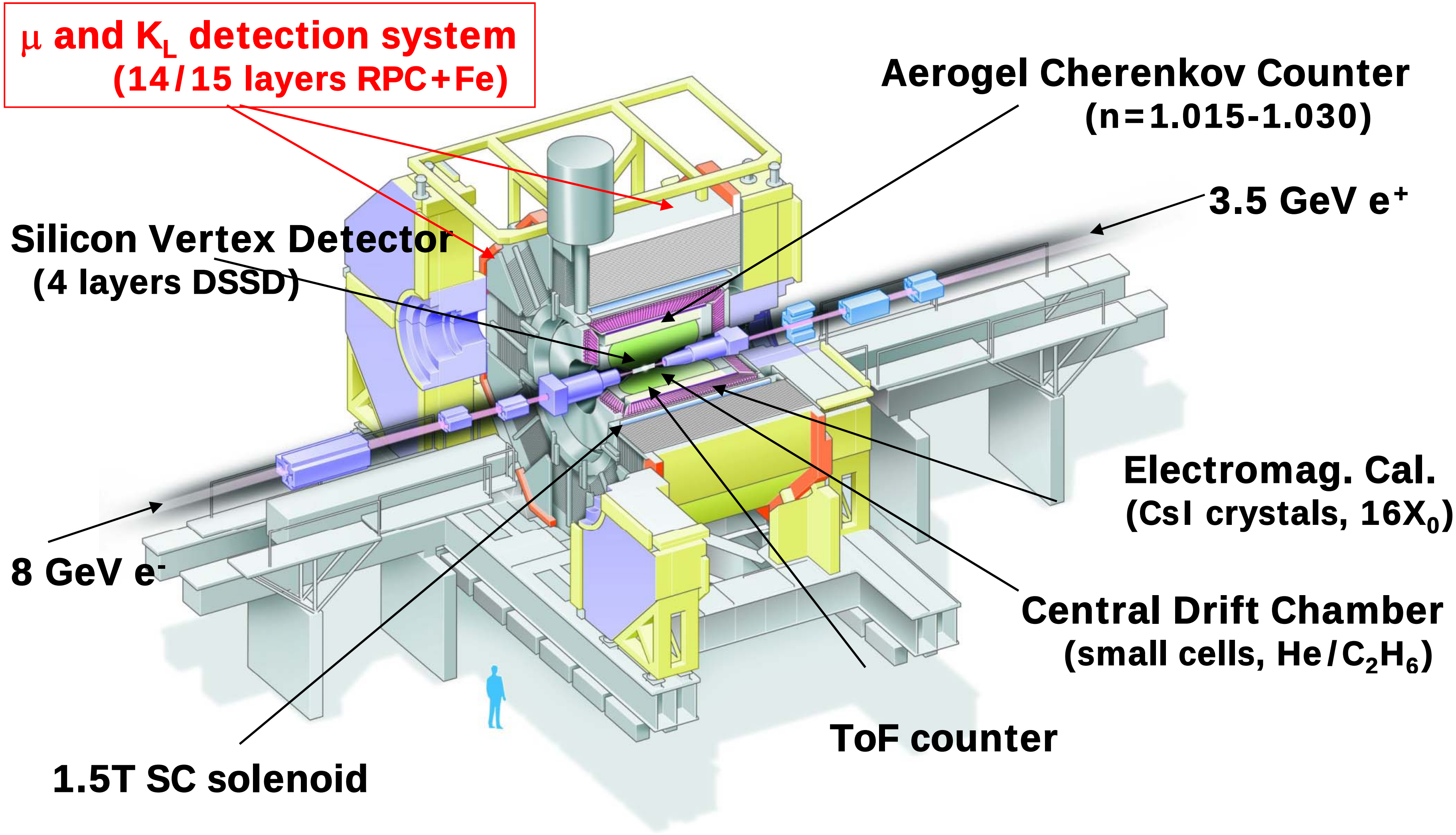

Muon and K_L detector

Up to 21 layers of resistive-plate chambers (RPCs) between iron plates of flux return

Bakelite RPCs at BABAR

Glass RPCs at Belle

(better choice)

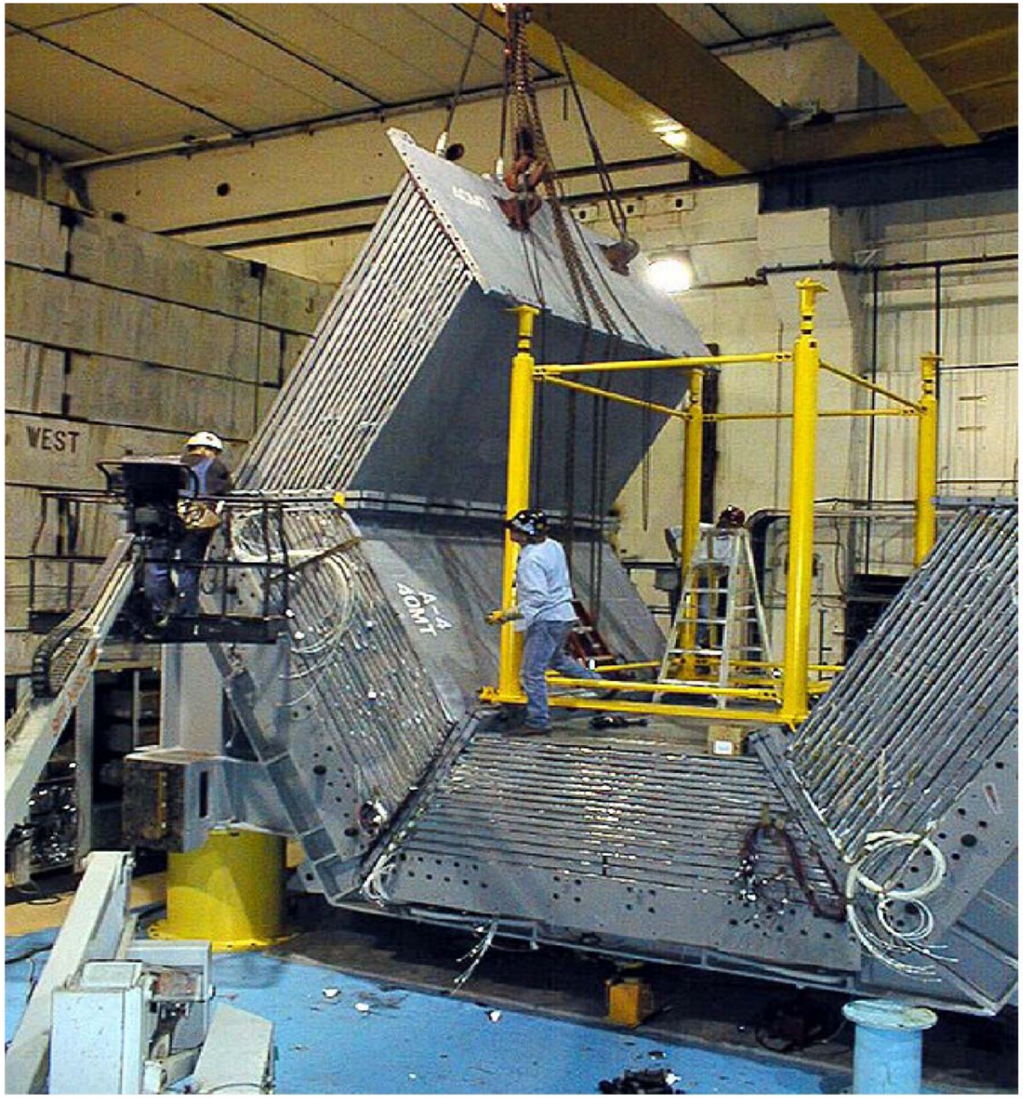

Muon and K_L detector

Example:

event with

- **two muons and a**
- **K_L**

and a pion that partly penetrated

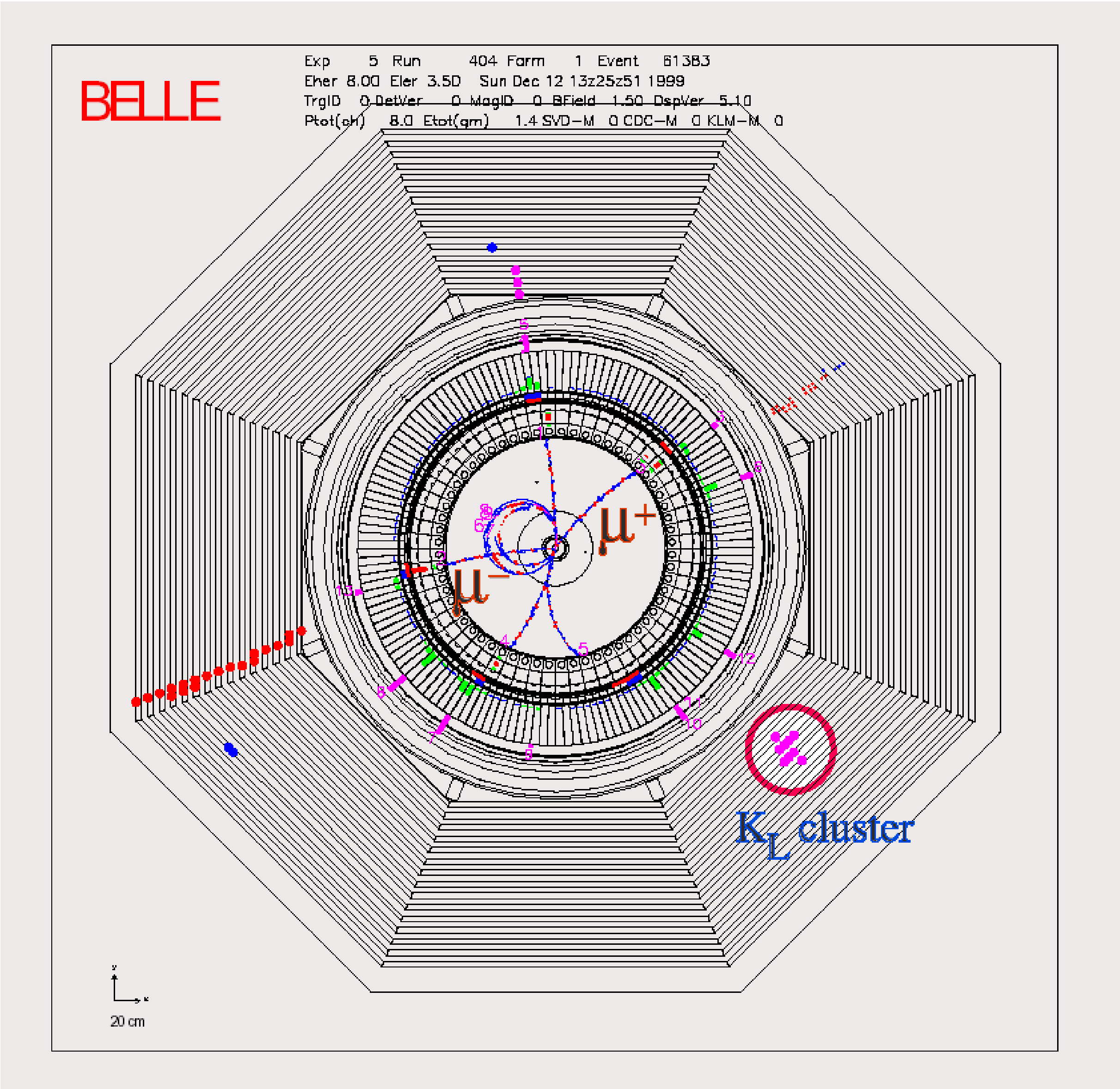

Muon and K_L detector performance

Muon identification: efficient for p>800 MeV/c

efficiency

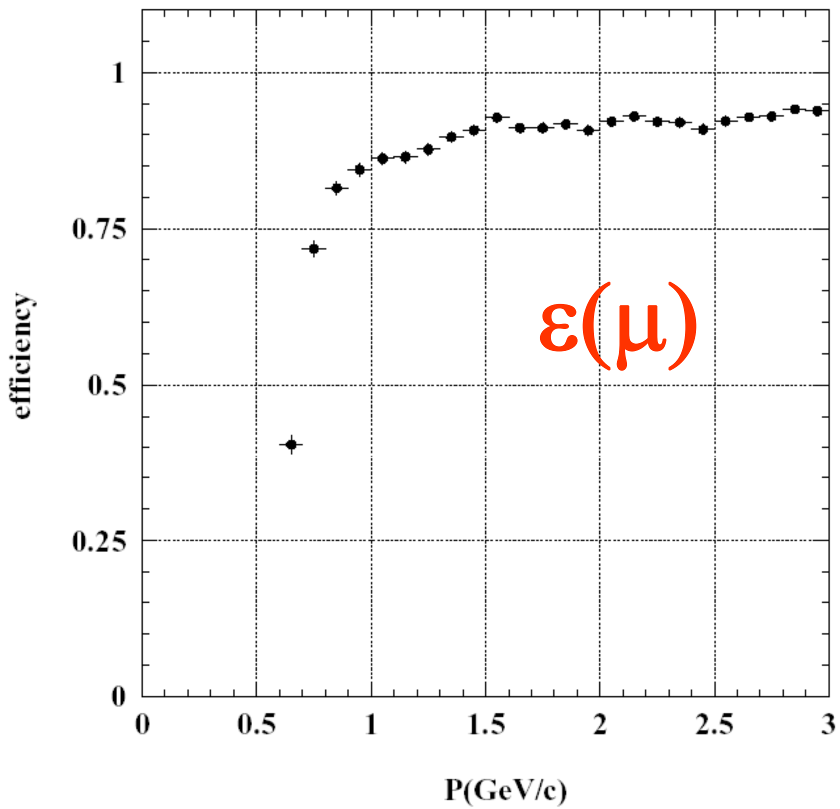

Fig. 109. Muon detection efficiency vs. momentum in KLM.

fake probability

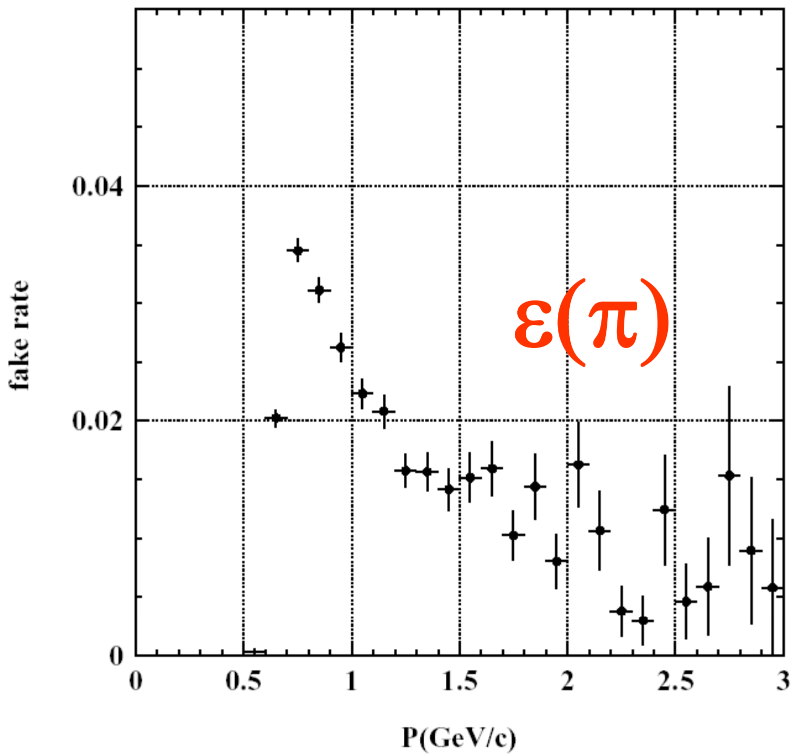

Fig. 110. Fake rate vs. momentum in KLM.

Muon and K_L detector performance

K_L detection: resolution in direction →

K_L detection: also with possible with electromagnetic calorimeter (0.8 interactin lengths)

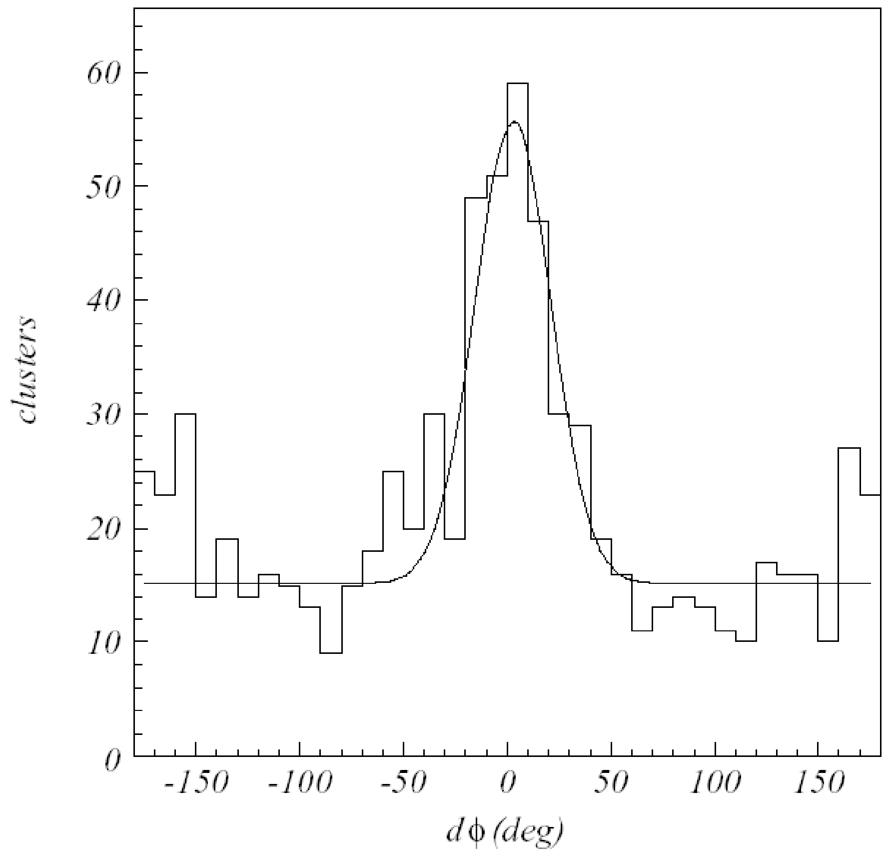

Fig. 107. Difference between the neutral cluster and the direction of missing momentum in KLM.

Identification of muons at LHC - example ATLAS

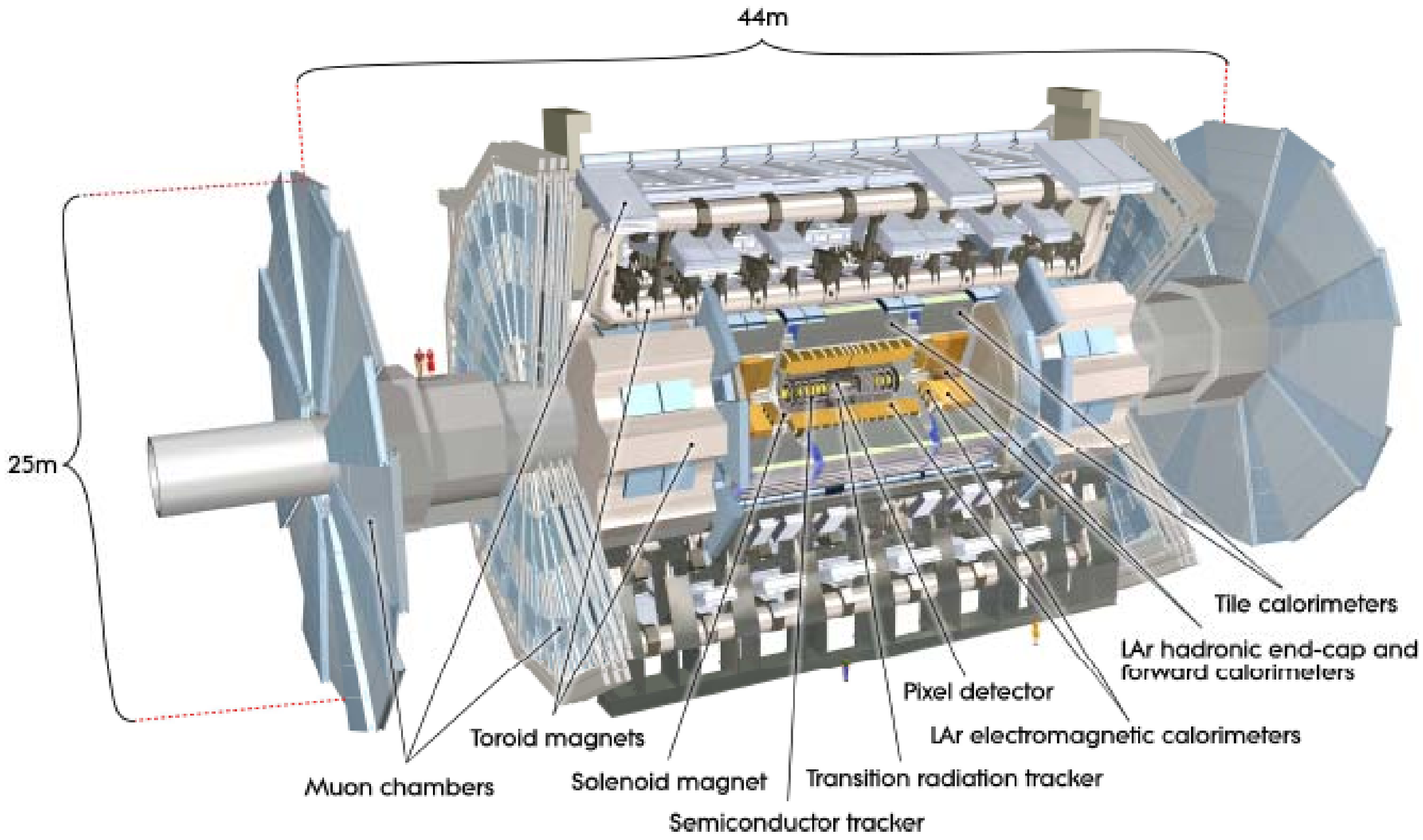

Identification of muons in ATLAS

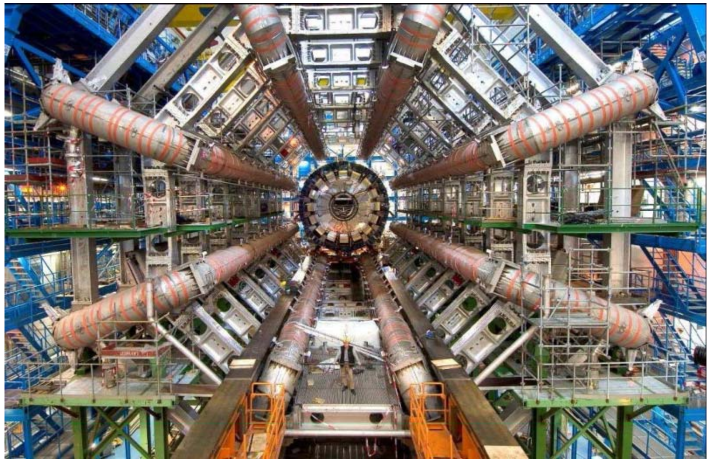

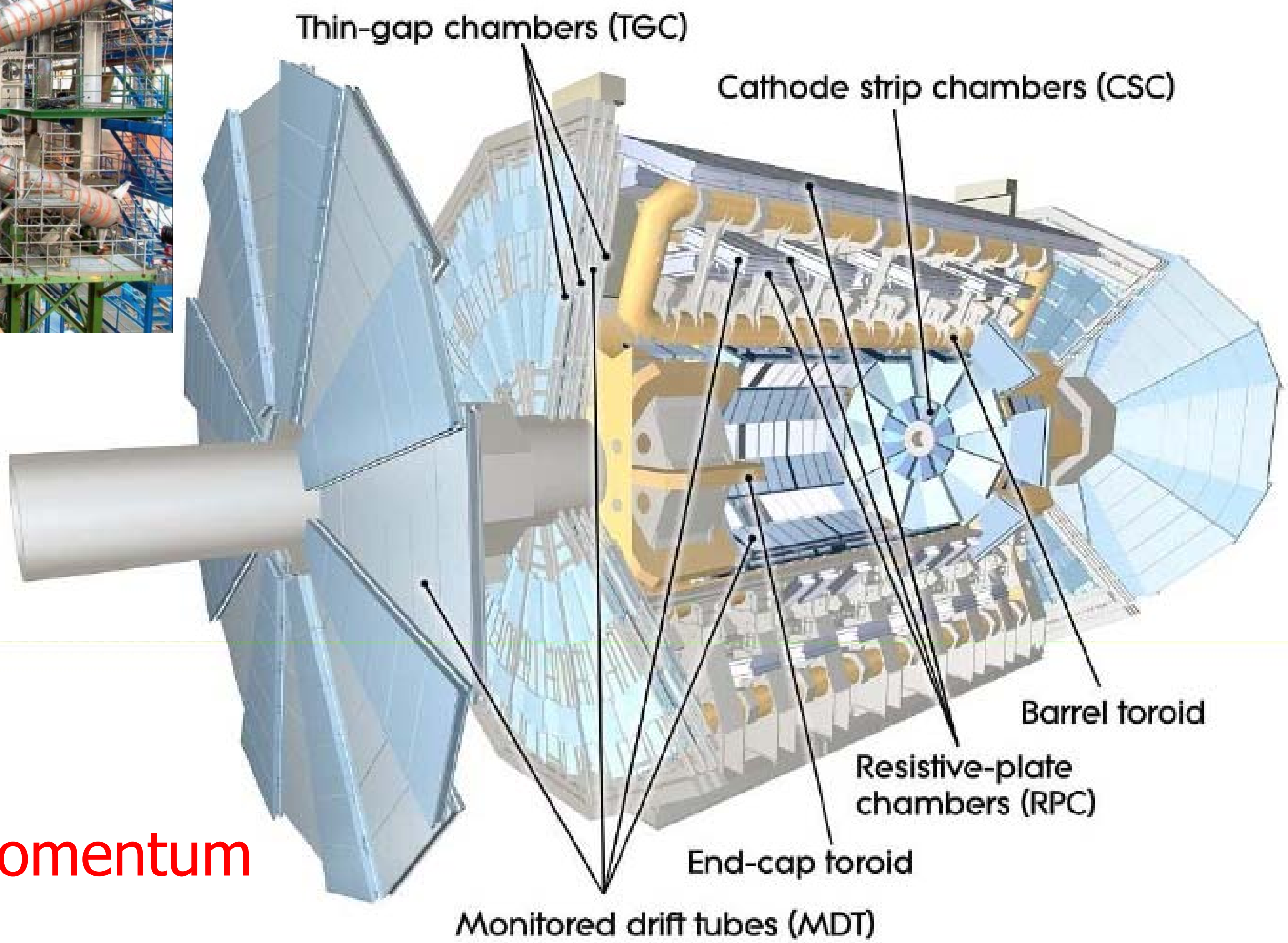

- Identify muons
- Measure their momentum

Muon spectrum

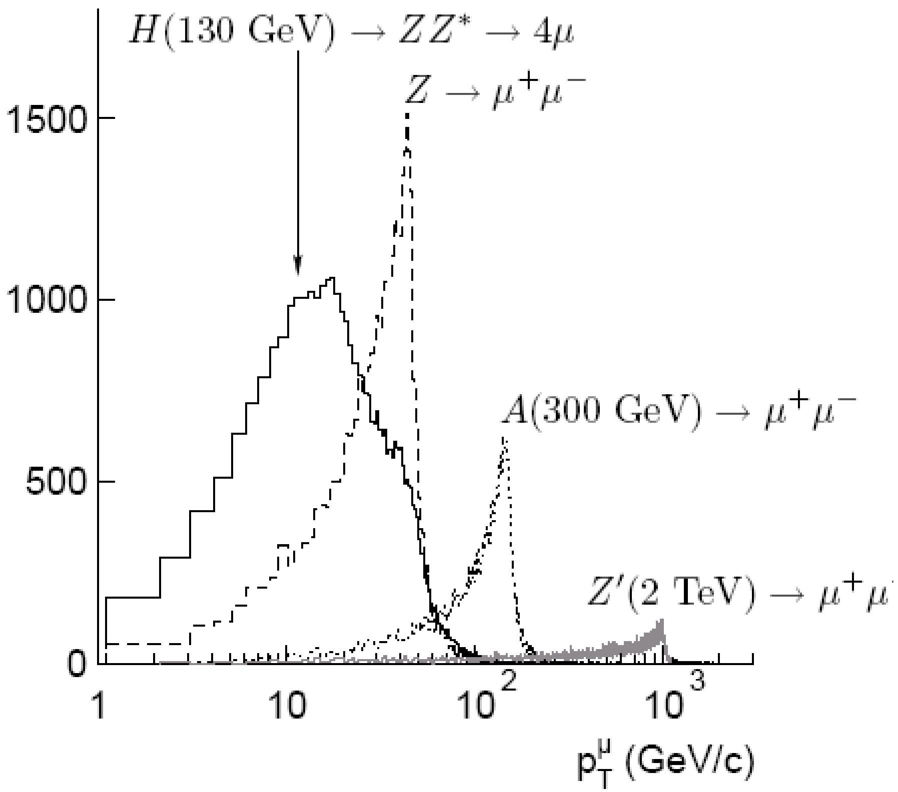

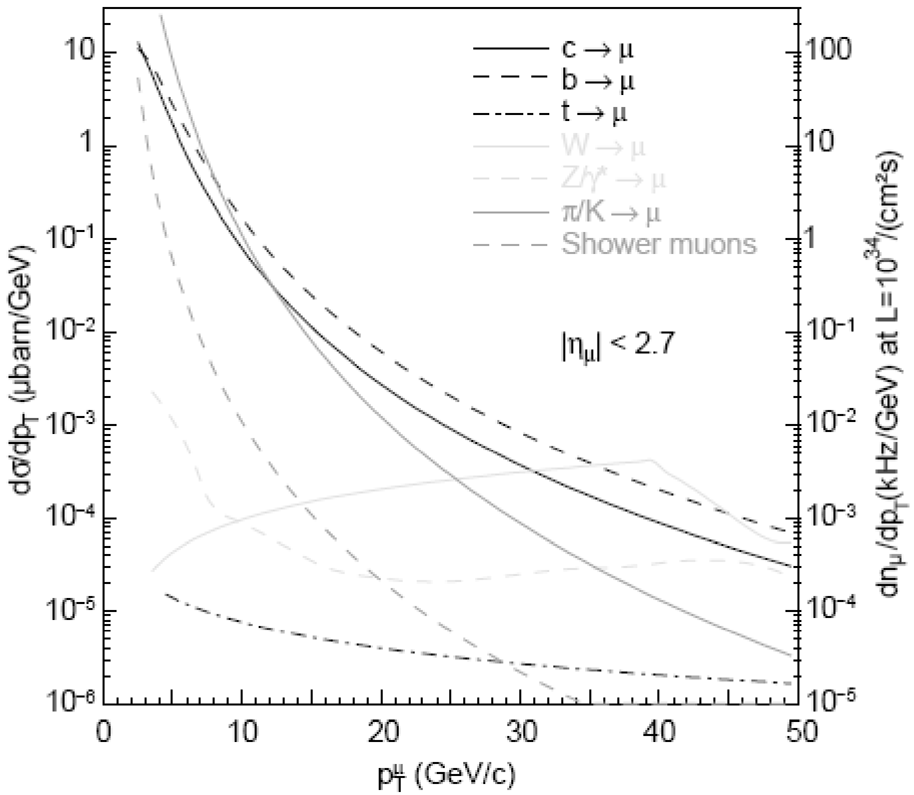

Muon identification in ATLAS

Material in front of the muon system

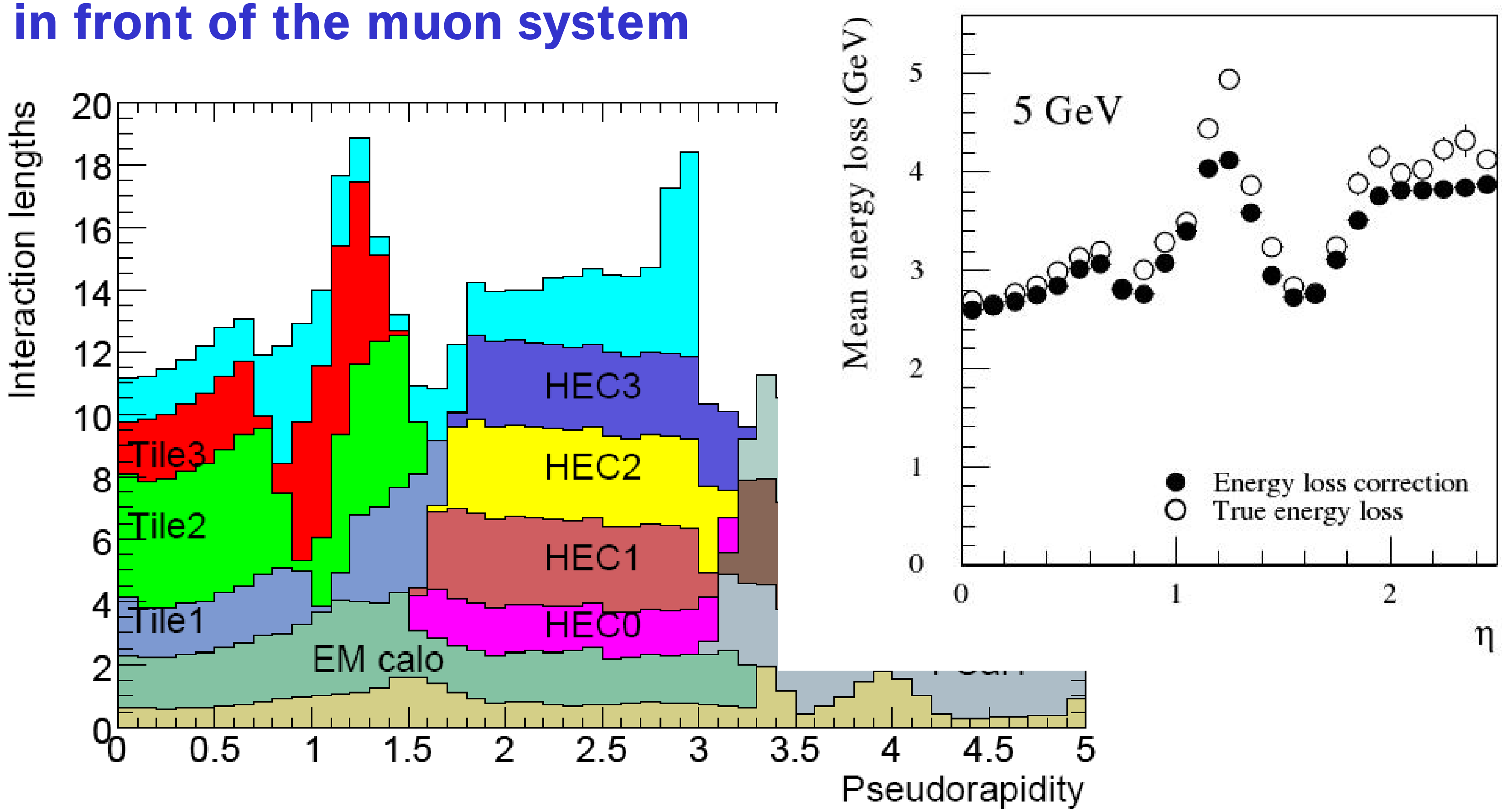

Figure 5.2: Cumulative amount of material, in units of interaction length, as a function of $|\eta|$, in front of the electromagnetic calorimeters, in the electromagnetic calorimeters themselves, in each hadronic layer, and the total amount at the end of the active calorimetry. Also shown for completeness is the total amount of material in front of the first active layer of the muon spectrometer (up to $|\eta| < 3.0$).

Muon identification efficiency

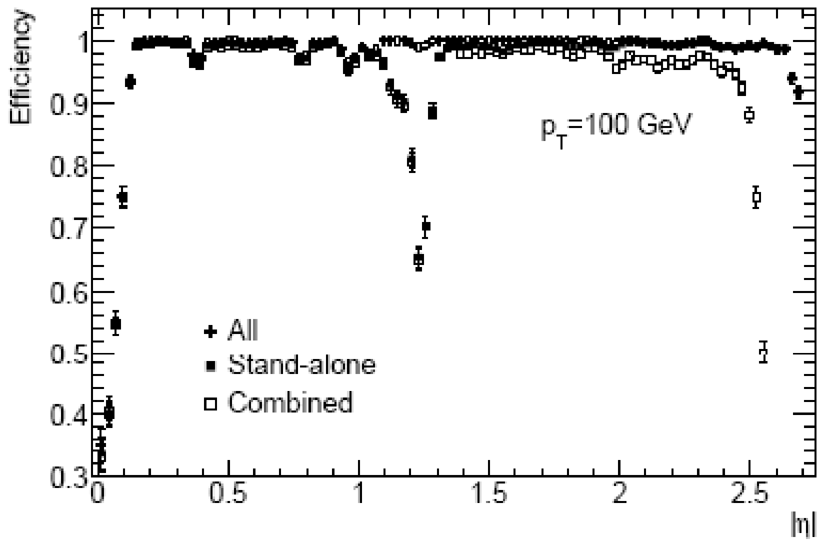

Figure 10.37: Efficiency for reconstructing muons with $p_T = 100\,\text{GeV}$ as a function of $|\eta|$. The results are shown for stand-alone reconstruction, combined reconstruction and for the combination of these with the segment tags discussed in the text.

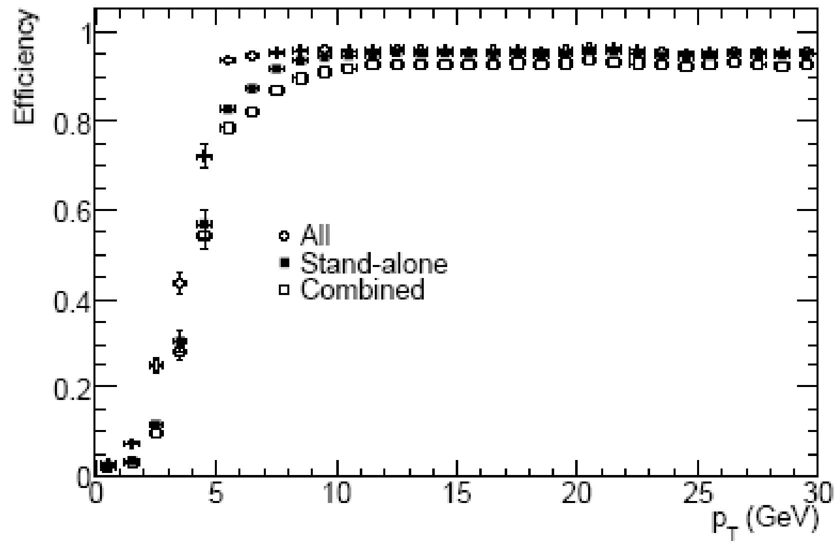

Figure 10.38: Efficiency for reconstructing muons as a function of p_T. The results are shown for stand-alone reconstruction, combined reconstruction and for the combination of these with the segment tags discussed in the text.

Muon fake probability

Sources of fakes:

-Hadrons: punch through negligible, >10 interaction legths of material in front of the muon system (remain: muons from pion and kaon decays)

-Electromagnetic showers triggered by energetic muons traversing the calorimeters and support structures lead to low-momentum electron and positron tracks, an irreducible source of fake stand-alone muons. Most of them can be rejected by a cut on their transverse momentum (pT > 5 GeV reduces the fake rate to a few percent per triggered event); can be almost entirely rejected by requiring a match of the muon-spectrometer track with an inner-detector track.

- Fake stand-alone muons from the background of thermal neutrons and low energy γ-rays in the muon spectrometer ("cavern background"). Again: pT > 5 GeV reduces this below 2% per triggered event at 10^{33} cm^{-2} s^{-1}. Can be reduced by almost an order of magnitude by requiring a match of the muon-spectrometer track with an inner-detector track.

Identification in astro-physics/astroparticle physics - 1

- Study composition of cosmic rays in balloon or satelite flights
- Identify (very) high energy cosmic rays and photons with detectors on the ground

Short flight small area detectors (Balloons)
Examples of Balloon-flown RICH detectors

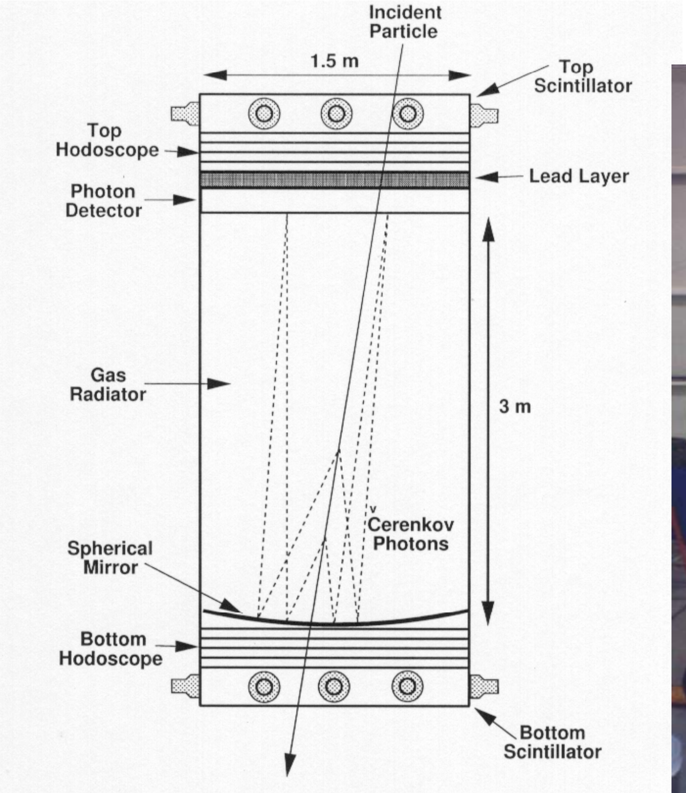

Fig. 1. Schematic cross-section of the instrument

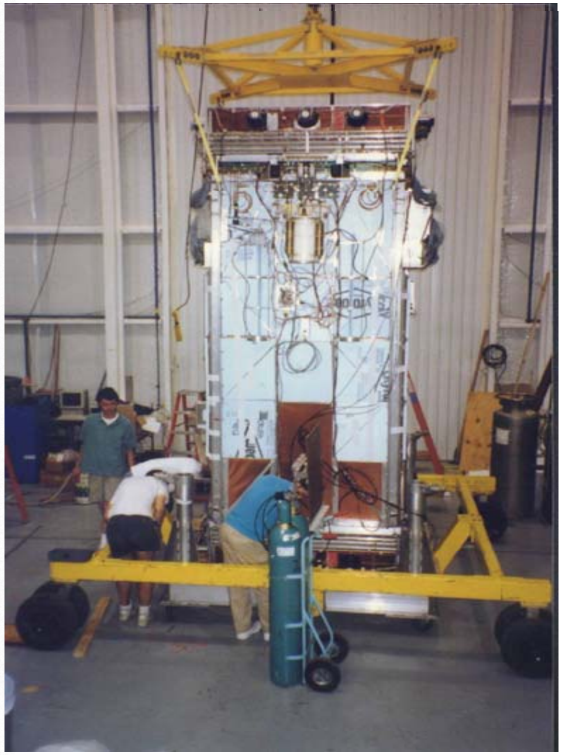

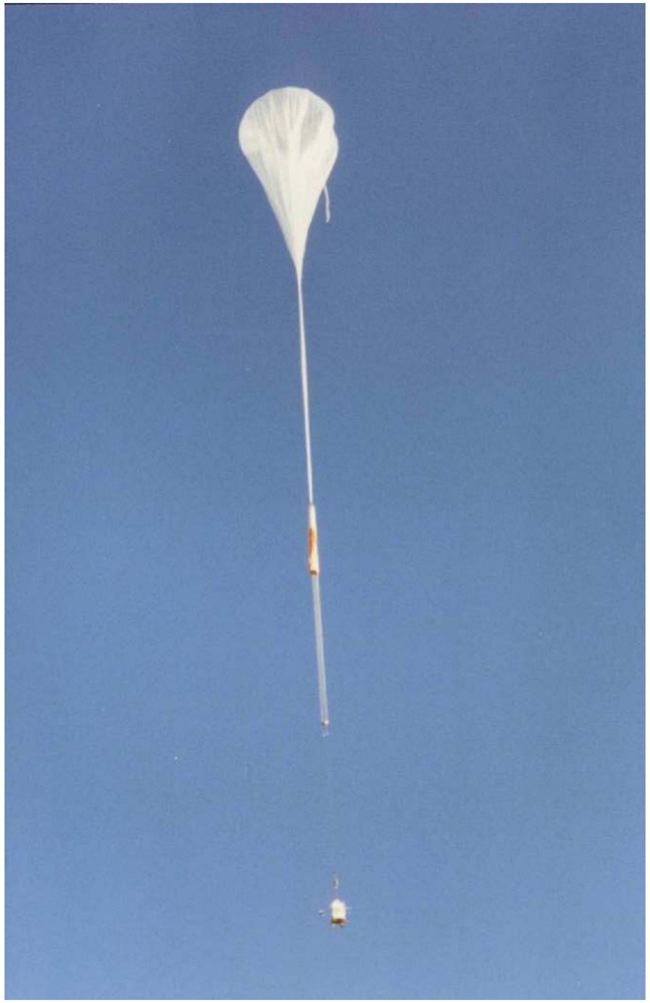

3-metre N_2 radiator, TMAE/CH_4: $\gamma_{th}=40$

p + He at high energy:

3-metre C_2F_6 radiator, TMAE/C_2H_6: $\gamma_{th}=25$

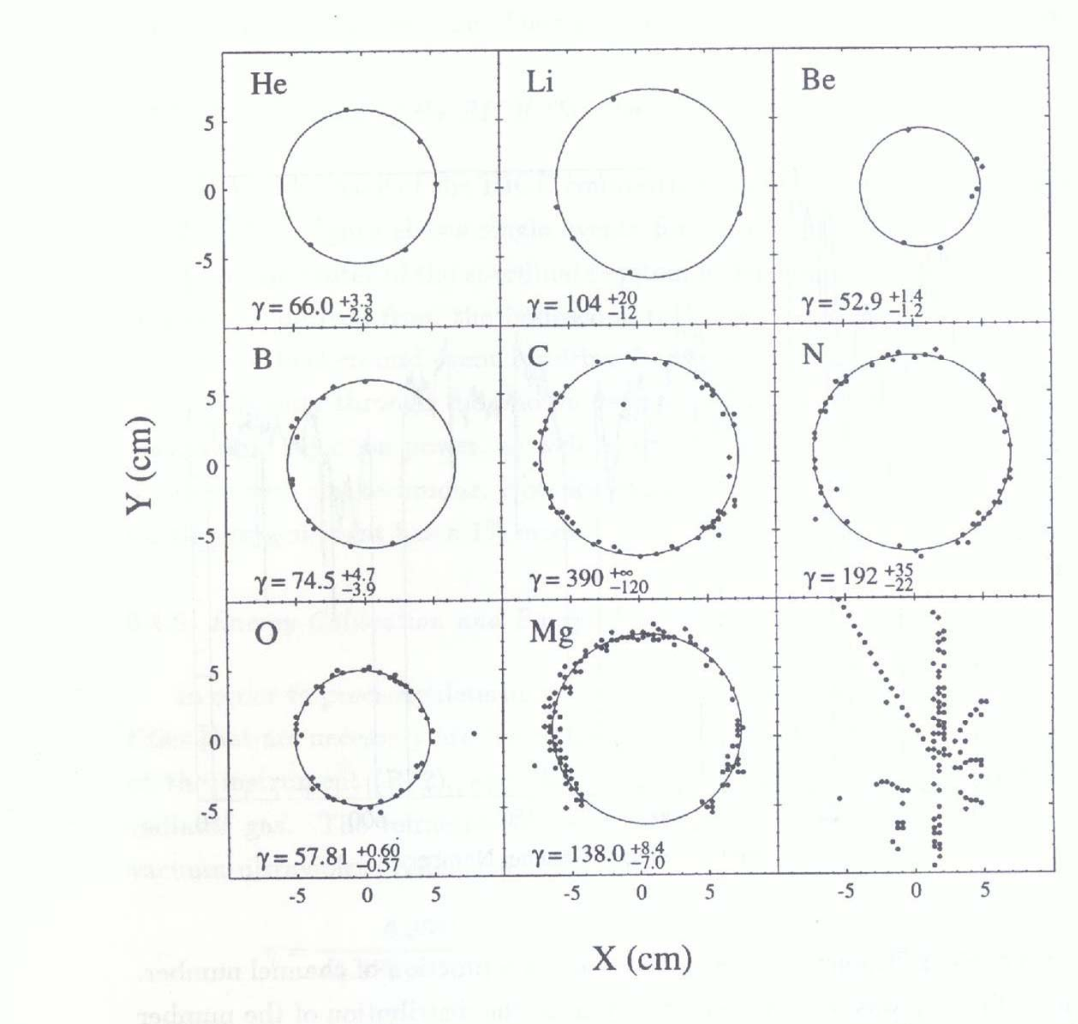

Heavy nucleus rings from 1991 flight –
Note that carbon here has total energy
~ 12*390 GeV = 4.6TeV

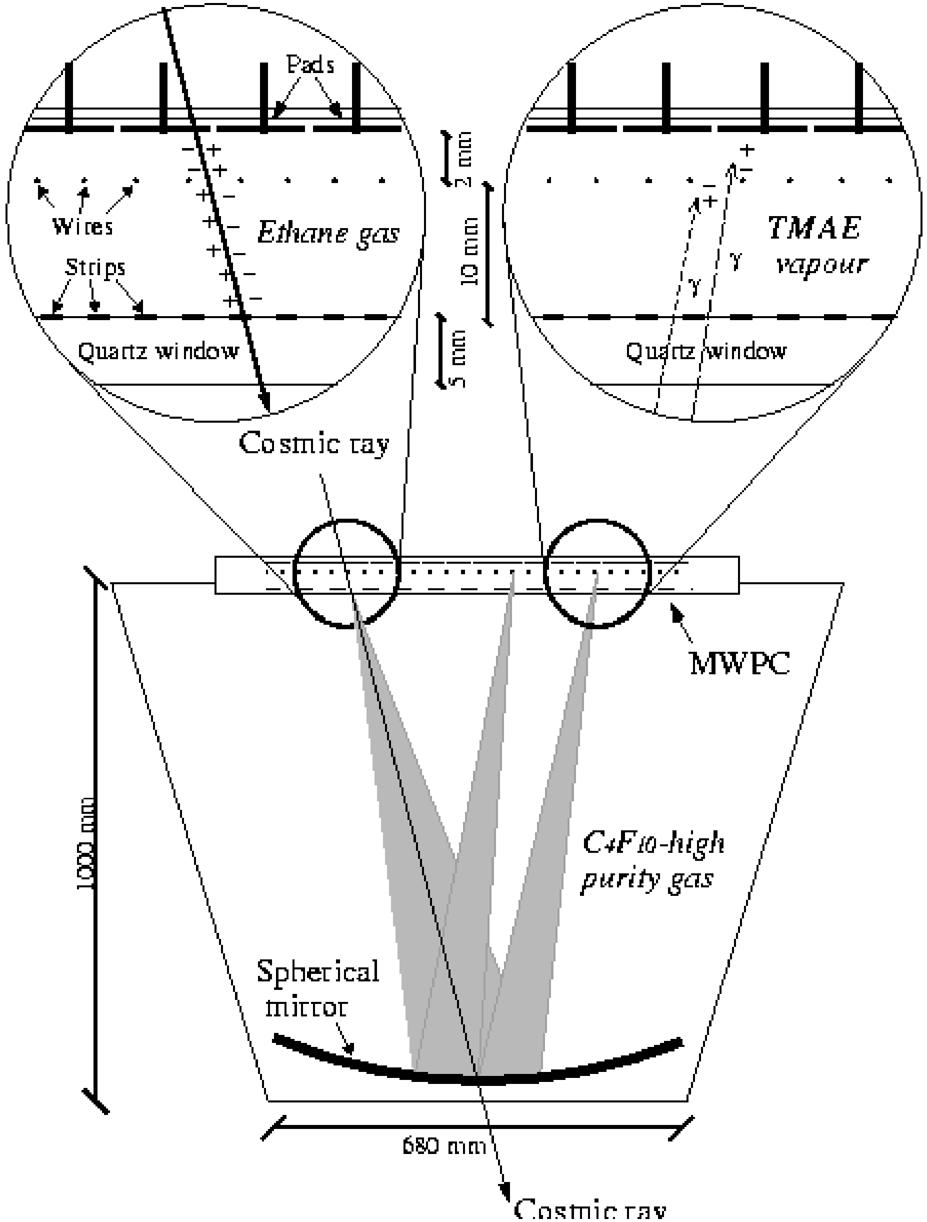

Figure 1.4: *Schematic view of the CAPRICE98 RICH detector.*

HESS 1 UHE Gamma Ray Telescope
Stereoscopic Quartet

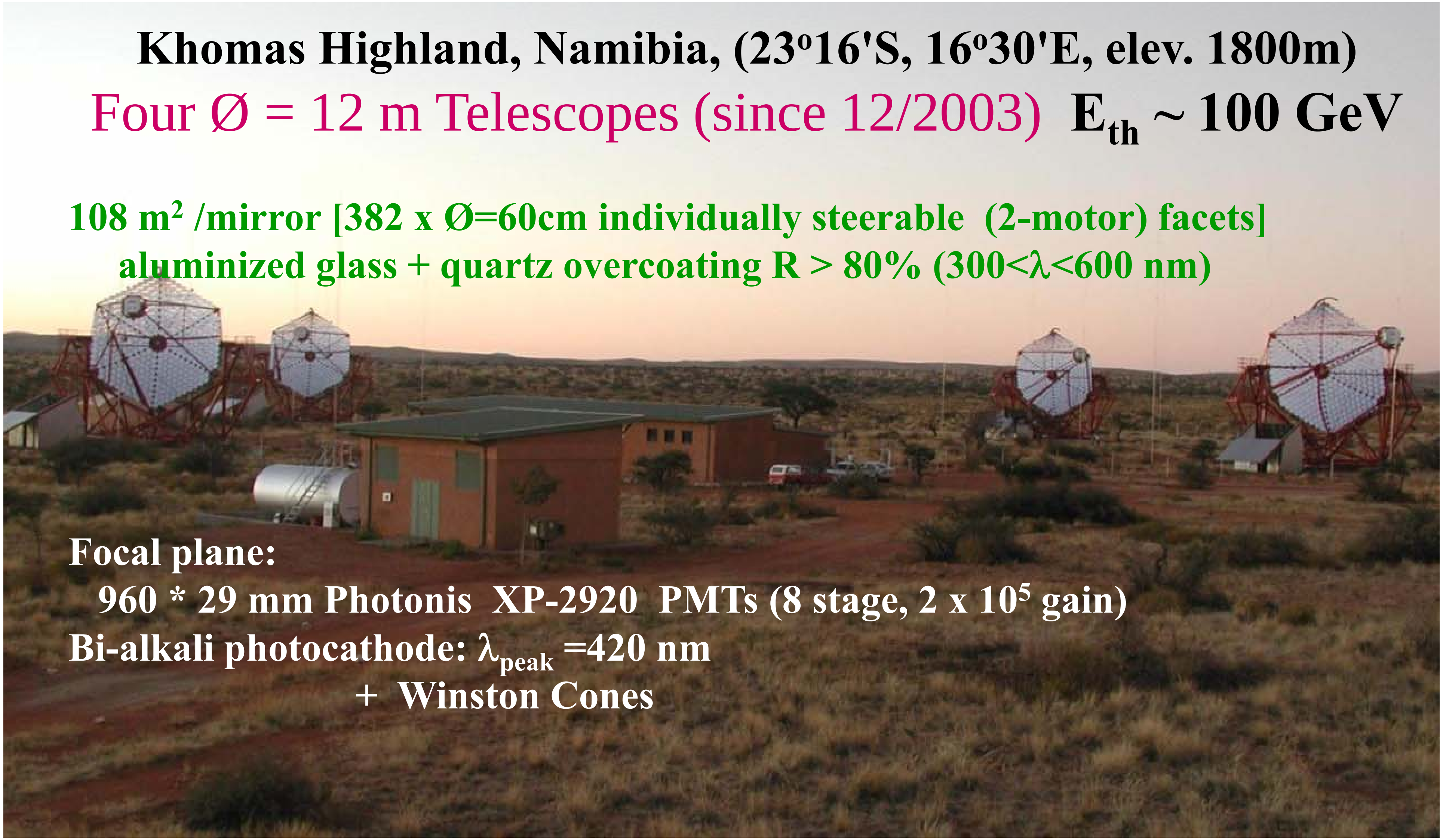

Khomas Highland, Namibia, (23°16'S, 16°30'E, elev. 1800m)

Four Ø = 12 m Telescopes (since 12/2003) **E_{th} ~ 100 GeV**

108 m^2 /mirror [382 x Ø=60cm individually steerable (2-motor) facets]
aluminized glass + quartz overcoating R > 80% (300<λ<600 nm)

Focal plane:
960 * 29 mm Photonis XP-2920 PMTs (8 stage, 2 x 10^5 gain)
Bi-alkali photocathode: λ_{peak} =420 nm
+ Winston Cones

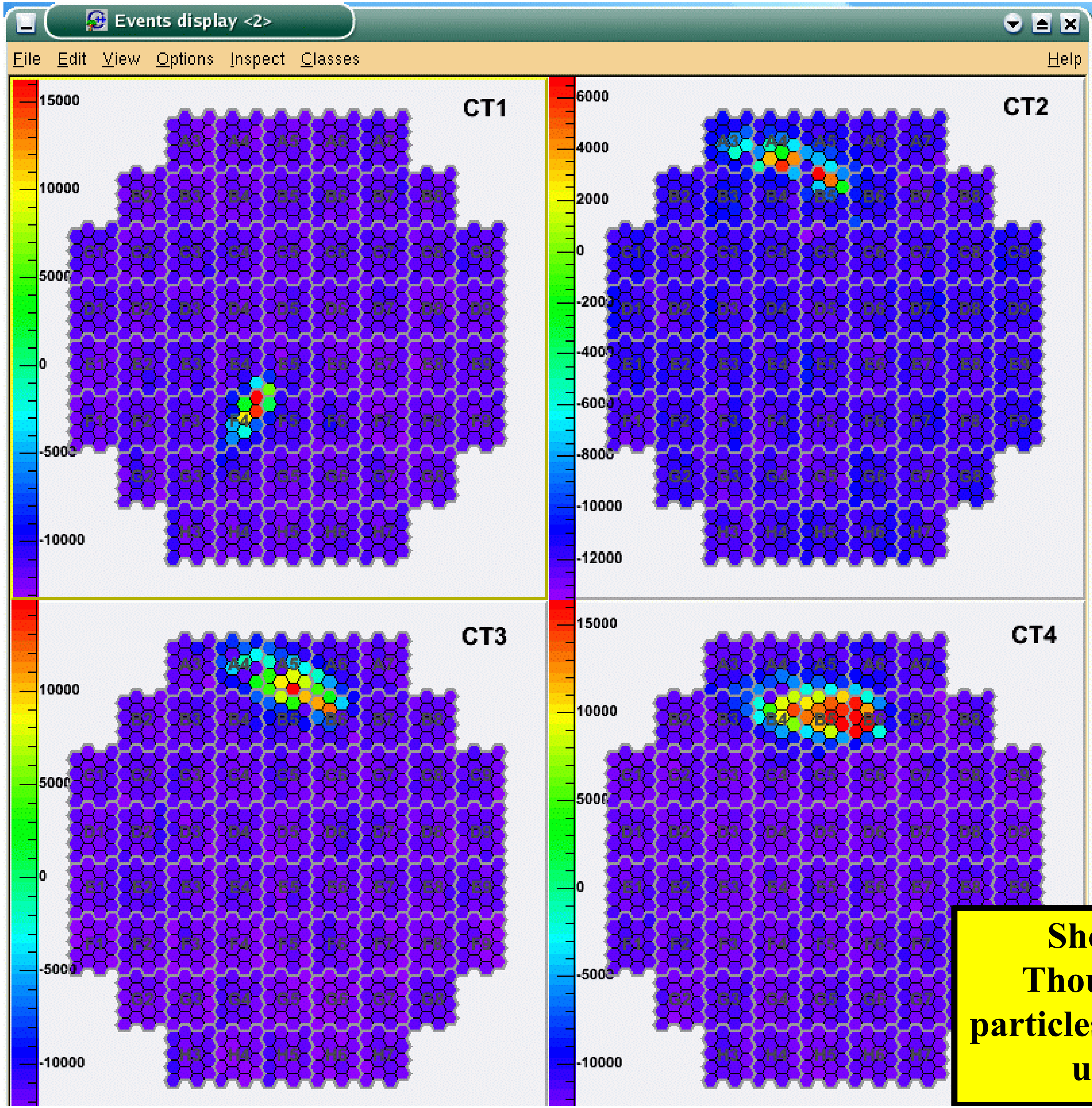

Detection of high-energy gamma rays

using Cherenkov telescopes

The HESS
Concept

Shower mainly E-M. Thousands of relativistic particles give Čerenkov light in upper atmosphere

Appendix A: derivation of dσ/d(hω) a la Allison, Cobb

– Solve Maxwell's Equations with charge density $\rho = e_0\delta^3(\vec{r} - \vec{\beta}ct)$ and current density $\vec{j} = \vec{\beta}c\rho \rightarrow$
$\phi(\vec{k},\omega) = \frac{e_0}{2\pi\epsilon\epsilon_0 k^2}\delta(\omega - \vec{k}\cdot\vec{\beta}c)$
$\vec{A}(\vec{k},\omega) = \frac{e_0}{2\pi\epsilon_0 c^2}\frac{(\omega\vec{k}/k^2 - \vec{\beta}c)}{(\epsilon\omega^2/c^2 - k^2)}\delta(\omega - \vec{k}\cdot\vec{\beta}c)$
$\rightarrow \vec{E}(\vec{r},t) =$
$\frac{1}{(2\pi)^2}\int\int\left[i\omega\vec{A}(\vec{k},\omega) - i\vec{k}\phi(\vec{k},\omega)\right]e^{i(\vec{k}\cdot\vec{r}-\omega t)}d^3k d\omega$ (A1)

– The energy loss is due to the component of this electric field in the direction β doing work on the particle at the point $\vec{r} = \vec{\beta}ct$:
$< \frac{dE}{dx} >= \frac{e_0}{\beta}\vec{E}(\vec{\beta}ct, t)\cdot\vec{\beta}$ (A2)

– The energy loss is re-written as a probability of energy transfers
$< \frac{dE}{dx} >=$
$-\int_0^\infty d(\hbar\omega)\int_{\frac{\hbar\omega}{\beta c}}^\infty d(\hbar k)\;\; n_e\hbar\omega\frac{d^2\sigma}{d(\hbar\omega)d(\hbar k)}$ (A3)
where n_e is the electron density and $\frac{d^2\sigma}{d(\hbar\omega)d(\hbar k)}$ is the double differential cross section per electron.

Appendix A: derivation of dσ/d(hω) a la Allison, Cobb - 2

Θ is the phase of $1 - \epsilon_1\beta^2 + i\epsilon_2\beta^2$.

Comments:

First term has a factor $\log(1 - \beta^2\epsilon_1)$, responsible for the relativistic rise of the energy-loss cross section and its saturation.

Third term: in the optical region σ_γ vanishes and only the second term contributes $\rightarrow$ Čerenkov radiation.

Phase: $\Theta = 0$ below, and π above threshold. We get the familiar formula for the number of emitted photons per unit track path length and photon energy interval $\frac{d^2N}{d(\hbar\omega)dx} = \frac{\alpha}{\hbar c}\left[1 - \frac{1}{\beta^2\epsilon}\right]$

When ϵ_2 and $\sigma\gamma$ do not vanish, the separate interpretation of this term in the cross section dissolves and it may even be negative.

Last term: constituent scattering from electrons. It is a Rutherford scattering term, shows no relativistic behaviour and is the only non-zero term for energy transfers $\hbar\omega$ in the far X-ray region, describes δ-ray production.